FREE CONVECTION AND TURBULENT FLUXES OVER COMPLEX TERRAIN

A dissertation submitted to the

FACULTY OF BIOLOGY, CHEMISTRY AND GEOSCIENCES

AT THE UNIVERSITY OF BAYREUTH, GERMANY

to attain the academic degree of

DR. RER. NAT.

presented by

RAFAEL EIGENMANN

Dipl. Geoökol.

born 29 April 1983

in Eichstätt, Germany

Bayreuth, January 2013

FREE CONVECTION AND TURBULENT FLUXES OVER COMPLEX TERRAIN

Supervisor: Prof. Dr. Thomas Foken

Die vorliegende Arbeit wurde in der Zeit von August 2008 bis Januar 2013 in Bayreuth an der Abteilung Mikrometeorologie unter Betreuung von Herrn Prof. Dr. Thomas Foken angefertigt.

Vollständiger Abdruck der von der Fakultät für Biologie, Chemie und Geowissenschaften der Universität Bayreuth genehmigten Dissertation zur Erlangung des akademischen Grades eines Doktors der Naturwissenschaften (Dr. rer. Nat.).

Dissertation eingereicht am: 09.01.2013
Zulassung durch die Prüfungskommission: 16.01.2013
Wissenschaftliches Kolloquium: 24.04.2013

Amtierender Dekan:
Prof. Dr. Beate Lohnert

Prüfungsausschuss:
Prof. Dr. Thomas Foken (Erstgutachter)
Prof. Dr. Andreas Held (Zweitgutachter)
Prof. Dr. John Tenhunen (Vorsitz)
Prof. Dr. Bernd Huwe
Prof. Dr. Michael Hauhs

Contents

List of manuscripts

The thesis is presented in cumulative form consisting of four manuscripts. Three manuscripts have been published in peer-reviewed journals. The fourth manuscript has been submitted for publication to a peer-reviewed journal.

Published manuscripts:

Eigenmann, R., Metzger, S., Foken, T., 2009. Generation of free convection due to changes of the local circulation system. Atmospheric Chemistry and Physics, 9: 8587–8600.

Previously published as: Eigenmann, R., Metzger, S., Foken, T., 2009. Generation of free convection due to changes of the local circulation system. Atmospheric Chemistry and Physics Discussions, 9: 11367–11411.

Eigenmann, R., Kalthoff, N., Foken, T., Dorninger, M., Kohler, M., Legain, D., Pigeon, G., Piguet, B., Schüttemeyer, D., Traulle, O., 2011. Surface energy balance and turbulence network during the Convective and Orographically-induced Precipitation Study (COPS). Quarterly Journal of the Royal Meteorological Society, 137: 57–69.

Zhou, D., Eigenmann, R., Babel, W., Foken, T., Ma, Y., 2011. Study of near-ground free convection conditions at Nam Co station on the Tibetan Plateau. Theoretical and Applied Climatology, 105: 217–228.

Submitted manuscript:

Brötz, B., Eigenmann, R., Dörnbrack, A., Foken, T., Wirth, V., 2013. Early-morning flow transition in a valley in low-mountain terrain. Boundary-Layer Meteorology, submitted.

Other publications not included in this thesis:

In peer-reviewed journals:

Kalthoff, N., Kohler, M., Barthlott, C., Adler, B., Mobbs, S.D., Corsmeier, U., Träumner, K., Foken, T., Eigenmann, R., Krauss, L., Khodayar, S., Di Girolamo, P., 2011. The dependence of convection-related parameters on surface and boundary-layer conditions over complex terrain. Quarterly Journal of the Royal Meteorological Society, 137: 70–80.

Wulfmeyer, V., Behrendt, A., Kottmeier, C., Corsmeier, U., Barthlott, C., Craig, G.C., Hagen, M., Althausen, D., Aoshima, F., Arpagaus, M., Bauer, H.-S., Bennett, L., Blyth, A., Brandau, C., Champollion, C., Crewell, S., Dick, G., Di Girolamo, P., Dorninger, M., Dufournet, Y., Eigenmann, R., Engelmann, R., Flamant, C., Foken, T., Gorgas, T., Grzeschik, M., Handwerker, J., Hauck, C., Höller, H., Junkermann, W., Kalthoff, N., Kiemle, C., Klink, S., König, M., Krauss, L., Long, C.N., Madonna, F., Mobbs, S., Neininger, B., Pal, S., Peters, G., Pigeon, G., Richard, E., Rotach, M.W., Russchenberg, H., Schwitalla, T., Smith, V., Steinacker, R., Trentmann, J., Turner, D.D., van Baelen, J., Vogt, S., Volkert, H., Weckwerth, T., Wernli, H., Wieser, A., Wirth, M., 2011. The Convective and Orographically-induced Precipitation Study (COPS): the scientific strategy, the field phase, and research highlights. Quarterly Journal of the Royal Meteorological Society, 137: 3–30.

In non-reviewed journals:

Metzger, S., Foken, T., Eigenmann, R., Kurtz, W., Serafimovich, A., Siebicke, L., Olesch, J., Staudt, K., Lüers, J., 2007. COPS experiment. Convective and orographically induced precipitation study. 01 June 2007 - 31 August 2007, Documentation. Work Report, University of Bayreuth, Dept. Micrometeorology, ISSN 1614-8916, 34, 72 pp.

Data sets at the World Data Center for Climate (WDCC) in Hamburg, Germany:

Dorninger, M., Eigenmann, R., Foken, T., 2012. cops_nebt_uv_flux: Surface layer scintillometer data from COPS energy balance network station run by University of Vienna during COPS 2007. World Data Center for Climate. DOI:10.1594/WDCC/cops_nebt_uv_flux.
http://dx.doi.org/10.1594/WDCC/cops_nebt_uv_flux

Eigenmann, R., Foken, T., 2012. cops_nebt_ubt_flux: Eddy-covariance turbulence data from COPS energy balance and turbulence network stations run by University of Bayreuth during COPS 2007. World Data Center for Climate. DOI:10.1594/WDCC/cops_nebt_ubt_flux.
http://dx.doi.org/10.1594/WDCC/cops_nebt_ubt_flux

Eigenmann, R., Foken, T., 2012. cops_nebt_ubt_mast: Profile data of wind speed, temperature and water vapor pressure at profile mast run by University of Bayreuth during COPS 2007. World Data Center for Climate. DOI:10.1594/WDCC/cops_nebt_ubt_mast.
http://dx.doi.org/10.1594/WDCC/cops_nebt_ubt_mast

Eigenmann, R., Foken, T., 2012. cops_nebt_ubt_met: Radiation and soil measurement data from COPS energy network stations run by University of Bayreuth during COPS 2007. World Data Center for Climate. DOI:10.1594/WDCC/cops_nebt_ubt_met.
http://dx.doi.org/10.1594/WDCC/cops_nebt_ubt_met

Eigenmann, R., Foken, T., 2012. cops_nsod_ubt: wind data from sodar-RASS run by University of Bayreuth during COPS 2007. World Data Center for Climate. DOI:10.1594/WDCC/cops_nsod_ubt.
http://dx.doi.org/10.1594/WDCC/cops_nsod_ubt

Kalthoff, N., Eigenmann, R., Foken, T., 2011. cops_nebt_imk_flux: Eddy-covariance turbulence data from COPS energy balance and turbulence network stations run by FZK/IMK-TRO during COPS 2007. World Data Center for Climate. DOI:10.1594/WDCC/cops_nebt_imk_flux.
http://dx.doi.org/10.1594/WDCC/cops_nebt_imk_flux

Kalthoff, N., Eigenmann, R., Foken, T., 2011. cops_nebt_imk_met: meteorological data from COPS energy balance and turbulence network run by FZK/IMK-TRO

during COPS 2007. World Data Center for Climate. DOI:10.1594/WDCC/cops_nebt_imk_met.
http://dx.doi.org/10.1594/WDCC/cops_nebt_imk_met

Pigeon, G., Eigenmann, R., Foken, T., Legain, D., Piguet, B., Traulle, O., 2012. cops_nebt_mf_flux: Eddy-covariance turbulence data from COPS energy balance and turbulence network stations run by Meteo-France/CNRM during COPS 2007. World Data Center for Climate. DOI:10.1594/WDCC/cops_nebt_mf_flux.
http://dx.doi.org/10.1594/WDCC/cops_nebt_mf_flux

Schüttemeyer, D., Eigenmann, R., Foken, T., 2012. cops_nebt_ubn_flux: Eddy-covariance turbulence data from COPS energy balance and turbulence network station run by University of Bonn during COPS 2007. World Data Center for Climate. DOI:10.1594/WDCC/cops_nebt_ubn_flux.
http://dx.doi.org/10.1594/WDCC/cops_nebt_ubn_flux

Acknowledgements

I would like to thank all persons who contributed to the success of this work and who supported me during the last years. Particularly, I would like to acknowledge:

- My supervisor Prof. Dr. Thomas Foken for his guidance through the progress of this thesis giving me continuous support and advice in manifold ways.
- B. Brötz (Institute of Atmospheric Physics, German Aerospace Center) for many valuable discussions on my work, especially on the first manuscript, and for the intensive cooperation during the preparation of the fourth manuscript.
- Prof. Dr. V. Wirth (Institute for Atmospheric Physics, University of Mainz) and Dr. A. Dörnbrack (Institute of Atmospheric Physics, German Aerospace Center) for their contributions to the fourth manuscript.
- All other co-authors of the publications for their individual contributions to the success of the corresponding manuscripts, especially Dr. D. Zhou (Centre for Monsoon System Research, Institute of Atmospheric Physics, Chinese Academy of Sciences), Dr. N. Kalthoff and M. Kohler (Institute for Meteorology and Climate Research, Karlsruhe Institute of Technology), Dr. D. Schüttemeyer (Meteorological Institute, University of Bonn), Ass.-Prof. Mag. Dr. M. Dorninger (Department of Meteorology and Geophysics, University of Vienna) and O. Traulle, D. Legain, Dr. G. Pigeon, Dr. B. Piguet (CNRM-GAME, Météo France).
- S. Metzger (NEON, USA) and the involved staff of the Department of Micrometeorology for their great work during the COPS field campaign 2007.
- All colleagues of the Department of Micrometeorology, especially W. Babel for his help on the data analysis for the first and third manuscript.
- My family, my friends and Henrietta.

This thesis was embedded within the framework of the Priority Program SPP 1167 “Quantitative Precipitation Forecast PQP (Praecipitationis Quantitativae Predictio)” funded by the German Science Foundation (DFG), subproject SALVE (Fo 226/19-1, Fo 226/23-1).

Summary

The impact of complex terrain on the land-atmosphere exchange is investigated in this thesis. Here, free convection, a very effective vertical transport mechanism as turbulence is predominantly driven by buoyant forces, is explicitly addressed. Recently, it was shown for certain situations over complex terrain that free convective injections of surface layer air masses into the atmospheric boundary layer (ABL) can alter the ABL properties significantly. This study aims at the general identification and description of such situations of near-ground free convection conditions (FCCs) over complex terrain. For this purpose, data obtained during the COPS (Convective and Orographically induced Precipitation Study) field campaign in summer 2007 were used. Within this project, several surface flux measurement stations were installed, mainly in valleys and on mountaintops of the Black Forest, southwestern Germany. Turbulent fluxes were calculated with the eddy-covariance (EC) method and were used to detect FCCs with the help of a stability parameter. The flux measurements were further combined with ABL profiling measurements (Sodar/RASS) and a large-eddy simulation (LES) model in order to investigate the impact of FCCs on ABL properties. The effect of complex terrain on the energy balance closure and on spatial and temporal flux differences was also studied with these flux data.

FCCs were detected on about 25% of the days during the three month COPS experiment. In situations of weak synoptic forcing, thermally driven orographic (e.g. valley winds) or local wind systems developed over the complex terrain due to heating differences. During the adaption of these wind systems to changing heating differences (e.g. during the reversal of the valley wind from down- to up-valley winds in the morning), the horizontal wind vanished. If, at the same time, the buoyancy flux was positive and enhanced, buoyant forces exceeded the usually prevailing shear forces in the surface layer and FCCs were detected. Moreover, it was demonstrated that FCCs are not restricted to the COPS region. Also, a data set of Nam Co station on the Tibetan Plateau showed FCCs during the reversal of a thermally driven land-lake breeze. However, at this high-altitude site, FCCs were more often detected in the afternoon compared to the COPS region due to the frequent change of heating differences during cloud cover periods.

The Sodar/RASS as well as the LES model showed the presence of coherent updraft structures in the developing early-morning convective boundary layer (CBL) in the

Kinzig valley (Black Forest) during FCCs. Spectral analysis of the EC data in these situations indicated the existence of large-eddy turbulent scales – typical for thermal updrafts in the CBL – already close to the ground. An ensemble and time mean analysis of the simulated flow field in the valley further confirmed that the Sodar/RASS was located preferably in an updraft region during FCCs. In a CBL over flat homogeneous terrain, the locations of convective structures would occur randomly. However, over the complex orography of the Kinzig valley, the updraft structures were found to develop in quasi-stationary patterns at specific locations relative to the surrounding mountain ridges. The model further showed that the flux through the valley boundary layer is mainly determined by the flux within these coherent updrafts. In combination with the Sodar/RASS observations, the model also showed that these updrafts deeply penetrated into the stably stratified valley boundary layer up to approximately the height of the surrounding mountains leading to an effective upward counter-gradient transport of surface layer air mass properties during FCCs.

The analysis of the turbulent fluxes at the different COPS sites showed that the flux values were strongly determined by varying land surface characteristics. Also an increase of the Bowen ratio with increasing altitude could be detected. These findings are in accordance with former studies in this area. As expected, the energy balance was found to be unclosed on average during the entire COPS period, with values of the residual typical for heterogeneous landscapes. However, regarding only the periods with FCCs, no residual occurred on average. This is due to the fact that the landscape heterogeneity is of minor importance in case of the more vertical oriented exchange regime during FCCs, so that missing advective flux components became strongly reduced in these situations. Moreover, it was found that in comparable periods with no FCCs, flux components were missing with exactly the proportions of the buoyancy flux ratio, thus suggesting a correction of the energy balance according to the buoyancy flux ratio approach. These results support recent publications on the energy balance closure problem.

Zusammenfassung

In der vorliegenden Arbeit wird die Auswirkung von komplexem Gelände auf den Austausch zwischen Land und Atmosphäre untersucht. Hierbei wird freie Konvektion, ein sehr effektiver vertikaler Transportmechanismus, da die Turbulenz hauptsächlich durch Auftriebskräfte gesteuert wird, ausführlich behandelt. Kürzlich wurde für bestimmte Situationen in komplexem Gelände gezeigt, dass der Eintrag bodennaher Luftmassen durch freie Konvektion in die atmosphärische Grenzschicht (ABL) zu einer erheblichen Änderung derer Eigenschaften führen kann. Diese Arbeit strebt eine generelle Identifizierung und Beschreibung solcher bodennaher Bedingungen freier Konvektion (FCCs) an. Dazu wurden Daten der COPS (Convective and Orographically induced Precipitation Study) Feldkampagne des Sommers 2007 verwendet. Im Rahmen dieses Projektes wurden mehrere Flussmessstationen, überwiegend in Tälern und auf Gipfeln des Schwarzwaldes in Süddeutschland, aufgebaut. Turbulente Flüsse wurden mit der Eddy-Kovarianz (EC) Methode berechnet und genutzt, um mit einem Stabilitätsparameter FCCs zu detektieren. Die Flussmessungen wurden überdies mit ABL Profilmessungen (Sodar/RASS) und einer Grobstruktursimulation (LES) verbunden, um die Auswirkung von FCCs auf die ABL zu untersuchen. Der Effekt komplexen Geländes auf die Energiebilanzschließung und auf räumliche sowie zeitliche Flussunterschiede wurde mit Hilfe dieser Flussdaten ebenfalls analysiert.

FCCs wurden an etwa 25% der Tage des dreimonatigen COPS Experimentes festgestellt. In Situationen schwachen synoptischen Forcings entwickelten sich über dem komplexen Gelände aufgrund von Wärmeunterschieden thermisch getriebene orographische (z.B. Talwinde) oder lokale Windsysteme. Während der Anpassung dieser Windsysteme an die sich ändernden Wärmeunterschiede (z.B. bei der Umkehr des Talwindsystems von Talab- zu Talaufwinden am Morgen), ging der Horizontalwind gegen Null. Falls zur selben Zeit der Auftriebsstrom positiv und erhöht war, übertrafen die Auftriebskräfte die üblicherweise in der Bodenschicht vorherrschenden Scherkräfte und FCCs wurden detektiert. Ferner wurde gezeigt, dass das Vorkommen von FCCs nicht auf die COPS Region beschränkt ist. Auch ein Datensatz der Nam Co Station auf der Tibetischen Hochebene wies FCCs während der Umkehrphase einer thermisch getriebenen Land-Seewind-Zirkulation auf. Jedoch wurden an diesem Höhenstandort im Vergleich zur COPS Region aufgrund häufiger Veränderungen der Wärmeunterschiede während Phasen mit Wolkenbedeckung FCCs vermehrt am Nachmittag festgestellt.

Das Sodar/RASS sowie die LES zeigten die Präsenz von kohärenten Aufwindstrukturen in der morgendlichen konvektiven Grenzschicht (CBL) im Kinzigtal (Schwarzwald) während FCCs. Eine Spektralanalyse der EC Daten in diesen Situationen hat gezeigt, dass großskalige Turbulenzstrukturen, typisch für thermische Aufwinde in der CBL, bereits bodennah auftraten. Eine Ensemble und Zeitmittelungsanalyse des simulierten Talströmungsfeldes bestätigte außerdem, dass sich das Sodar/RASS bei FCCs bevorzugt in einer Aufwindregion befand. In einer CBL über flachem, homogenem Gelände würden die konvektiven Strukturen zufällig auftreten. Über dem komplexen Gelände des Kinzigtals bildeten sich die Aufwindstrukturen jedoch in quasi-stationären Mustern an bestimmten Stellen relativ zu den umliegenden Höhenrücken aus. Die LES zeigte zudem, dass der Fluss durch die Talgrenzschicht hauptsächlich durch den Fluss in den Aufwindstrukturen bestimmt wird. Zusammen mit den Sodar/RASS Beobachtungen zeigte die LES auch, dass diese Aufwindstrukturen tief in die stabil geschichtete Talgrenzschicht bis zu Höhen von etwa den umliegenden Bergen eindrangen, und dadurch bei FCCs zu einem effektiven aufwärts und gegen den Gradienten gerichteten Transport von bodennahen Luftmassen führten.

Die Analyse der turbulenten Flüsse an den unterschiedlichen COPS Standorten ergab, dass die Flüsse stark durch variierende Eigenschaften der Geländeoberfläche bestimmt wurden. Auch konnte ein Anstieg des Bowen Verhältnisses mit zunehmender Höhe festgestellt werden. Diese Ergebnisse stimmen mit früheren Untersuchungen in diesem Gebiet überein. Wie erwartet wurde im Mittel bei Betrachtung des gesamten COPS Zeitraumes eine ungeschlossene Energiebilanz mit Werten des Residuums typisch für heterogenes Gelände gefunden. Dagegen trat bei ausschließlicher Betrachtung der Perioden mit FCCs im Mittel kein Residuum auf. Dies liegt darin begründet, dass die Landschaftsheterogenität im Falle des eher vertikal orientierten Austauschregimes während FCCs von geringerer Bedeutung ist, so dass fehlende Flussanteile in diesen Situationen stark reduziert wurden. Außerdem wurde in vergleichbaren Perioden ohne FCCs festgestellt, dass Flussanteile genau mit dem Verhältnis des Auftriebsstroms fehlten, was eine Korrektur der Energiebilanz gemäß dem Auftriebsstromverhältnis nahe legt. Diese Ergebnisse stützen kürzlich publizierte Befunde zur Energiebilanz-schließungsproblematik.

1 Introduction

Altering land surface properties, such as vegetation, roughness, albedo, emissivity and soil properties, and orography, e.g. valleys and mountains, are typical features of complex terrain. Heterogeneities of surface properties can lead to spatial variations of turbulent fluxes (e.g. Mahrt et al., 1994; Lyons and Halldin, 2004; LeMone et al., 2007) and thus to an impact on boundary layer dynamics (e.g. Mahrt and Ek, 1993; Sun et al., 1998; Brunsell et al., 2011). Different temporal and spatial scales can be affected (e.g. Betts et al., 1996). Many experimental studies, e.g. the LITFASS-2003 experiment (Beyrich and Mengelkamp, 2006), were carried out in the last twenty years in order to study the influence of surface heterogeneities on boundary layer conditions (e.g. Maronga and Raasch, 2012). Besides circulations induced by differential terrain heating (Pielke and Segal, 1986; Segal and Arritt, 1992), thermally induced orographic wind systems, e.g. slope and valley winds (Defant, 1949; Whiteman, 1990; Whiteman, 2000; Zardi and Whiteman, 2013), strongly influence the turbulent fluxes of heat, moisture and momentum through the atmospheric boundary layer (ABL). The turbulent exchange processes, e.g. in a steep Alpine valley, were shown to strongly depend on orography and stratification in a mountainous boundary layer (e.g. Weigel et al., 2007; Rotach et al., 2008). In the past, much research was done to determine the scale of surface heterogeneity λ relative to the boundary layer height z_i necessary to have a significant effect on ABL characteristics. In addition to theoretical (e.g. Mahrt, 2000) and experimental (e.g. Strunin et al., 2004; Bange et al., 2006) investigations, numerical studies with large-eddy simulation (LES) models (e.g. Hadfield et al., 1991, 1992; Avissar and Schmidt, 1998; Baidya Roy and Avissar, 2000; Gopalakrishnan et al., 2000; Gopalakrishnan and Avissar, 2000; Letzel and Raasch, 2003; Patton et al., 2005; Couralt et al., 2007; Huang et al., 2009; Huang and Margulis, 2009) are a widely used tool to study the influence of surface heterogeneity on the ABL. Small-scale surface heterogeneities ($\lambda/z_i \approx 0.27-1.2$) were studied with LES by Shen and Leclerc (1995) and Raasch and Harbusch (2001). These authors observed that the most vigorous vertical energy transport in a convective boundary layer (CBL) is produced when $\lambda \approx z_i$. For very small patches ($\lambda << z_i$) it is recognized by researchers that these heterogeneities are blended and above a certain height level a uniform and area-averaged flux can be assumed. This theory is referred to as the concept of blending

height (Mason, 1988). However, in the case of very low wind speeds (free convection regime), even patch lengths considerably smaller than the boundary layer height ($\lambda < z_i$, $\lambda \approx 250$ m) are sufficient to affect the turbulence structure of the CBL (Shen and Leclerc, 1994; 1995).

Free convection is a common phenomenon in the mixed layer of a CBL on clear sunny days with light wind speeds. It prevails when the part of turbulence kinetic energy (TKE) created by buoyancy dominates over that created by shear (e.g. Stull, 1988). Vertical motion is then primarily induced by density differences within the fluid. Coherent vertical structures (e.g. plumes or thermal updrafts) exist in the CBL during free convection leading to an effective vertical transport. The present thesis is focused on specific situations in which free convection is already observed over certain patches of land use very close to the ground (in the surface layer), where normally shear processes dominate. Air masses close to the surface show different characteristics than air masses further up in the boundary layer, e.g., are humid or have a characteristic chemical composition. These characteristics can then be transported upwards very effectively by free convection which starts already close to the ground. In the surface layer, free convection can be detected with the help of the stability parameter ζ for values of $\zeta < -1$ (e.g. Webb, 1962; Foken, 2008a). ζ is the quotient of the height *z* and the Obukhov length *L* (Obukhov, 1946):

$$\zeta = \frac{z}{L} = -\frac{z\,\kappa\,g\,\left(\overline{w'\theta_v'}\right)_0}{\overline{\theta_v}\,u_*^3} \tag{1}$$

Here, u_* is the friction velocity, g the acceleration due to gravity, $\overline{\theta_v}$ the mean virtual potential temperature, $\left(\overline{w'\theta_v'}\right)_0$ the buoyancy flux at the surface and κ the Kármán constant ($\kappa \approx 0.4$). According to Businger et al. (1971), ζ is related approximately linearly to the Richardson number for unstable conditions ($\zeta < 0$). The flux Richardson number R_f is defined as the quotient of the buoyancy term *B* to the shear term *S* of the TKE budget equation (e.g. Stull, 1988; Garratt, 1992):

$$R_f = B/S = \frac{g}{\overline{\theta_v}}\,\overline{w'\theta_v'} \Bigg/ \left(\overline{u'w'}\,\frac{\partial \overline{u}}{\partial z}\right) \tag{2}$$

Regarding a coordinate system aligned with the mean wind, the shear term *S* is the

product of the momentum flux $\overline{u'w'}$ and the wind shear $\partial\bar{u}/\partial z$. With the knowledge of $\zeta \approx R_f$ in an unstable surface layer, $|L|$ can be interpreted as the height above the surface at which buoyant production first dominates over mechanical production of TKE (e.g. Stull, 1988). In other words, $\zeta < -1$ means that buoyancy-driven turbulence dominates over shear-generated turbulence for $|L| < z$. Thus, the requirement of $\zeta < -1$ is used in this thesis (Eigenmann et al., 2009, Appendix B; Eigenmann et al., 2011, Appendix C; Zhou et al., 2011, Appendix D; Brötz et al., 2013, Appendix E) to detect situations of near-ground free convection conditions (FCCs). Regarding Eq. (1), free convection is achieved by the conditions $u_* \to 0$ and $\left(\overline{w'\theta_v'}\right)_0 > 0$. The surface turbulent fluxes, u_* and $\left(\overline{w'\theta_v'}\right)_0$, can easily be measured by e.g. the eddy-covariance (EC) method (e.g. Swinbank, 1951; Foken et al., 2012).

Recently, Mayer et al. (2008) observed the free convective coherent vertical transport of surface layer trace gases into upper regions of the boundary layer in the Alpine foreland during early-morning situations of low wind speed. The ceasing wind speeds could often be related to the onset of a mesoscale circulation system called Alpine pumping (see Lugauer and Winkler, 2005). During the period of changing wind direction, the horizontal wind speed vanished. The trace gases, transported upwards vertically by free convection, were then translocated advectively with the mean wind towards a mountain summit and altered the trace gas observations there significantly. Situations of near-ground free convection can also be seen in the stability and data quality analysis of EC data obtained in an Alpine valley in Switzerland (see Hiller et al., 2008), although these authors did not address these events. Following these studies, the main objective of this thesis is to investigate in general the occurrence of FCCs over complex terrain and its impact on ABL characteristics. For this purpose, data of the three month field campaign of the Convective and Orographically induced Precipitation Study (COPS, e.g. Wulfmeyer et al., 2011) in summer 2007 were mainly used. The experiment took place over a heterogeneous low-mountain region typical for Central Europe, i.e. the Vosges Mountains and the Black Forest. These low-mountain ranges are well known to induce thermally driven orographic wind systems (e.g. Kossmann and Fiedler, 2000; Kalthoff et al., 2000; Barthlott et al., 2006; Meißner et al., 2007), which can be expected to trigger free convective situations similar to Mayer et al. (2008).

Complex terrain also has an impact on turbulence flux measurements, e.g. on the EC

measurements as used in this thesis. It is a well known phenomenon that, in micrometeorological field experiments conducted over complex terrain, the energy balance cannot be closed (e.g. Oncley et al., 2007; Foken, 2008b). Theoretically, the input of energy at the surface by net radiation ($-Q_S^*$) must balance the sum of the sensible (Q_H), latent (Q_E), ground (Q_G) and storage heat flux (ΔQ_S):

$$-Q_S^* = Q_H + Q_E + Q_G + \Delta Q_S \tag{3}$$

The sum of Q_H and Q_E was found to only amount to about 70–90% of the available energy ($-Q_S^*-Q_G-\Delta Q_S$) at the surface (e.g. Aubinet et al., 2000; Wilson et al., 2002; Mauder et al., 2006; Franssen et al., 2010). Contrary to that, in landscapes without heterogeneities, a closure of the energy balance was reported (e.g. Heusinkveld et al., 2004; Mauder et al., 2007; Foken, 2008b). For that reason, it is concluded that the landscape heterogeneity plays an important role for the non-closure of the energy balance. It is recognized that the missing flux components are transported within large-scale eddies caused by the landscape heterogeneity (e.g. Foken, 2008b, Foken et al., 2010; 2011). These large-scale eddies cannot be captured by a single-point EC station, as they are organized above the EC tower, are quasi-stationary in space or have a longer wavelength than the usual 30 min averaging period of the EC fluxes. Indeed, strong indications exist that the residual over complex terrain is transported within advective and low-frequency flux contributions (e.g. Sakai et al., 2001; Finnigan, 2003; Malhi et al., 2004; Foken et al., 2006; Mauder and Foken, 2006) and within quasi-stationary circulations (e.g. Kanda et al., 2004; Inagaki et al., 2006; Steinfeld et al., 2007; Huang et al., 2008; Foken et al., 2010; Stoy et al., 2013). These secondary circulations are mainly buoyancy-driven due to differences in thermal heating of the land surface. Consequently, to partition the residual according to the buoyancy flux ratio, as proposed by Charuchittipan et al. (2013), seems to be an appropriate approach to close the energy balance.

Based on the theoretical background introduced above, the overarching goal of this thesis is the investigation and description of FCCs detected at the height of EC measurements (≈ 2 m) over complex terrain. Major points of interest are the identification of the (micro-) meteorological and synoptical conditions which lead to these free convective events, the frequency and time of their occurrence and their

impact on boundary layer properties. Moreover, this thesis aims to investigate the impact of complex terrain on turbulence flux measurements and on the energy balance closure.

Regarding the manuscripts attached to this thesis, Eigenmann et al. (2009, Appendix B) introduces the method for the detection of FCCs with EC flux measurements and investigates their occurrence using data obtained in the Kinzig valley in the Black Forest during the COPS experiment. This study also addresses the impact of FCCs on ABL properties by analyzing ABL profiling measurements in the Kinzig valley and studying the spectral characteristics of the turbulence during FCCs.

Within the COPS field campaign, an energy balance network was operated (see Sect. 2.1). This network consisted of sixteen individual EC stations distributed over the complex terrain of the COPS region. Different types of land use and different topographical features (valleys and mountaintops) were probed. Energy balance measurements in the COPS region were already carried out within the REKLIP project (e.g. Wenzel et al., 1997), although this project had a more climatological focus. These earlier investigations revealed a significant dependence of the energy balance components on the altitude and on the land-use types in the COPS area (Kalthoff et al., 1999; Wenzel and Kalthoff et al., 2000). Thus, the study of Eigenmann et al. (2011, Appendix C) aims at comparing the flux measurements obtained during COPS with the results of the REKLIP project. Moreover, this study calculates and discusses the energy balance closure at the COPS stations with regard to the surrounding heterogeneous terrain. Also, the occurrence of FCCs within the entire COPS region in relation to different land-use types and topographical features is investigated.

In order to demonstrate that FCCs can also be detected within different settings of complex terrain besides the study area of COPS, a data set of Nam Co station on the Tibetan Plateau (see Sect. 2.2) is further investigated in this thesis (see Zhou et al., 2011, Appendix D). The dominating land-use type (Alpine steppe) at Nam Co station is rather homogeneous and the terrain in the immediate vicinity is flat. However, heterogeneity in this study is given by a land-lake surface and by frequently changing heating differences during cloud cover periods. These surface heating differences during cloud cover periods are enhanced on the Tibetan Plateau compared to lowland sites as diffuse radiation components are strongly reduced at high altitudes. A numerical simulation of the ABL flow characteristics at Nam Co station by Lu et al. (2008) recently indicated the occurrence of a thermally driven land-lake circulation system.

A further main objective of this thesis is to adapt a LES model (see Sect. 2.3) to the heterogeneous terrain of a segment of the Kinzig valley using COPS data (Brötz et al., 2013, Appendix E). The aim of the model is to simulate the exchange processes in the ABL during the observed FCCs. Especially, the organisation of turbulence in the convective mixed layer, crucial for further vertical transport of the convectively released surface layer air masses, is studied. Therefore, simulations of the flow transition from the free covective low wind speed situation to the following period of along-valley wind are performed. An initial stable stratification in the early-morning hours is considered. The model provides the opportunity to estimate how far surface layer air masses are transported upwards within convective structures during the observed FCCs.

2 Experimental data sets and the LES model

The results presented in the studies of Eigenmann et al. (2009, Appendix B; 2011, Appendix C) are based on data sets obtained within the framework of the COPS project (Sect. 2.1). The publication of Zhou et al. (2011, Appendix D) uses a seven month data set of measurements at Nam Co station on the Tibetan Plateau provided by the project partners involved in this specific study (Sect. 2.2). In the LES study of Brötz et al. (2013, Appendix E), data of the COPS project were used as boundary conditions of the model (Sect. 2.3).

2.1 The COPS field campaign

The Convective and Orographically induced Precipitation Study (COPS) was an international field campaign (Wulfmeyer et al., 2008) embedded within the German 6-year Priority Program SPP 1167 “Quantitative Precipitation Forecast PQP (Praecipitationis Quantitativae Predictio)” of the German Science Foundation (DFG). The field campaign was carried out from 1 June to 31 August 2007 in a low-mountain area in southwestern Germany and eastern France covering the Vosges Mountains, the Upper Rhine valley, the Black Forest and the Swabian Mountains. It was organized into different Intensive Observation Periods (IOPs), which observed specific convective situations with a synergy of meteorological instruments in order to identify the physical and chemical processes responsible for the deficiencies in Quantitative Precipitation Forecast (QPF) in low-mountain regions (Wulfmeyer et al., 2011). The investigation of the initiation of (moist) convection was a main part of the research efforts (e.g. Aoshima et al., 2008; Kottmeier et al., 2008; Kalthoff et al., 2009, 2011; Behrendt et al., 2011; Bennett et al., 2011, Corsmeier et al., 2011). During COPS, a large number of state-of-the-art meteorological instrumentation, combining a synergy of in situ and remote-sensing systems (e.g. radar and lidar systems), was operated (see Wulfmeyer et al., 2008, 2011). Measurements were obtained from networks (see Sect. 2.1.1; Eigenmann et al., 2011, Appendix C; Hauck et al., 2011), aircraft (e.g. Kiemle et al., 2011) and satellites and were intensified at specific sites (supersites). In the following, only the data sets of the COPS campaign used in this thesis will be introduced.

2.1.1 Surface energy balance and turbulence network

Under weak synoptic forcing, spatial heterogeneities of surface characteristics result in heterogeneities of turbulent fluxes of heat and moisture into the ABL and hence may determine if and where convection is initiated (e.g. Kottmeier et al., 2008; Kalthoff et al., 2011). Moreover, land surface exchange processes modulate thermally induced orographic flow systems, which in turn influence the initiation of convection (e.g. Barthlott et al., 2006; Meißner et al., 2007, Kalthoff et al., 2009). Therefore, a surface energy balance and turbulence network (Eigenmann et al., 2011, Appendix C) was set up during COPS. Data of high-quality surface flux measurements as well as standard surface micrometeorological measurements was stored at the World Data Center for Climate (WDCC) in Hamburg, Germany. This provided data is further used within the COPS community for the forcing and validation of the applied mesoscale models.

The surface network consisted of sixteen stations operated by five collaborating institutes (Table 1). The EC measuring technique was applied in order to provide surface turbulent flux data of momentum, sensible and latent heat, expect at one site where scintillometer measurements were used. Latent heat flux was only measured at nine sites. At most of the sites, the remaining components of the surface energy balance were obtained by additional soil (Hauck et al., 2011) and radiation measurements. The instrumentation of the soil and radiation measurements is listed in Table V in Eigenmann et al. (2011, Appendix C). Heterogeneity in the COPS region exists due to orography and due to a patchy land-use structure. Therefore, measuring sites included locations in the valleys (Murg, Kinzig and Rench valley) and on mountaintops (Hornisgrinde, Igelsberg) of the Black Forest, locations in the Upper Rhine valley and locations on the eastern edge of the Black Forest. Moreover, the turbulent fluxes were measured over different types of land use, mainly grassland and agricultural fields. Table 1 summarizes all above-mentioned information. At some of these stations, Sodar/RASS instruments were also operated for profiling wind components and virtual temperature. In this thesis, only the Sodar/RASS system installed in the Kinzig valley is used (Eigenmann et al., 2009, Appendix B; Brötz et al., 2013, Appendix E). More details about the experimental setup can be looked up in Metzger et al. (2007) and Eigenmann et al. (2009, Appendix B; 2011, Appendix C).

Tabelle 1: Turbulence measuring sites of the COPS field campaign. The column 'Code' abbreviates the responsible institute: UBT (University of Bayreuth), IMK (Karlsruhe Institute of Technology), MF (Météo France), UV (University of Vienna), UBN (University of Bonn). Also given are the coordinates and the altitude above sea level (a.s.l.) of the sites as well as the applied instruments of the EC system (sonic anemometer, hygrometer - CSAT3: sonic anemometer by Campbell Scientific Inc., USA; USA-1: sonic anemometer by METEK GmbH, Germany; Solent R1012: sonic anemometer by Gill Instruments Ltd., UK; Young 81000: sonic anemometer by R. M. Young Company, USA; Solent HS: sonic anemometer by Gill Instruments Ltd., UK; KH20: krypton hygrometer by Campbell Scientific Inc., USA; LI-7500: open-path CO_2/H_2O gas analyzer by LI-COR Biosciences, USA). The station UV1 used the Optical Energy Balance Measurement System (OEBMS1) with a Scintillometer SLS20 system by Scintec AG, Germany. The column 'Land use' indicates the target land-use type: grassland (G), maize (M), strawberry (S), fallow (F) and wheat (W). The column 'Location' sorts the stations by their location: valley (V) sites, mountaintop (T) sites, Upper Rhine (R) valley sites and sites in the lee (L) of the Black Forest. Table taken from Eigenmann et al. (2011, Appendix C), modified.

Code	Site	Coordinates (lat., long.)	Altitude	Land use	Sonic anemometer	Hygrometer	Location
UBT1	Fußbach I *	48° 22′ 7.82″ 8° 1′ 21.17″	178	M	CSAT3	LI-7500	V
UBT2	Fußbach II	48° 22′ 0.88″, 8° 1′ 16.68″	180	F	USA-1	-	V
UBT3	Fischerbach *	48° 16′ 57.40″, 8° 7′ 56.28″	226	G	CSAT3	KH20	V
UBT4	Hagenbuch *	48° 16′ 54.59″, 8° 12′ 16.81″	245	G	CSAT3	LI-7500	V
IMK1	Hornisgrinde *	48° 36′ 12.95″, 8° 12′ 4.88″	1158	G	Solent R1012	LI-7500	T
IMK2	Baden Airpark *	48° 46′ 40.51″, 8° 4′ 25.20″	120	G	Solent R1012	LI-7500	R
IMK3	Linkenheim *	49° 8′ 9.24″, 8° 23′ 32.21″	96	W	Young 81000	-	R
IMK4	Sasbach	48° 39′ 4.20″, 8° 5′ 19.53″	133	G	Solent R1012	-	R
IMK5	Oberkirch	48° 31′ 19.15″, 8° 5′ 54.00″	203	S	Solent R1012	-	V
IMK6	Bad Rotenfels	48° 49′ 29.35″, 8° 17′ 30.55″	127	G	Solent R1012	-	V
IMK7	Igelsberg	48° 31′ 40.85″, 8° 25′ 50.35″	770	G	Solent R1012	-	T
IMK8	Burnhaupt	47° 42′ 33.52″, 7° 9′ 16.07″	299	M	Solent R1012	-	R
MF1	Niederrott *	48° 26′ 34.40″, 7° 32′ 38.36″	155	M	Solent HS	LI-7500	R
MF2	Nordfeld *	48° 27′ 58.22″, 7° 32′ 22.35″	156	M	Solent HS	LI-7500	R
UV1	Deckenpfronn *	48° 38′ 21.12″, 8° 49′ 7.86″	574	G	-	-	L
UBN1	Deckenpfronn *	48° 38′ 21.12″, 8° 49′ 7.86″	574	G	CSAT3	LI-7500	L

* Additional measurement of radiation and soil components.

2.1.2 Post-processing and quality control of the turbulence data

In order to receive a data set of high-quality turbulent fluxes, a post-processing and quality control scheme was consistently applied to all turbulence stations. This allows for a high comparability of the surface fluxes between different sites. The scheme included the processing of the turbulence raw data with the software package TK2 (Mauder and Foken, 2004; Mauder et al., 2008) as well as a footprint analysis (Göckede et al., 2004, 2006) and a check for internal boundary layers (Raabe, 1983; Jegede and Foken, 1999) at each site. Detailed information about the individual post-processing and quality control steps and the corresponding references of the applied methods are given in Eigenmann et al. (2011, Appendix C). In this publication, also the application of the data quality control scheme for the selection of data can be looked up. The applied methods are in agreement with the recent recommendations by Foken et al. (2012).

2.2 Data set of Nam Co station

The data set of Nam Co station on the Tibetan Plateau used in the study of Zhou et al. (2011, Appendix D) was provided by the project partners involved in this research and covers a time period of seven month from 21 March 2007 to 21 October 2007. Nam Co station was established by the Institute of Tibetan Plateau Research, Chinese Academy of Sciences in August 2005. Besides standard meteorological, radiation and soil measurements, flux measurements were carried out with an EC system. The turbulence data was processed in a similar way as the COPS data (see Sect. 2.1.2). More details are given in Zhou et al. (2011, Appendix D).

2.3 LES model

In the framework of this thesis, a LES model was run by the DFG project partners to simulate turbulent exchange processes in a segment of the Kinzig valley. The used numerical model was the multiscale geophysical flow solver EULAG (Smolarkiewicz et al., 1997; Prusa et al., 2008). Among the broad range of application documented in literature, EULAG was also successfully applied to the ABL (see Smolarkiewicz et al., 2007; Piotrowski et al., 2009). A realistic topography was implemented into the model. The boundary conditions were chosen according to the COPS observations in the Kinzig valley at Fußbach (see Table 1). A detailed description of the model and the setup of the simulations can be looked up in Brötz et al. (2013, Appendix E). The objectives of the model application in respect of this thesis are formulated in Sect. 1.

3 Results

3.1 Turbulent fluxes and energy balance closure over complex terrain

The COPS data set (see Sect. 2.1.1) allowed an investigation of the influence of land use and topographical location on the turbulent fluxes of sensible and latent heat. Fluxes were found to differ strongly between different types of land use (see Eigenmann et al., 2011, Appendix C). In the afternoon, the oasis effect (e.g. Stull, 1988) caused negative values of sensible heat over highly evapotranspirating land-use types (e.g. maize), while over others (e.g. grassland) this effect did not occur. However, flux differences could also be observed between sites with the same type of land use. This was because of varying surface characteristics even over the same type of land use due to different times of mowing of the grassland sites or due to different stages of the vegetation development in general. It became clear that on a specific day the flux values were strongly determined by different types of land use and surface characteristics, while the effect of altitude (mountaintop or valley) plays a minor role. Interpreting these findings within the scope of the COPS project, which deals with the initiation of convection over complex terrain, it can be concluded that on convective days with weak synoptic forcing, the spatial distribution of land-use characteristics may be decisive if and where convection is initiated. Hot spots of increased transport of heat or moisture into the ABL may form over certain patches of land use. However, it should be mentioned that thermally driven wind systems, which frequently occur in the Black Forest (e.g. Kossmann and Fiedler, 2000; Kalthoff et al., 2000; Barthlott et al., 2006; Meißner et al., 2007) may redistribute the surface-initiated heat and moisture distribution in the ABL and thus may modulate the local forcing of the initiation of convection by surface fluxes.

To study the effect of altitude on flux differences, the fluxes over one type of land use (here: grassland, as most frequently measured) were averaged over the entire COPS period (see Eigenmann et al., 2011, Appendix C). The averaging minimized temporal flux differences due to mowing and vegetation development. Higher Bowen ratios were found at the top of the mountains and lower values in the valleys. This is in accordance with the former findings by Wenzel et al. (1997) and Kalthoff et al. (1999) in the framework of the REKLIP project. These authors also found an increase of the Bowen ratio from the Rhine valley to the top of the Black Forest within a one year data set.

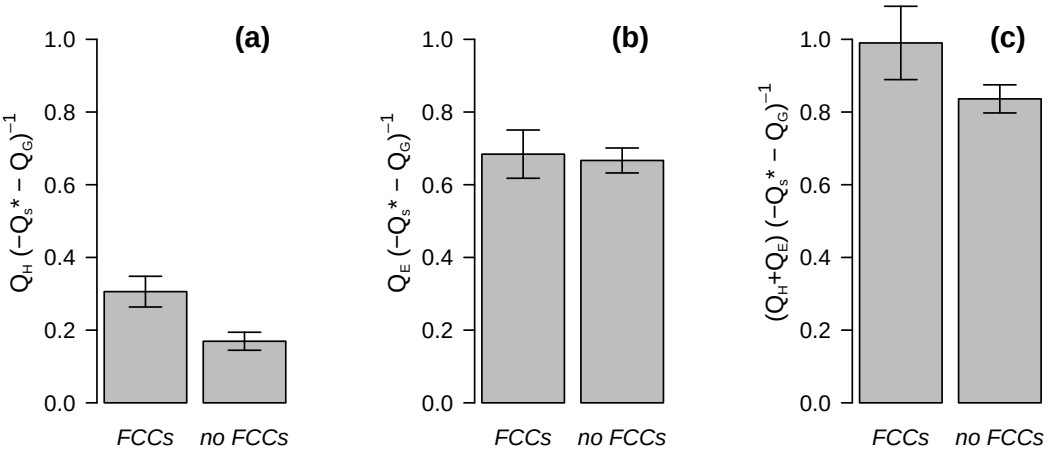

Figure 1: Bar plots of the mean of (a) Q_H, (b) Q_E and (c) the sum of both normalized with the available energy ($-Q^*_S - Q_G$) for the periods with FCCs and for the first 2 hours of the following along-valley wind periods with no FCCs. Averaging is done for the 23 days with FCCs at the Fubach I site in the Kinzig valley (see Fig. 2). Also shown are the 95% confidence intervals which indicate significant differences in the mean values for (a) and (c). The storage heat flux in the upper soil layer is included in Q_G. From Brötz et al. (2013, Appendix E), modified.

A standard investigation of the energy balance closure at the COPS sites was carried out by Eigenmann et al. (2011, Appendix C). The average residual for the entire COPS measurement period at the individual sites was found to range between 17% and 36%. This is comparable to the range reported by e.g. Mauder et al. (2006) for different agricultural sites (residual: 20–30%) during the LITFASS-2003 experiment (Beyrich and Mengelkamp, 2006).

According to the introduction (see Sect. 1), this thesis aimed at the detection and investigation of near-ground free convection conditions (FCCs) with the help of the stability parameter ζ using COPS data. In the Kinzig valley, periods with FCCs in the morning hours were detected on 23 days of the three month COPS field campaign in summer 2007, which means that FCCs occured on about 25% of all days (see also Fig. 2 in Sect. 3.2). For these observed periods with FCCs, the energy balance closure was further investigated. Regarding average conditions during the periods with FCCs, the energy balance was found to be closed (Fig. 1c). However, in a comparable time period in the following along-valley wind period directly after these FCCs (no FCCs), a residual of 16% was found on average (Fig. 1c). This value is close to the average residual of 21% found during the entire COPS campaign at this site (see Eigenmann et al., 2011, Appendix C). According to Fig. 1a and b, the relative flux contributions missing in the period with no FCCs compared to the period with FCCs have exactly the

proportions of the buoyancy flux ratio, which would distribute about 85% of the residual to Q_H and 15% to Q_E for a typical Bowen ratio of about 0.45 in the observed early-morning situations. As such, Fig. 1 supports the suggestion of Charuchittpan et al. (2013) to rather correct the energy balance according to the buoyancy flux ratio approach than with the usually used approach by Twine et al. (2000) which distributes the residual according to the Bowen ratio. The missing flux components in the period with no FCCs are assumed to be transported within buoyancy-driven secondary circulations not captured by the EC measurements (see Sect. 1 and e.g. Foken, 2008b). The transfer of the missing energy into these secondary circulations mainly happens at significant surface heterogeneities which can be found over complex terrain. Advection-dominated processes (also not captured by the EC) lead to the transport of the missing energy to these heterogeneities. As wind speeds are vanishing in the periods with FCCs, the landscape heterogeneity becomes less important so that no missing energy is transferred into secondary circulations and the energy balance is closed in this period. However, landscape heterogeneity becomes more important in the period of along-valley wind (no FCCs) leading to missing advective flux components and thus to the observed residual in this period. However, the recent study of Leuning et al. (2012) gives some hints that advective fluxes alone cannot explain the energy imbalance at half-hourly time scales indicating that the surface energy imbalance problem is still a micrometeorological issue and some further research is necessary.

Moreover, the energy balance closure was investigated in situations of the oasis effect. It was found that, with the onset of the oasis effect shortly after midday, the residual of the investigated maize field strongly increased (see Eigenmann et al., 2011, Appendix C). In this case study, the increase of the residual can also be ascribed to an increase of missing advective flux components during the oasis effect which transport sensible heat towards the evaporating surface.

3.2 Near-ground free convection conditions (FCCs) over complex terrain

The stability parameter ζ is used in this thesis to identify situations of FCCs at the height of EC measurements (≈ 2 m) (see Sect. 1). According to the theory (see Eq. 1), vanishing wind speeds ($u_* \to 0$) and positive buoyancy fluxes ($\left(\overline{w'\theta_v'}\right)_0 > 0$) are the conditions for the occurrence of free convection ($\zeta < -1$), i.e. the dominance of buoyancy versus shear-driven turbulence. A threshold of $\left(\overline{w'\theta_v'}\right)_0 > 20$ Wm^{-2} was introduced into the detection routine (see Zhou et al., 2011, Appendix D), which is defined by the accuracy of EC fluxes nowadays achievable (Mauder et al., 2006). This procedure was applied to the EC turbulence measuring sites in the COPS region, which were set up over different land-use types and at topographically different locations (see Sect. 2.1.1). Two IOPs were selected: IOP 8b (15 July 2007) and IOP 9c (20 July 2007). These IOPs are exemplary for two totally different (and most frequent: see Kottmeier et al., 2008) cases of initiation of convection and are well understood and intensively investigated in the COPS community (e.g. Kalthoff et al., 2009; Barthlott et al., 2010; Corsmeier et al., 2011). IOP 8b was a high pressure situation with high solar radiation, weak synoptic forcing and locally initiated convection, while IOP 9c was characterized by convection near convergence lines or frontal zones. The main findings were (see Eigenmann et al., 2011, Appendix C):

- At all sites in the Kinzig, Rench and Murg valley in the Black Forest, a thermally driven valley wind system, characterized by up-valley winds during the daytime and down-valley winds at night (> 4 ms^{-1}), was observed during IOP 8b. During the reversal of the valley wind system from down- to up-valley winds in the morning, wind speeds vanished in the entire valley (as observed by the Sodar) and FCCs were detected. No FCCs occurred during IOP 9c at these sites.
- At the mountaintop sites (Hornisgrinde, Igelsberg), FCCs were not observed on both IOPs. Enhanced wind speeds at the exposed mountaintops resulted in mainly neutral conditions during the daytime.
- In the Upper Rhine valley, FCCs occured during the entire daytime in IOP 8b. During IOP 9c, FCCs were only detected before the passage of the frontal structure in the morning hours. Vanishing wind speeds were responsible for the detection of FCCs. The reasons for these situations are complex and probably

bound to an interaction of mesoscale flow features and local circulation structures which break down and re-establish.

- FCCs which occured during midday and afternoon in the Upper Rhine valley in IOP 8b were found to depend on the underlying land-use type. FCCs were only detected at stations over grassland, while stations over maize did not show FCCs. That was because of the negative sensible heat flux during the occurrence of the oasis effect over the highly evapotranspirating maize fields (see Sect. 3.1).

Focusing on a certain site – Fußbach I in the Kinzig valley – the occurrence of FCCs during the entire COPS period following the study of Eigenmann et al. (2009, Appendix B) shall now be highlighted (see Fig. 2). The periods with FCCs are indicated by red lines. 23 days with FCCs were identified during the three month field campaign. The FCCs were mainly detected in the morning hours with the mean time of occurrence at 08:15 UTC and a standard deviation of one hour and were strongly related to the times of onset of the up-valley wind direction. The duration of FCCs (mean: 84 min, standard deviation: 57 min) is strongly determined by the period of low wind speeds during the reversal of the valley wind system. A slight adjustment of the times of FCCs to the seasonal change of sunrise is obvious in the individual months indicating that a certain time of insolation is required until the valley wind system is reversed in the morning hours. During the reversal from up- to down-valley winds in the evening, buoyancy fluxes are already very small or even negative so that FCCs were not detected.

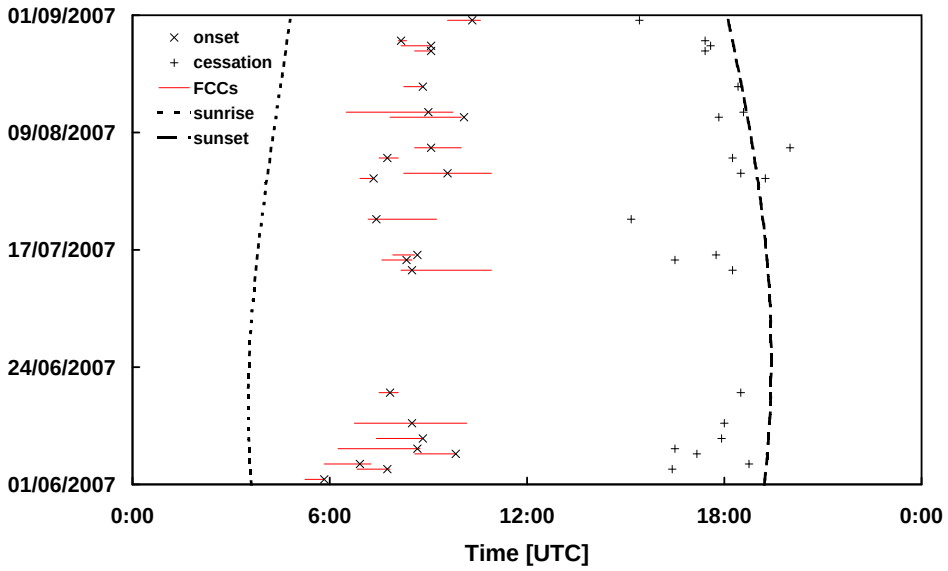

Figure 2: Onset and cessation times of the up-valley wind direction and the corresponding periods with FCCs at the Fußbach I site in the Kinzig valley for the entire COPS period. Also depicted are the times of sunrise and sunset. From Eigenmann et al. (2009, Appendix B).

The data set of EC measurements at Nam Co station on the Tibetan Plateau (see Sect. 2.2) was used to adapt the detection routine for FCCs also to another study area and to investigate the occurrence of FCCs within this different setting of complex terrain (see also Sect. 1). Two types of generation of FCCs were identified (see Zhou et al., 2011, Appendix D). It was found that FCCs were detected (1) in the morning during the reversal of a thermally driven diurnal land-lake wind circulation system or (2) during the whole daytime due to the adaption of the land-lake wind circulation system to surface heating differences in combination with cloud cover periods. The first type is similar to the observations during COPS (see Eigenmann et al., 2009, Appendix B), while the second type is typical for Nam Co station. Due to the high altitude of Nam Co station, diffuse radiation components are strongly reduced compared to lowland sites causing a strong cooling of the land surface during cloud cover periods. During these periods, the land-lake circulation is weakened or reversed, dependent on the temperature gradient between the land and the lake. The adaptation of the land-lake breeze to the alternating situation of heating difference leads to periods of vanishing wind speeds and thus to FCCs. The distribution of FCCs regarding the entire measurement period in Fig. 3 indicates that FCCs can be mainly attributed to case (1) during the non-monsoon period, while FCCs are generated by both mechanisms (1 and 2) during the monsoon season. The second peak in the afternoon during monsoon can be related to cloud cover frequency of high clouds, which was found by Fujinami et al. (2005) to be higher in the afternoon than in the morning in the latitudinal zone where Nam Co station is located.

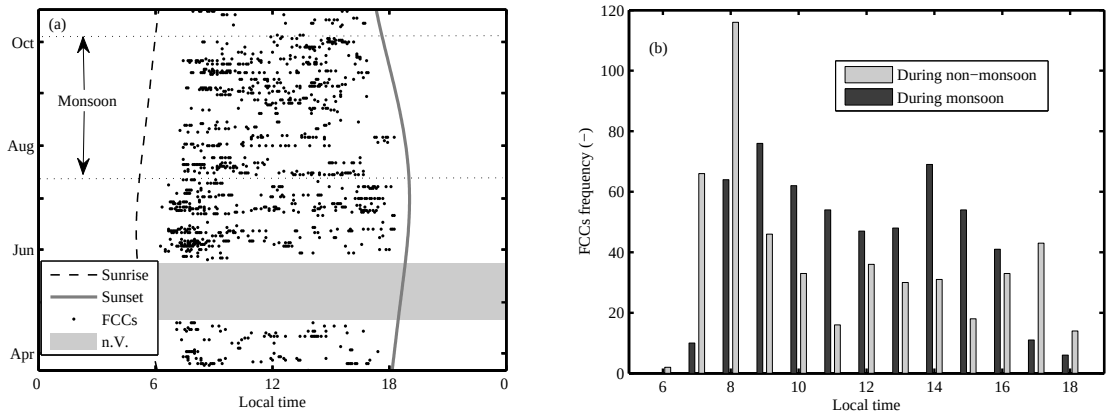

Figure 3: (a) The distribution of FCCs during the entire measurement period at Nam Co station and (b) the corresponding frequencies in the course of the day as a histogram. From Zhou et al. (2011, Appendix D), modified.

3.3 Convective structures in the boundary layer during FCCs

Observations in the Kinzig valley (see Sect. 2.1.1) were combined with LES (see Sect. 2.3) in order to study the impact of the observed FCCs (see Sect. 3.2) on the turbulence structure in the boundary layer.

The scale of turbulent eddies at the height of the EC measurements during periods with FCCs was investigated by applying spectral analysis methods to the EC data (see Eigenmann et al., 2009, Appendix B). Figure 4 shows for COPS IOP 8b (15 July 2007) the normalized wavelet power spectra of the vertical wind speed and the sonic temperature from 05:00–13:00 UTC. This day is exemplary for all 23 days with FCCs (see Fig. 2). During the period with FCCs (07:35–08:40 UTC, black dotted vertical lines), a strong gain of significant areas of enhanced spectral power within turbulent scales of a few minutes (maxima from 4 to 13 min) is obvious. These time scales can be related to the presence of large coherent vertical structures (e.g. plumes or updrafts) with a spatial extent in the order of the boundary layer height, which are known to be responsible for the majority of the transport within the CBL (see e.g. Stull, 1988; Chandra et al., 2010). The occurrence of these turbulent scales in the ground-based EC data indicates that air very close to the ground is able to be transported upwards very efficiently by non-local large-eddy transport processes during FCCs. With the onset of the up-valley wind, these turbulent scales disappear from the data indicating that the vertical transport of near-ground air becomes less effective.

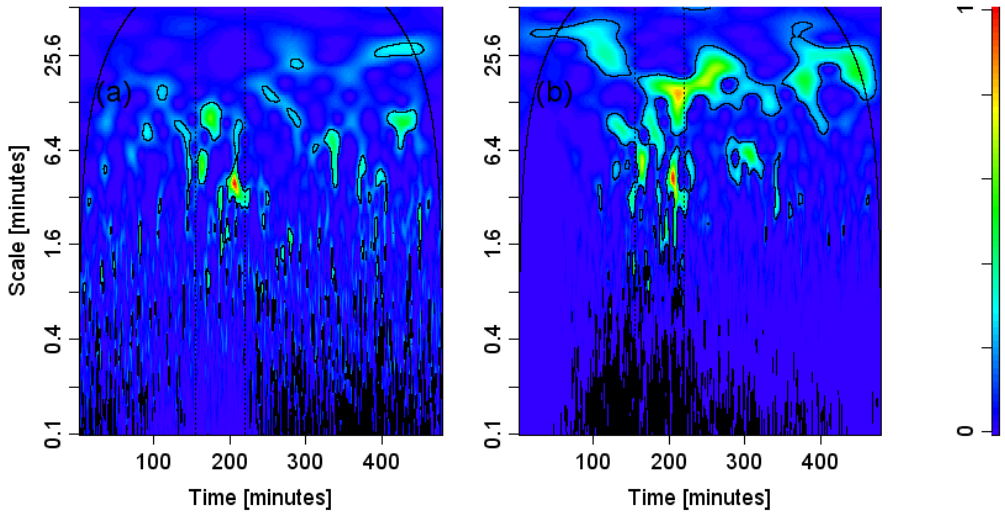

Figure 4: Normalized wavelet power spectra of (a) the vertical wind speed and (b) sonic temperature from 05:00–13:00 UTC (480 min) for COPS IOP 8b (15 July 2007) at the Fußbach I site in the Kinzig valley. The period with FCCs (07:35–08:40 UTC) is indicated by the black dotted vertical lines. From Eigenmann et al. (2009, Appendix B).

Indeed, strong updrafts could be frequently observed in the valley boundary layer by the Sodar/RASS system during FCCs. The morning evolution of the vertical wind speed is exemplarily shown for COPS IOP 15b (13 August 2007) in Fig. 5 (lower panel). It can be seen that during FCCs – especially from 07:50 to 10:30 UTC – vertical wind speeds are strongly enhanced with values of locally more than 0.8 ms^{-1} (10 min average value). Such values can also be found within other studies using boundary layer profiling techniques (e.g. Barlow et al., 2011; Kiemle et al., 2011). Moreover, the corresponding profiles of virtual potential temperature in Fig. 5 (upper panel) give insight into the stratification of the valley boundary layer. As expected, at times of strong coherent updrafts (Fig. 5b and d), the stratification is approximately neutral or slightly unstable. However, in the short period of interruption of stronger updrafts at 09:10 UTC (Fig. 5c), stable stratification becomes evident with a profile similar to that observed before the period with FCCs (Fig. 5a). This indicates that outside of the updrafts the valley atmosphere is still stably stratified and that the observed updrafts deeply penetrate into the stably stratified valley boundary layer during FCCs.

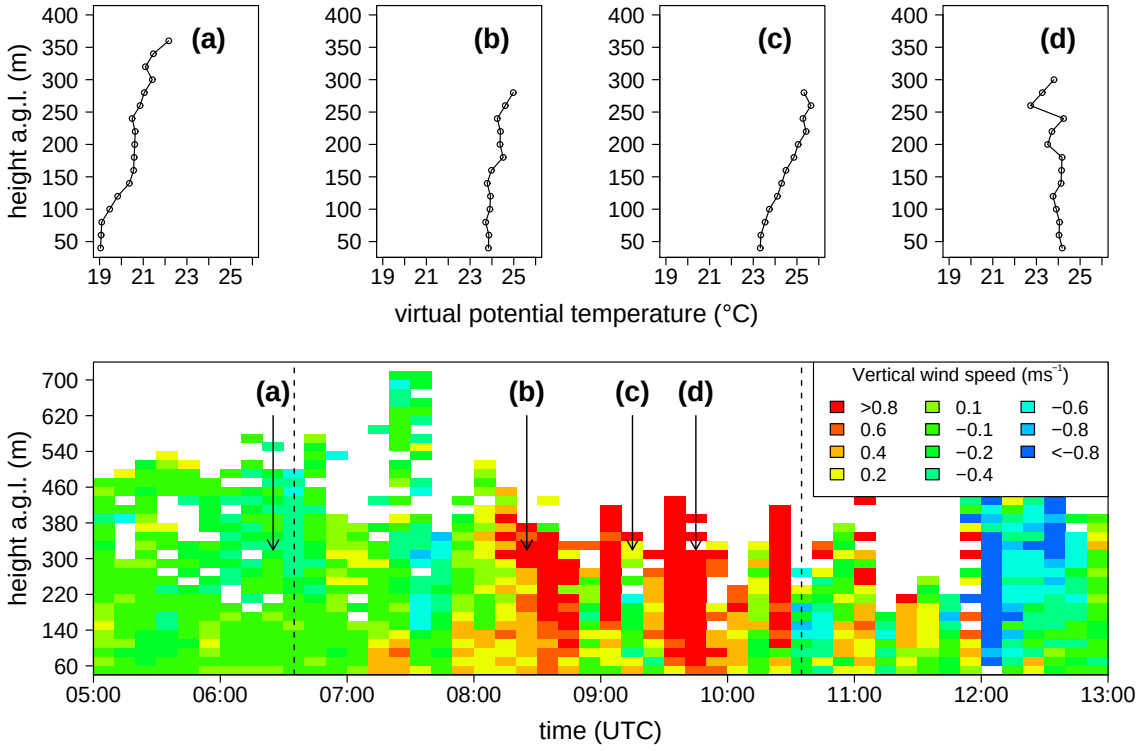

Figure 5: Upper panel (a-d): profiles of the virtual potential temperature measured by the Sodar/RASS in the morning hours of COPS IOP 15b (13 August 2007) at Fußbach. The times of the profiles are marked in the lower panel. Lower panel: corresponding Sodargramm of the vertical wind speed in colour from 05:00-13:00 UTC. The black dashed vertical lines indicate the period with FCCs (06:30–10:30 UTC). From Brötz et al. (2013, Appendix E), modified.

To answer the question how these coherent updraft structures get organized during FCCs in the boundary layer of the Kinzig valley, the LES model was adapted to the conditions of the Kinzig valley (see Brötz et al., 2013, Appendix E). Flux differences between different types of land surfaces were found to be negligible in the observed early-morning periods with FCCs (see Eigenmann et al., 2011, Appendix C). Orography was assumed to mainly determine the convective structures in the valley in these periods. Indeed, the application of an ensemble and time mean analysis (see Brötz et al., 2013, Appendix E) of the vertical wind speed revealed that the complex orography imposes the valley flow coherent convective motions at specific locations during FCCs (see Fig. 6). Their persistence relative to the mountain ridges is in contrast to the changing locations of coherent structures in a CBL over flat homogeneous terrain. The quasi-stationary patterns of up- and downdrafts in the valley are shown in Fig. 6 at about 130 m above the valley floor (300 m a.s.l.). This pattern resembles the typical spoke patterns known for CBLs with zero mean wind speed (e.g. Schmidt and Schumann, 1989). Regarding the location of the measurement site indicated in Fig. 6, it can be seen that it lies within an area of preferred coherent updraft during FCCs. Thus, the simulations support the observations of strong updrafts by the Sodar/RASS (see Fig. 5) during FCCs. An analysis of probability density functions of the simulated and measured vertical wind speed as described in Brötz et al. (2013, Appendix E) also showed that the site is located preferably in an updraft area during FCCs.

The situation of turbulent transport in the valley during FCCs was further analysed by means of LES. The simulated TKE budget terms (see Fig. 8 in Brötz et al., 2013, Appendix E) showed that the boundary layer is buoyancy-driven during FCCs. A strong transport of TKE from the lower half of the valley boundary layer into upper regions can be seen in the simulations. However, the simulated following along-valley wind period with no FCCs showed that the quasi-stationary spoke patterns during FCCs are dissolved and irregular streak-like patterns become evident (see Fig. 5 in Brötz et al., 2013, Appendix E), typical for shear-driven boundary layers (e.g. Moeng and Sullivan, 1994; Weckwerth et al., 1997; Drobinski et al., 1998; Drobinski and Foster, 2003). The TKE transport term in the along-valley wind situation is much weaker compared to the period with FCCs.

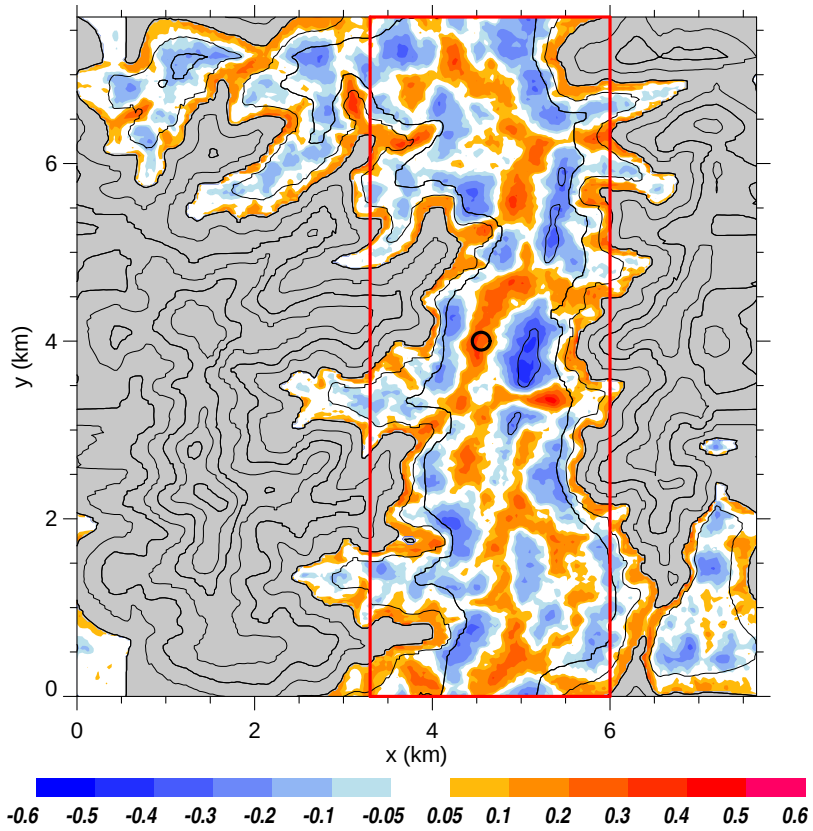

Figure 6: Ensemble and time mean of the simulated vertical wind speed in ms^{-1} at 300 m a.s.l. in the Kinzig valley during FCCs (color-coded). Black solid lines mark the orography in steps of 50 m. Grey contours indicate the intersection with the orography. The red frame represents the section of the valley used for Fig. 7. The location of the measurement site is marked by the black circle. From Brötz et al. (2013, Appendix E).

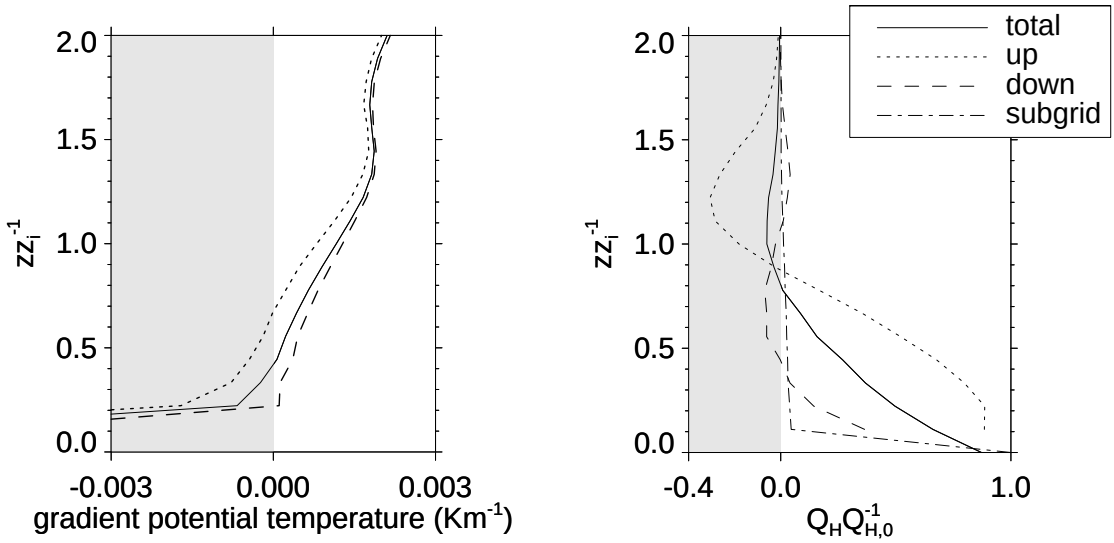

Figure 7: (left panel) Simulated vertical profiles of the gradient of the potential temperature and (right panel) of Q_H (normalized) during FCCs. The solid line shows the values for all points in the valley (see red frame in Fig. 6), while the dotted (dashed) line shows the profiles for the updraft (downdraft) areas in the valley. The contribution to Q_H from the sub-grid model is shown in the right panel as dash-dotted line. From Brötz et al. (2013, Appendix E), modified.

To further highlight the effective vertical transport during FCCs, Fig. 7 shows the simulated profiles of the flux of sensible heat and the corresponding vertical profiles of the gradient of the potential temperature for the valley area (see red frame in Fig. 6). The mean total profile and the mean profiles for up- and downdraft areas are depicted separately. Regarding the total flux of sensible heat in the valley, it can be seen that the flux is counter to the temperature gradient in the center of the valley between about 0.4 z_i and 0.8 z_i. The total heat flux is mainly determined by the flux within the updraft areas. Regarding the updraft areas, the heat flux follows the (unstable to neutral) temperature gradient up to a height of 0.65 z_i. A counter-gradient flux remains above this height up to about 0.9 z_i. Counter-gradient fluxes are a common feature in turbulent flows (e.g. Schumann, 1987) and can also be found within forest canopies (see e.g. Denmead and Bradley, 1985). The described counter-gradient flux is a very effective transport mechanism for surface layer air mass properties to reach higher altitudes in the stably stratified valley. For illustration, Fig. 8 shows for the vertical wind and the temperature stratification an instantaneous vertical slice through the model domain during FCCs. Strong convective updraft structures can be seen within the valley penetrating through the stably stratified valley atmosphere up to approximately the height of the surrounding mountains. The simulated vertical counter-gradient transport in the valley agrees well with the Sodar/RASS observations shown in Fig. 5.

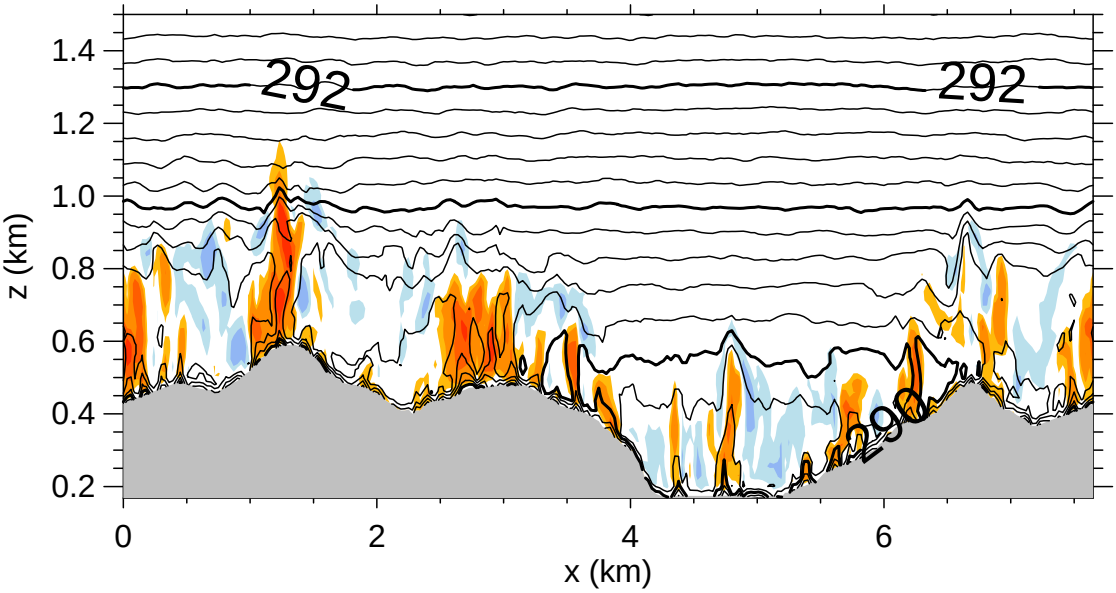

Figure 8: Instantaneous situation of the simulated vertical wind speed in ms^{-1} (color-coded) shown in a vertical cross section perpendicular to the axis of the valley during FCCs. Black lines are isolines of potential temperature in steps of 0.2 K. Intersection with the orography is shaded in grey. From Brötz et al. (2013, Appendix E), modified.

4 Conclusions

The following conclusions related to free convection and turbulent fluxes over complex terrain can be drawn:

(i) High effort was put into a uniform processing and quality control of the surface turbulent flux measurements conducted at sixteen stations during COPS (Eigenmann et al., 2011, Appendix C). This allowed for a high comparability of the measurements as methodical differences could be excluded. Differences in flux values on days with weak synoptic forcing were found to be strongly determined by varying land surface characteristics. The role of altitude plays a minor role, although a slight increase of the Bowen ratio from the valleys to the mountaintops – similar to former experiments in this area (Wenzel et al., 1997; Kalthoff et al., 1999) – could be found. From this it can be concluded that on a single day with weak synoptic forcing, the initiation of convection can be forced locally by the spatial distribution of land surface characteristics.

(ii) Values of the non-closure of the energy balance typical for agricultural sites were found at the sites of the COPS field campaign regarding average conditions. The landscape heterogeneity causing not measurable advective and low-frequency flux components is assumed to be responsible for the observed residual. This hypothesis is reinforced by the fact that the residual was found to increase with the onset of the oasis effect. Moreover, in the observed low wind speed situations with free convection conditions (FCCs) – characterized by a more vertically oriented turbulent exchange regime – the residual was found to vanish on average. Due to the more vertical orientation of the exchange regime during FCCs, the landscape heterogeneity at a single measurement site is of minor importance and missing advective flux components are strongly reduced. With the onset of the wind after the periods with FCCs, the heterogeneity of the surrounding landscape becomes again more important and advective flux components and other heterogeneity effects lead again to an unclosed energy balance.

(iii) It was shown that the relative contributions of sensible and latent heat missing in the considered periods with no FCCs compared to the periods with FCCs have exactly the proportions of the buoyancy flux ratio. This

finding supports the theory (e.g. Foken et al. 2008b) that the missing flux components are transported within buoyancy-driven secondary circulations which develop over heterogeneous terrain. Moreover, this finding also supports the recent suggestion of Charuchittipan et al. (2013) to use the buoyancy flux ratio approach for the correction of the energy balance. The usually used approach by Twine et al. (2000) to distribute the residual according to the Bowen ratio seems to be not appropriate.

(iv) FCCs could be frequently observed in situations of weak synoptic forcing during COPS. This finding confirmed the initial question of this thesis based on the work of Mayer et al. (2008) whether FCCs occur in general over complex terrain. As the occurrence of FCCs is bound to vanishing wind speeds ($u_* \rightarrow 0$) and simulataneously enhanced positive values of the buoyancy flux ($\left(\overline{w'\theta_v'}\right)_0 > 20$ Wm^{-2}), FCCs were observed in all probed valleys of the Black Forest during the reversal of the valley wind system from down- to up-valley winds in the morning hours. Thus, the occurrence of FCCs is mainly controlled by the adaption of thermally driven orographic or local wind systems to heating differences over complex terrain. However, also the surface characteristics with their impact on the resulting turbulent fluxes may control the occurrence of FCCs. For instance, it was shown that the negative values of sensible heat during the oasis effect inhibit FCCs.

(v) With the data set of Nam Co station on the Tibetan Plateau, the conclusions drawn in (iv) could be confirmed. However, FCCs were more frequently observed in the afternoon in combination with cloud cover periods at this site. As diffuse radiation components are strongly reduced at the altitude of the Tibetan Plateau compared to lowland sites, the cloud cover periods caused a strong cooling of the land surface within a short time. Thus, the adaption of the land-lake breeze at Nam Co station to the changing situation of heating differences led to more periods of vanishing wind speeds and thus to more FCCs in combination with cloud cover periods compared to the COPS region.

(vi) A spectral analysis of the turbulent scales and an analysis of the vertical wind speeds measured by the Sodar/RASS revealed the existence of coherent updraft structures in the Kinzig valley during FCCs. The Sodar/RASS

measurements further showed that these updrafts penetrate into the stably stratified valley boundary layer indicating that surface layer air mass characteristics can be effectively injected into higher regions of the valley boundary layer during FCCs. It can be assumed that these fluxes in the early-morning hours are crucial for the preconditioning of the CBL for a further development of moist convection in the course of the day. However, the experimental design of COPS – contrary to the trace gas measurements in the study of Mayer et al. (2008) which tracked a pulse of surface layer trace gases up to a mountain summit – was not able to answer such questions. An experiment similar to that of COPS, but focused on a certain segment of e.g. the Kinzig valley, should be considered in future plans of boundary layer experiments.

(vii) The application of the LES model confirmed that the measurement site in the Kinzig valley is located preferably in an updraft region during FCCs. This was demonstrated by an ensemble and time mean analysis of the vertical wind speed in the valley, which showed that the complex orography forces the valley flow to form coherent convective structures at spatially fixed locations relative to the surrounding mountain ridges. This is in contrast to the random locations of convective structures in case of a CBL over flat homogeneous terrain.

(viii) Simulated profiles of the sensible heat flux showed that the total flux out of the valley is mainly determined by the flux within these coherent updraft structures during FCCs. The total heat flux was found to be a flux counter to the temperature gradient in these early-morning situations. This finding underlines the observations summarized in (vi) that surface layer air mass properties can be effectively transported into higher regions of the stably stratified valley boundary layer during FCCs. According to the simulation, these updrafts reach up to approximately the height of the surrounding mountains. From this, it can be concluded that the vertically transported surface layer air mass properties during FCCs can be horizontally translocated with the above-valley or large-scale flow and can also alter ABL characteristics elsewhere.

References

Aoshima, F., Behrendt, A., Bauer, H.-S., Wulfmeyer, V., 2008. Statistics of convection initiation by use of Meteosat rapid scan data during the Convection and Orographically-induced Precipitation Study (COPS). Meteorol. Z., 17: 921–930.

Aubinet, M., Grelle, A., Ibrom, A., Rannik, Ü., Moncrieff, J., Foken, T., Kowalski, A. S., Martin, P.H., Berbigier, P., Bernhofer, Ch., Clement, R., Elbers, J., Granier, A., Grünwald, T., Morgenstern, K., Pilegaard, K., Rebmann, C., Snijders, W., Valentini, R., Vesala, T., 2000. Estimates of the annual net carbon and water exchange of forests: the EUROFLUX methodology. Adv. Ecol. Res., 30: 113–175.

Avissar, R., Schmidt, T., 1998. An evaluation of the scale at which ground-surface heat flux patchiness affects the convective boundary layer using large-eddy simulations. J. Atmos. Sci., 55: 2666–2689.

Baidya Roy, S., Avissar, R., 2000. Scales of response of the convective boundary layer to land surface heterogeneity. Geophys. Res. Lett., 27, 533–536.

Bange, J., Spieß, T., Herold, M., Beyrich, F., Hennemuth, B., 2006. Turbulent fluxes from Helipod flights above quasi-homogeneous patches within the LITFASS area. Bound.-Lay. Meteorol., 121: 127–151.

Barlow, J.F., Dunbar, T.M., Nemitz, E.G. Wood, C.R., Gallagher, M.W., Davies, F., O'Connor, E., Harrison, R.M., 2011. Boundary layer dynamics over London, UK, as observed using Doppler lidar during REPARTEE-II. Atmos. Chem. Phys., 11: 2111–2125.

Barthlott, C., Corsmeier, U., Meißner, C., Braun, F., Kottmeier, C., 2006. The influence of mesoscale circulation systems on triggering convective cells over complex terrain. Atmos. Res., 81: 150–175.

Barthlott, C., Schipper, J.W., Kalthoff, N., Adler, B., Kottmeier, C., Blyth, A., Mobbs, S., 2010. Model representation of boundary-layer convergence triggering deep convection over complex terrain: A case study from COPS. Atmos. Res., 95: 172–185.

Behrendt, A., Pal, S., Aoshima, F., Bender, M., Blyth, A., Corsmeier, U., Cuesta, J., Dick, G., Dorninger, M., Flamant, C., Di Girolamo, P., Gorgas, T., Huang, Y., Kalthoff, N., Khodayar, S., Mannstein, H., Träumner, K., Wieser, A., Wulfmeyer, V., 2011. Observation of convection initiation processes with a suite of state-of-the-art research instruments during COPS IOP 8b. Q. J. R. Meteorol. Soc., 137: 81–100.

Bennett, L.J., Blyth, A.M., Burton, R.R., Gadian, A.M., Weckwerth, T.M., Behrendt, A., Di Girolamo, P., Dorninger, M., Lock, S.-J., Smith, V.H., Mobbs, S.D., 2011. Initiation of convection over the Black Forest mountains during COPS IOP15a. Q. J. R. Meteorol. Soc., 137: 176–189.

Betts, A.K., Ball, J.H., Beljaars, A.C.M., Miller, M.J., Viterbo, P.A., 1996. The land surface-atmosphere interaction: A review based on observational and global modeling perspectives. J. Geophys. Res., 101: 7209–7225.

Beyrich, F., Mengelkamp, H.-T., 2006. Evaporation over a heterogeneous land surface: EVA_GRIPS and the LITFASS-2003 experiment - an overview. Bound.-Lay. Meteorol., 121:5–32.

Brötz, B., Eigenmann, R., Dörnbrack, A., Foken, T., Wirth, V., 2013. Early-morning flow transition in a valley in low-mountain terrain. Bound.-Lay. Meteorol., submitted.

Brunsell, N.A., Mechem, D.B., Anderson, M.C., 2011. Surface heterogeneity impacts on boundary layer dynamics via energy balance partitioning. Atmos. Chem. Phys., 11: 3403–3416.

Businger, J.A., Wyngaard, J.C., Izumi, Y., Bradley, E.F., 1971. Flux-profile relationships in the atmospheric surface layer. J. Atmos. Sci., 28: 181–189.

Chandra, A.S., Kollias, P., Giangrande, S.E., Klein, S.A., 2010. Long-term observations of the convective boundary layer using insect radar returns at the SGP ARM climate research facility. J. Clim., 23: 5699–5714.

Charuchittipan, D., Babel, W., Mauder, M., Beyrich, F., Leps, J.P., Foken, T., 2013. Extension of the averaging time of the eddy-covariance measurement and its effect on the energy balance closure. Bound.-Lay. Meteorol., to be submitted.

Corsmeier, U., Kalthoff, N., Barthlott, C., Aoshima, F., Behrendt, A., Di Girolamo, P., Dorninger, M., Handwerker, J., Kottmeier, C., Mahlke, H., Mobbs, S.D., Norton, E.G. Wickert, J., Wulfmeyer, V., 2011. Processes driving deep convection over complex terrain: A multi-scale analysis of observations from COPS-IOP 9c. Q. J. R. Meteorol. Soc., 137: 137–155.

Courault, D., Drobinski, P., Brunet, Y., Lacarrere, P., Talbot, C., 2007. Impact of surface heterogeneity on a buoyancy-driven convective boundary layer in light winds, Bound.-Lay. Meteorol., 124: 383–403.

Defant, F., 1949. Zur Theorie der Hangwinde, nebst Bemerkungen zur Theorie der Berg- und Talwinde. Arch. Meteorol. Geophys. Bioklim., A1: 421–450.

Denmead, D.T., Bradley, E.F., 1985. Flux-gradient relationships in a forest canopy. In: B.A. Hutchison, Hicks B.B. (Editors), The forest-atmosphere interaction, D. Reidel Publ. Comp., Dordrecht, Boston, London, pp 421–442.

Drobinski, P., Brown, R.A., Flamant, P.H., Pelon, J., 1998. Evidence of organized large eddies by ground-based doppler lidar, sonic anemometer and sodar. Bound.-Lay. Meteorol., 88: 343–361.

Drobinski, P., Foster, R.C., 2003. On the origin of near-surface streaks in the neutrally-stratified planetary boundary layer. Bound.-Lay. Meteorol., 108: 247–256.

Eigenmann, R., Metzger, S., Foken, T., 2009. Generation of free convection due to changes of the local circulation system. Atmos. Chem. Phys., 9: 8587–8600.

Eigenmann, R., Kalthoff, N., Foken, T., Dorninger, M., Kohler, M., Legain, D., Pigeon, G., Piguet, B., Schüttemeyer, D., Traulle, O., 2011. Surface energy balance and turbulence network during the Convective and Orographically-induced Precipitation Study (COPS). Q. J. R. Meteorol. Soc., 137: 57–69.

Finnigan, J.J., Clement, R., Malhi, Y., Leuning, R., Cleugh, H.A., 2003. A re-evaluation of long-term flux measurement techniques. Part I: Averaging and coordinate rotation. Bound.-Lay. Meteorol., 107: 1–48.

Foken, T., Wimmer, F., Mauder, M., Thomas, C., Liebethal, C., 2006. Some aspects of the energy balance closure problem. Atmos. Chem. Phys., 6: 4395–4402.

Foken, T., 2008a. Micrometeorology. Springer, Berlin, Heidelberg, 308 pp.

Foken, T., 2008b. The energy balance closure problem: An overview. Ecol. Appl., 18: 1351–1367.

Foken, T., Mauder, M., Liebethal, C., Wimmer, F., Beyrich, F., Leps, J.P., Raasch, S., DeBruin, H.A.R., Meijninger, W.M.L., Bange, J., 2010. Energy balance closure for the LITFASS-2003 experiment. Theor. Appl. Climatol., 101: 149–160.

Foken, T., Aubinet, M., Finnigan, J.J., Leclerc, M.Y., Mauder, M., K.T., Paw U, 2011. Results of a panel discussion about the energy balance closure correction for trace gases. B. Am. Meteorol. Soc., 92(4): ES13–ES18.

Foken, T., Leuning, R., Oncley, S.P., Mauder, M., Aubinet, M., 2012. Corrections and data quality. In: M. Aubinet et al. (Editors), Eddy covariance: A practical guide to measurement and data analysis, Springer, Dordrecht, Heidelberg, London, New York, pp. 85–131.

Franssen, H.J.H., Stöckli, R., Lehner, I., Rotenberg, E., Seneviratne, S.I., 2010. Energy balance closure of eddy-covariance data: A multisite analysis for European

FLUXNET stations. Agr. Forest Meteorol., 150: 1553–1567.

Fujinami, H., Nomura, S., Yasunari, T., 2005. Characteristics of diurnal variations in convection and precipitation over the southern Tibetan Plateau during summer. SOLA, 1: 49–52.

Garratt, J.R., 1992. The Atmospheric Boundary Layer. Cambridge University Press, 316 pp.

Göckede, M., Rebmann, C., Foken, T., 2004. A combination of quality assessment tools for eddy covariance measurements with footprint modelling for the characterisation of complex sites. Agr. Forest Meteorol., 127: 175–188.

Göckede, M., Markkanen, T., Hasager, C.B., Foken, T., 2006. Update of a footprint-based approach for the characterisation of complex measurement sites. Bound.-Lay. Meteorol., 118: 635–655.

Gopalakrishnan, S.G., Avissar, R., 2000. An LES study of the impacts of land surface heterogeneity on dispersion in the convective boundary layer. J. Atmos. Sci., 57: 352–371.

Gopalakrishnan, S.G., Baidya Roy, S., Avissar, R., 2000. An evaluation of the scale at which topographical features affect the convective boundary layer using large eddy simulations. J. Atmos. Sci., 57: 334–351.

Hadfield, M.G., Cotton, W.R., Pielke, R.A., 1991. Large-eddy simulations of thermally forced circulations in the convective boundary layer. Part I: Small-scale circulation with zero wind. Bound.-Lay. Meteorol., 57: 79–114.

Hadfield, M.G., Cotton, W.R., Pielke, R.A., 1992. Large-eddy simulations of thermally forced circulations in the convective boundary layer. Part II: The effect of changes in wavelength and wind speed. Bound.-Lay. Meteorol., 58: 307–327.

Hauck, C., Barthlott, C., Krauss, L., Kalthoff, N., 2011. Soil moisture variability and its influence on convective precipitation over complex terrain. Q. J. R. Meteorol. Soc., 137: 42–56.

Heusinkveld, B.G., Jacobs, A.F.G., Holtslag, A.A.M., Berkowicz, S.M., 2004. Surface energy balance closure in an arid region: role of soil heat flux. Agr. Forest Meteorol., 122: 21–37.

Hiller, R., Zeeman, M. J., Eugster, W., 2008. Eddy-covariance flux measurements in the complex terrain of an Alpine valley in Switzerland. Bound.-Lay. Meteorol., 127: 449–467.

Huang, J., Lee, X., Patton, E.G. 2008. A modelling study of flux imbalance and the

influence of entrainment in the convective boundary layer. Bound.-Lay. Meteorol., 127: 273–292.

Huang, H.-Y., Lee, X., Patton, E.G. 2009. Dissimilarity of scalar transport in the convective boundary layer in inhomogeneous landscapes. Bound.-Lay. Meteorol., 130: 327–345.

Huang, H.-Y., Margulis, S.A., 2009. On the impact of surface heterogeneity on a realistic convective boundary layer. Water Resour. Res., 45: W04425, doi:10.1029/2008WR007175.

Inagaki, A., Letzel, M.O., Raasch, S., Kanda, M., 2006. Impact of surface heterogeneity on energy imbalance: A study using LES. J. Meteorol. Soc. Jpn., 84: 187–198.

Jegede, O.O., Foken, T., 1999. A study of the internal boundary layer due to a roughness change in neutral conditions observed during the LINEX field campaigns. Theor. Appl. Climatol., 62: 31–41.

Kalthoff, N., Fiedler, F., Kohler, M., Kolle, O., Mayer, H., Wenzel, A., 1999. Analysis of energy balance components as a function of orography and land use and comparison of results with the distribution of variables influencing local climate. Theor. Appl. Climatol., 62: 65–84.

Kalthoff, N., Horlacher, V., Corsmeier, U., Volz-Thomas, A., Kolahgar, B., Geiß, H., Möllmann-Coers, M., Knaps, A., 2000. Influence of valley winds on transport and dispersion of airborne pollutants in the Freiburg-Schauinsland area. J. Geophys. Res.- Atmos., 105: 1585–1597.

Kalthoff, N., Adler, B., Barthlott, C., Corsmeier, U., Mobbs, S., Crewell, S., Träumner, K., Kottmeier, C., Wieser, A., Smith, V., Di Girolamo, P., 2009. The impact of convergence zones on the initiation of deep convection: A case study from COPS. Atmos. Res., 93: 680–694.

Kalthoff, N., Kohler, M., Barthlott, C., Adler, B., Mobbs, S.D., Corsmeier, U., Träumner, K., Foken, T., Eigenmann, R., Krauss, L., Khodayar, S., Di Girolamo, P., 2011. The dependence of convection-related parameters on surface and boundary-layer conditions over complex terrain. Q. J. R. Meteorol. Soc., 137: 70–80.

Kanda, M., Inagaki, A., Letzel, M.O., Raasch, S., Watanabe, T., 2004. LES study of the energy imbalance problem with eddy covariance fluxes. Bound.-Lay. Meteorol., 110: 381–404.

Kiemle, C., Wirth, M., Fix, A., Rahm, S., Corsmeier, U., Di Girolamo, P., 2011. Latent heat flux measurements over complex terrain by airborne water vapour and wind

lidars. Q. J. R. Meteorol. Soc., 137: 190–203.

Kossmann, M. Fiedler, F., 2000. Diurnal momentum budget analysis of thermally induced slope winds. Meteorol. Atmos. Phys., 75: 195–215.

Kottmeier, C., Kalthoff, N., Corsmeier, U., Barthlott, C., van Baelen, J., Behrendt, A., Behrendt, R., Blyth, A., Coulter, R., Crewell, S., Di Girolamo, P., Dorninger, M., Flamant, C., Foken, T., Hagen, M., Hauck, C., Höller, H., Konow, H., Kunz, M., Mahlke, H., Mobbs, S., Richard, E., Steinacker, R., Weckwerth, T., Wieser, A., Wulfmeyer, V., 2008. Mechanisms initiating deep convection over complex terrain during COPS. Meteorol. Z., 17: 931–948.

LeMone, M.A., Chen, F., Alfieri, J.G., Tewari, M., Geerts, B., Miao, Q., Grossman, R.L., Coulter, R.L., 2007. Influence of land cover and soil moisture on the horizontal distribution of sensible and latent heat fluxes in southeast Kansas during IHOP_2002 and CASES-97. J. Hydrometeorol., 8: 68–87.

Letzel, M.O., Raasch, S., 2003. Large eddy simulation of thermally induced oscillations in the convective boundary layer. J. Atmos. Sci., 60: 2328–2341.

Leuning, R., van Gorsel, E., Massman, W.J., Isaac, P.R., 2012. Reflections on the surface energy imbalance problem. Agr. Forest Meteorol., 156: 65–74.

Lu, Y., Ma, Y., Li, M., Yang, X., 2008. Numerical simulation of typical atmospheric boundary layer characteristics over lake Namco region, Tibetan Plateau in summer (in Chinese with English abstract). Plateau Meteorol., 27: 733–740.

Lugauer, M., Winkler, P., 2005. Thermal circulation in South Bavaria – climatology and synoptic aspects. Meteorol. Z., 14: 15–30.

Lyons, T., Halldin, S., 2004. Surface heterogeneity and the spatial variation of fluxes. Agr. Forest Meteorol., 121: 153–165.

Mahrt, L., Ek, M., 1993. Spatial variability of turbulent fluxes and roughness lengths in HAPEX-MOBILHY. Bound.-Lay. Meteorol., 65: 381–400.

Mahrt, L., MacPherson, I., Desjardins, R., 1994. Observations of fluxes over heterogeneous surfaces. Bound.-Lay. Meteorol., 67: 345–367.

Mahrt, L., 2000. Surface heterogeneity and vertical structure of the boundary layer. Bound.-Lay. Meteorol., 96: 33–62.

Malhi, Y., McNaughton, K.G., von Randow, C., 2004. Low frequency atmospheric transport and surface flux measurements. In: X. Lee, W. Massman, B. Law (Editors), Handbook of micrometeorology: a guide for surface flux measurement and analysis. Kluwer Academic Publishers, Dordrecht, pp. 101–118.

Maronga, B., Raasch, S., 2012. Large-eddy simulations of surface heterogeneity effects on the convective boundary layer during the LITFASS-2003 experiment. Bound.-Lay. Meteorol., 146: 17–44.

Mason, P.J., 1988. The formation of areally-averaged roughness lengths. Q. J. R. Meteorol. Soc., 114: 399–420.

Mauder, M., Foken, T., 2004. Documentation and instruction manual of the eddy covariance software package TK2. Work Report, University of Bayreuth, Dept. Micrometeorology, ISSN 1614-8916, 26, 45 pp.

Mauder, M., Foken, T., 2006. Impact of post-field data processing on eddy covariance flux estimates and energy balance closure. Meteorol. Z., 15: 597–609.

Mauder, M., Liebethal, C., Göckede, M., Leps, J.P., Beyrich, F., Foken, T., 2006. Processing and quality control of flux data during LITFASS-2003. Bound.-Lay. Meteorol., 121: 67–88.

Mauder, M., Jegede, O.O., Okogbue, E.C., Wimmer, F., Foken, T., 2007. Surface energy balance measurements at a tropical site in West-Africa during the transition from dry to wet season. Theor. Appl. Climatol., 89: 171–183.

Mauder, M., Foken, T., Clement, R., Elbers, J.A., Eugster, W., Grünwald, T., Heusinkveld, B., Kolle, O., 2008. Quality control of CarboEurope flux data – Part 2: Inter-comparison of eddy-covariance software. Biogeosciences, 5: 451–462.

Mayer, J.-C., Staudt, K., Gilge, S., Meixner, F.X., Foken, T., 2008. The impact of free convection on late morning ozone decreases on an Alpine foreland mountain summit. Atmos. Chem. Phys., 8: 5941–5956.

Meißner, C., Kalthoff, N., Kunz, M., Adrian, G., 2007. Initiation of shallow convection in the Black Forest mountains. Atmos. Res., 86: 42–60.

Metzger, S., Foken, T., Eigenmann, R., Kurtz, W., Serafimovich, A., Siebicke, L., Olesch, J., Staudt, K., Lüers, J., 2007. COPS experiment. Convective and orographically induced precipitation study. 01 June 2007 - 31 August 2007, Documentation. Work Report, University of Bayreuth, Dept. Micrometeorology, ISSN 1614-8916, 34, 72 pp.

Moeng, C.-H., Sullivan, P.P., 1994. A comparison of shear- and buoyancy-driven planetary boundary layer flows. J. Atmos. Sci., 51: 999–1022.

Obukhov, A.M., 1946. Turbulence in the atmosphere with inhomogeneous temperature. Tr. Geofiz. Inst. Akad. Nauk SSSR, 1: 95–115.

Oncley, S.P., Foken, T., Vogt, R., Kohsiek, W., DeBruin, H.A.R., Bernhofer, C.,

Christen, A., van Gorsel, E., Grantz, D., Feigenwinter, C., Lehner, I., Liebethal, C., Liu, H., Mauder, M., Pitacco, A., Ribeiro, L., Weidinger, T., 2007. The energy balance experiment EBEX-2000. Part I: overview and energy balance. Bound.-Lay. Meteorol., 123: 1–28.

Patton, E.G. Sullivan, P.P., Moeng, C.-H., 2005. The influence of idealized heterogeneity on wet and dry planetary boundary layers coupled to the land surface. J. Atmos. Sci., 62: 2078–2097.

Pielke, R.A., Segal, M., 1986. Mesoscale circulations forced by differential terrain heating. In: P.S. Ray (Editor), Mesoscale Meteorology and Forecasting. American Meteorological Society, Boston, USA, pp. 516–548.

Piotrowski, Z., Smolarkiewicz, P., Malinowski, S., Wyszogrodzki, A., 2009. On numerical realizability of thermal convection. J. Comput. Phys., 228: 6268–6290.

Prusa, J.M., Smolarkiewicz, P.K., Wyszogrodzki, A.A., 2008. EULAG, a computational model for multiscale flows. Comput. Fluids, 37: 1193–1207.

Raabe, A., 1983. On the relation between the drag coefficient and fetch above the sea in the case of off-shore wind in the near-shore zone. Z. Meteorol., 33: 363–367.

Raasch, S., Harbusch, G., 2001. An analysis of secondary circulations and their effects caused by small-scale surface inhomogeneities using large-eddy simulation. Bound.-Lay. Meteorol., 101: 31–59.

Rotach, M.W., Andretta, M., Calanca, P., Weigel, A.P., Weiss, A., 2008. Boundary layer characteristics and turbulent exchange mechanisms in highly complex terrain. Acta Geophys., 56:194–219.

Sakai, R.K., Fitzjarrald, D.R., Moore, K.E, 2001. Importance of low-frequency contributions to eddy fluxes observed over rough surfaces. J. Appl. Meteorol., 40: 2178–2192.

Schmidt, H., Schumann, U., 1989. Coherent structure of the convective boundary layer derived from large-eddy simulations. J. Fluid Mech., 200: 511–562.

Schumann, U., 1987. The countergradient heat flux in turbulent stratified flows. Nucl. Eng. Des., 100: 255–262.

Segal, M., Arritt, R.W., 1992. Nonclassical mesoscale circulations caused by surface sensible heat-flux gradients. B. Am. Meteorol. Soc., 73:1593–1604.

Shen, S., Leclerc, M.Y., 1994. Large-eddy simulation of small-scale surface effects on the convective boundary-layer structure. Atmos. Ocean, 32: 717–731.

Shen, S., Leclerc, M.Y., 1995. How large must surface inhomogeneities be before they

influence the convective boundary layer structure? A case study. Q. J. R. Meteorol. Soc., 121: 1209–1228.

Smolarkiewicz, P.K., Grubisic, V., Margolin, L.G., 1997. On forward-in-time differencing for fluids: Stopping criteria for iterative solutions of anelastic pressure equations. Mon. Weather Rev., 125: 647–654.

Smolarkiewicz, P.K., Sharman, R., Weil, J., Perry, S.G., Heist, D., Bowker, G., 2007. Building resolving large-eddy simulations and comparison with wind tunnel experiments. J. Comput. Phys., 227: 633–653.

Steinfeld, G., Letzel, M.O., Raasch, S., Kanda, M., Inagaki, A., 2007. Spatial representativeness of single tower measurements and the imbalance problem with eddy-covariance fluxes: results of a large-eddy simulation study. Bound.-Lay. Meteorol., 123: 77–98.

Stoy, P., Mauder, M., Foken, T., Marcolla, B., Boegh, E., Ibrom, A., Arain, MA., Arneth, A., Aurela, M., Bernhofer, C., Cescatti, A., Dellwik, E., Duce, P., Gianelle, D., van Gorsel, E., Kiely, G., Knohl, A., Mangolis, H., McCaughey, H., Merbold, L., Montagnani, L., Papale, D., Reichstein, M., Serrano-Ortiz, P., Sottocornola, M., Saunders, M., Spano, D., Vaccari, F., Varlagin, A., 2013. A data-driven analysis of energy balance closure across FLUXNET research sites: The role of landscape-scale heterogeneity. Agr. Forest Meteorol., accepted.

Strunin, M.A., Hiyama, T., Asanuma, J., Ohata, T., 2004. Aircraft observations of the development of thermal internal boundary layers and scaling of the convective boundary layer over non-homogeneous land surfaces. Bound.-Lay. Meteorol., 111: 491–522.

Stull, R.B., 1988. An Introduction to Boundary Layer Meteorology. Kluwer Academic Publishers, Dordrecht, The Netherlands, 666 pp.

Sun, J., Desjardins, R., Mahrt, L., MacPherson, I., 1998: Transport of carbon dioxide, water vapor, and ozone by turbulence and local circulations. J. Geophys. Res., 103, 25873–25885.

Swinbank, W.C., 1951. The measurement of vertical transfer of heat and water vapor by eddies in the lower atmosphere. J. Meteorol., 8: 135–145.

Twine, T.E., Kustas, W.P., Norman, J.M., Cook, D.R., Houser, P.R., Meyers, T.P., Prueger, J.H., Starks, P.J., Wesely, M.L., 2000. Correcting eddy-covariance flux underestimates over a grassland. Agr. Forest Meteorol., 103: 279–300.

Webb, E.K., 1962. Thermal convection with wind shear. Nature, 193: 840–842.

Weckwerth, T.M., Wilson, J.W., Wakimoto, R.M., Crook, N.A., 1997. Horizontal convective rolls: determining the environmental conditions supporting their existence and characteristics. Mon. Weather Rev., 125: 505–526.

Weigel, A.P., Chow, F.K., Rotach, M.W., 2007b. The effect of mountainous topography on moisture exchange between the "surface" and the free atmosphere. Bound.-Lay. Meteorol., 125: 227–244.

Wenzel, A., Kalthoff, N., Fiedler, F., 1997. On the variation of the energy-balance components with orography in the Upper Rhine Valley. Theor. .Appl. Climatol., 57: 1–9.

Wenzel, A., Kalthoff, N., 2000. Method for calculating the whole-area distribution of sensible and latent heat fluxes based on climatological observations. Theor. Appl. Climatol., 66: 139–160.

Whiteman, C.D., 1990. Observations of thermally developed wind systems in mountainous terrain. In: W. Blumen (Editor), Atmospheric processes over complex terrain. Meteorological Monographs, 23 (45), American Meteorological Society, Boston, USA, pp. 5–42.

Whiteman, C.D., 2000. MountainMeteorology: Fundamentals and Applications. Oxford University Press, USA, 355 pp.

Wilson, K., Goldstein, A., Falge, E., Aubinet, M., Baldocchi, D., Berbigier, P., Bernhofer, Ch., Ceulemans, R., Dolman, H., Field, C., Grelle, A., Ibrom, A., Law, B.E., Kowalski, A., Meyers, T., Moncrieff, J., Monson, R., Oechel, W., Tenhunen, J., Valentini, R., Verma, S., 2002. Energy balance closure at FLUXNET sites. Agr. Forest Meteorol., 113: 223–243.

Wulfmeyer, V., Behrendt, A., Bauer, H.S., Kottmeier, C., Corsmeier, U., Blyth, A., Craig G., Schumann, U., Hagen, M., Crewell, S., Di Girolamo, P., Flamant, C., Miller, M., Montani, A., Mobbs, S., Richard, E., Rotach, M.W., Arpagaus, M., Russchenberg, H., Schlüssel, P., König, M., Gärtner, V., Steinacker, R., Dorninger, M., Turner, D.D., Weckwerth, T., Hense, A., Simmer, C., 2008. The Convective and Orographically induced Precipitation Study: A research and development project of the World Weather Research Program for improving quantitative precipitation forecasting in low-mountain regions. B. Am. Meteorol. Soc. 89: 1477–1486.

Wulfmeyer, V., Behrendt, A., Kottmeier, C., Corsmeier, U., Barthlott, C., Craig, G.C., Hagen, M., Althausen, D., Aoshima, F., Arpagaus, M., Bauer, H.-S., Bennett, L., Blyth, A., Brandau, C., Champollion, C., Crewell, S., Dick, G., Di Girolamo, P.,

Dorninger, M., Dufournet, Y., Eigenmann, R., Engelmann, R., Flamant, C., Foken, T., Gorgas, T., Grzeschik, M., Handwerker, J., Hauck, C., Höller, H., Junkermann, W., Kalthoff, N., Kiemle, C., Klink, S., König, M., Krauss, L., Long, C.N., Madonna, F., Mobbs, S., Neininger, B., Pal, S., Peters, G., Pigeon, G., Richard, E., Rotach, M.W., Russchenberg, H., Schwitalla, T., Smith, V., Steinacker, R., Trentmann, J., Turner, D.D., van Baelen, J., Vogt, S., Volkert, H., Weckwerth, T., Wernli, H., Wieser, A., Wirth, M., 2011. The Convective and Orographically-induced Precipitation Study (COPS): the scientific strategy, the field phase, and research highlights. Q. J. R. Meteorol. Soc., 137: 3–30.

Zardi, D., Whiteman, C.D., 2013. Diurnal mountain wind systems. In: F.K. Chow, S.F. De Wekker, B.J. Snyder (Editors), Mountain Weather Research and Forecasting, Springer, Dordrecht, Heidelberg, New York, London, pp. 35–119.

Zhou, D., Eigenmann, R., Babel, W., Foken, T., Ma, Y., 2011. Study of near-ground free convection conditions at Nam Co station on the Tibetan Plateau. Theor. Appl. Climatol., 105: 217–228.

List of appendices

Appendix A: Individual contributions to the joint publications

The results presented in this cumulative thesis were obtained in collaboration with other scientists. Thus, many authors contributed to the publications listed in the appendices B to E in different ways. This section is to specify my own contributions to the individual manuscripts.

Appendix B

Eigenmann, R., Metzger, S., Foken, T., 2009. Generation of free convection due to changes of the local circulation system. Atmospheric Chemistry and Physics, 9: 8587–8600.

- The data used in this publication were obtained during the COPS field campaign and include the measurements of one energy balance and turbulence station and a nearby Sodar/RASS system. The set-up and maintenance of the instruments and the routinely performed data quality control during the experiment involved many people of the Department of Micrometeorology (A. Serafimovich, L. Siebicke, K. Staudt, J. Lüers, J. Olesch). S. Metzger was mainly responsible for the on-site data collection and continuous operation during the three month field campaign. I also supported the field work of S. Metzger during a two weeks stay.
- I alone was responsible for the post-processing of the eddy-covariance, low-frequency soil and radiation measurements and the Sodar/RASS data. The innovative data analysis procedure for the detection of near-ground free convection conditions (FCCs), the analysis of spectral characteristics of the turbulence during these situations and the analysis of the Sodar/RASS data was performed by myself. W. Babel supported me with his knowledge about spectral analysis methods. I alone wrote the complete text of the manuscript.
- B. Brötz contributed with many fruitful discussions and comments, especially in the review process of the publication.
- T. Foken supervised this work and contributed with many helpful ideas and discussions.

Appendix C

Eigenmann, R., Kalthoff, N., Foken, T., Dorninger, M., Kohler, M., Legain, D., Pigeon, G., Piguet, B., Schüttemeyer, D., Traulle, O., 2011. Surface energy balance and turbulence network during the Convective and Orographically-induced Precipitation Study (COPS). Quarterly Journal of the Royal Meteorological Society, 137: 57–69.

- This publication is an overview over the post-processing and quality control of the turbulence data of all sixteen stations of the surface energy balance and turbulence network during COPS. The network consisted of five different institutions (Department of Micrometeorology, University of Bayreuth; Institute for Meteorology and Climate Research, Karlsruhe Institute of Technology; Meteorological Institute, University of Bonn; Department of Meteorology and Geophysics, University of Vienna; CNRM-GAME, Météo France). Each institution conducted the field work during the experiment independently. Responsibilities for the field work of the Department of Micrometeorology were already mentioned with the publication above. Most institutions provided the results of the processing of the turbulence raw data with the software package TK2. For the University of Bonn and for our department, the processing of the data with TK2 was done by myself.

- My contribution was the development of a consistent turbulence data post-processing scheme applied to all sixteen measuring sites. I alone did the quality control of the turbulence data, including a footprint analysis and a check for internal boundary layers. For this purpose, each institution provided land use data for the corresponding sites.

- I myself performed the data analysis about some typical features of turbulent flux data and the occurrence of FCCs within the entire COPS region. I alone wrote the text of the manuscript including some comments of the coauthors.

- My supervisor T. Foken contributed to this publication through many discussions and initiated the scientific exchange between the different institutions involved.

Appendix D

Zhou, D., Eigenmann, R., Babel, W., Foken, T., Ma, Y., 2011. Study of near-ground free convection conditions at Nam Co station on the Tibetan Plateau. Theoretical and Applied Climatology, 105: 217–228.

- The data used in this publication were provided by the Institute of Tibetan Plateau Research, Chinese Academy of Sciences, within the framework of the scientific collaboration of this study originated by T. Foken and Y. Ma. This study aimed at demonstrating the applicability of the method for the detection of FCCs also in another investigation area with a different setting of heterogeneity (land-lake surface).
- I myself, W. Babel and T. Foken introduced D. Zhou into the post-processing of the turbulence data, including the usage of TK2 and footprint analysis tools, and into the investigation and relevance of FCCs at Nam Co station.
- D. Zhou performed the processing of the data under close instruction of myself and W. Babel. D. Zhou also wrote a first version of the manuscript.
- I myself intensively revised and rephrased the initial manuscript version of D. Zhou before submission.
- T. Foken, W. Babel and Y. Ma contributed to the progress of the manuscript in several discussions.

Appendix E

Brötz, B., Eigenmann, R., Dörnbrack, A., Foken, T., Wirth, V., 2013. Early-morning flow transition in a valley in low-mountain terrain. Boundary-Layer Meteorology, submitted.

- B. Brötz was responsible for the performance of the applied large-eddy simulations (LES) under the guidance of V. Wirth and A. Dörnbrack.
- The observational data from COPS, necessary for the adaption of the model to the complex terrain of a segment of the Kinzig valley, were provided by myself and T. Foken.

- The scientific content of this study was intensively discussed in many fruitful meetings of the coauthors. Each of them contributed with ideas on data analyses in manifold ways. The study aimed at investigating the convective structures in the valley during the observed FCCs responsible for the transport of surface layer air masses into higher regions of the boundary layer. Simulated data was compared with the observations. A great number of telephone conferences between myself and B. Brötz refined the content of the manuscript and led to its final version.
- The text was written in close cooperation with myself and B. Brötz considering many helpful comments of the supervisors. I myself mainly wrote the introduction of the observational data (Section 2.1), the interpretation of the modification of the energy balance closure during FCCs (Section 3.1) and the interpretation of the observations and the simulations with respect to the vertical transport situation during FCCs (Section 3.3). A. Dörnbrack strongly supported the writing in the part of the description of the model (Section 2.2).

Appendix B: Eigenmann et al. (2009)

Atmos. Chem. Phys., 9, 8587–8600, 2009
www.atmos-chem-phys.net/9/8587/2009/

Atmospheric Chemistry and Physics

Generation of free convection due to changes of the local circulation system

R. Eigenmann[1], **S. Metzger**[1,*], **and T. Foken**[1]

[1]Department of Micrometeorology, University of Bayreuth, Bayreuth, Germany
[*]now at: Institute for Meteorology and Climate Research – Atmospheric Environmental Research (IMK-IFU), Karlsruhe Institut of Technology, Garmisch-Partenkirchen, Germany

Received: 31 March 2009 – Published in Atmos. Chem. Phys. Discuss.: 7 May 2009
Revised: 29 October 2009 – Accepted: 5 November 2009 – Published: 12 November 2009

Abstract. Eddy-covariance and Sodar/RASS experimental measurement data of the COPS (Convective and Orographically-induced Precipitation Study) field campaign 2007 are used to investigate the generation of near-ground free convection conditions (FCCs) in the Kinzig valley, Black Forest, Southwest Germany. The measured high-quality turbulent flux data revealed that FCCs are initiated near the ground in situations where moderate to high buoyancy fluxes and a simultaneously occurring drop of the wind speed were present. The minimum in wind speed – observable by the Sodar measurements through the whole vertical extension of the valley atmosphere – is the consequence of a thermally-induced valley wind system, which changes its wind direction from down to up-valley winds in the morning hours. Buoyancy then dominates over shear within the production of turbulence kinetic energy near the ground. These situations are detected by the stability parameter (ratio of the measurement height to the Obukhov length) when the level of free convection, which starts above the Obukhov length, drops below that of the sonic anemometer. An analysis of the scales of turbulent motions during FCCs using wavelet transform shows the occurrence of large-scale turbulence structures. Regarding the entire COPS measurement period, FCCs in the morning hours occur on about 50% of all days. Enhanced surface fluxes of latent and sensible heat are found on these days.

1 Introduction

The COPS (Convective and Orographically-induced Precipitation Study) field campaign was undertaken from 1 June to 31 August 2007 within the low mountain range of the Black Forest, the Vosges Mountains and the Swabian Jura with the Rhine rift valley as a pronounced topographic lowland plain in between (Wulfmeyer et al., 2008). Rainfall in the COPS area is characterized by subgrid-scale convection initiation (CI) processes, e.g. orographically or thermally-induced local circulation systems, triggered by the complex terrain, thus complicating the exact modeling and forecasting of precipitation events (Meißner et al., 2007; Barthlott et al., 2006). The problems of modeling convective clouds and precipitation – its time, amount and location – are the premature initiation of convection, the simulation of convective precipitation events as being too spatially widespread and the overestimation of precipitation on the windward compared to the lee side over low-mountain ranges, e.g. the Black Forest (Schwitalla et al., 2008).

The interaction of the land surface with the overlying atmosphere crucially affects the energy and water cycle over many temporal and spatial scales (Betts et al., 1996). The spatial distribution and patchiness of individual land use elements can have a strong impact on the atmospheric boundary layer (ABL) evolution and its thermodynamic structure, as changes of the surface energy budget directly influence the surface turbulent fluxes of moisture, momentum and heat, which act as the link between the atmosphere and the underlying soil-vegetation system (Pielke, 2001). Dynamical phenomena in the ABL can be related to changing surface characteristics, since gradients in sensible heat flux produced by evapotranspiration, albedo and soil property discontinuities induce local or secondary circulation systems (Segal and Arritt, 1992). Together with diurnal mountain winds developing over mountainous terrain (Whiteman, 1990), land surface-atmosphere interactions and the related physical processes within complex terrain are the key to the local occurrence and timing of the initiation of convection, cloud formation and precipitation (Hanesiak et al., 2004; Pielke, 2001; Chen and Avissar, 1994; Rabin et al., 1990; Banta, 1990, 1984; Raymond and Wilkening, 1980). Besides land-surface

Correspondence to: R. Eigenmann
(rafael.eigenmann@uni-bayreuth.de)

interactions and orography, mesoscale and synoptic scale features are important for convective processes (Wulfmeyer et al., 2007). Kottmeier et al. (2008) discusses several mechanisms relevant for CI in the COPS region.

The present study aims at the detection and the description of near-ground free convection conditions (FCCs) by using eddy-covariance (EC) measurements. FCCs can be detected at the height of the EC measurement (see Sect. 2.1) close to the ground with the help of the stability parameter (see Sect. 3.2) and occur if the buoyancy term dominates over the shear term within the turbulence kinetic energy equation. In the case of detection of FCCs near the ground, convective elements are closely related to ground sources and can more effectively transport quantities of moisture, heat and trace gases enhanced in near-ground regions into the ABL. Moreover, following Shen and Leclerc (1995), the dimensions of our targeted land use type (corn field) of the EC measurements (see Sect. 2.1) are large enough (>250 m) that the surface fluxes are able to exert a major influence on ABL thermodynamics and turbulence structure.

Recently, Mayer et al. (2008) found that FCCs detected close to the bottom of a valley result in a strong and sudden ozone decrease at a mountain summit (Hohenpeissenberg) in the morning hours. In their study, the FCCs are triggered by a simultaneously occurring wind speed minimum, which reduces shear and leads to a dominance of buoyancy. On about half of the days these wind speed minima could be attributed to the onset of Alpine Pumping in the alpine foreland (Lugauer and Winkler, 2005) associated with a change of wind direction causing a drop of the horizontal wind speed. Hence, other mesoscale or local circulation systems initiated by complex terrain – e.g. the well known slope and valley winds in the Black Forest (Kossmann and Fiedler, 2000; Kalthoff et al., 2000) – are expected to trigger FCCs.

For that reason, the focus of the present study is to demonstrate the applicability of the EC method to the detection of FCCs in experimental data obtained during the COPS field campaign in the Kinzig valley (Black Forest), which was found in earlier studies (e.g., Meißner et al., 2007) to establish a pronounced diurnal thermally-induced valley wind system. Moreover, the processed turbulent flux data passing through a detailed quality assurance and control effort are used to select and describe these FCCs in detail.

2 Materials and methods

2.1 Site description and experiment set-up

During the COPS field campaign, a network of 17 energy balance and turbulence stations was set up over the entire COPS region (Wulfmeyer et al., 2007). The energy balance and turbulence station under investigation in the present study is located in the Kinzig valley near Fußbach (48°22′7.8″ N, 8°1′21.2″ E, 178 m a.s.l) on the western edge

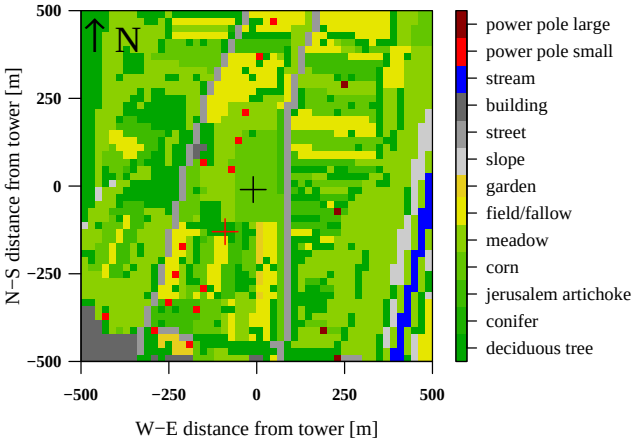

Fig. 1. Land use map ($1\times1\,km^2$) at the Fußbach site with the location of the eddy-covariance station indicated as a black cross in the middle of the map above the target land use type (corn). The additional red cross marks the position of the Sodar/RASS system. Fetch distances of the eddy-covariance system depending on wind sector can be obtained from Table 1.

of the Black Forest, Southwest Germany. The Kinzig valley at Fußbach is oriented in a N-S direction, thus specifying the main wind direction, and has a valley width of about 1.3 km. Mountain crests in the immediate vicinity of the Fußbach site reach maximal values of about 450 m a.s.l. The target land use type was a corn field (length: 260 m, width: 140 m) located within the patchy, agricultural land use of the Kinzig valley (see Fig. 1).

In this study, data of an EC tower and a nearby Sodar/RASS system are used. The EC system (measurement height: 2.29 m, sampling rate: 20 Hz) measured turbulent fluxes of momentum, sensible and latent heat as well as carbon dioxide (CO_2) above the corn field using a CSAT3 (Campbell Scientific, Inc.) sonic anemometer for recording the wind vector and the sonic temperature T_S and a LI-7500 (LI-COR Biosciences) open-path gas analyser for water vapor (H_2O) and CO_2 concentrations. The Sodar/RASS system consisted of a phase array Doppler Sodar DSDPA.90-64 with a 1290 MHz RASS extension by Metek GmbH and provided vertical profiles of wind velocity components, wind direction and acoustic temperature with a vertical resolution of 20 m and a temporal resolution of 10 min. More detailed information about the measuring set-up and background data can be obtained from Metzger et al. (2007).

2.2 Quality control effort

The EC flux data measured at the Fußbach site was processed and quality controlled applying the latest micrometeorological post-field data processing standards (e.g., Mauder et al., 2006) in order to obtain a data set of the desired quality and accuracy, which can be utilized for further fundamental

research. Accordingly, the turbulent flux raw data recorded with the EC method was post-processed with the comprehensive software package TK2 developed at the University of Bayreuth (Mauder and Foken, 2004), which comprises state of the art flux corrections and post-field quality control including tests on the fulfillment of integral turbulence characteristics and stationarity (Foken and Wichura, 1996; Foken et al., 2004).

Theoretical assumptions actually restrict the EC method to homogeneous terrain, but the increasing requirement for continuous monitoring of flux data (Aubinet et al., 2000; Baldocchi et al., 2001) forced the application of the EC method within highly structured terrain such as that in the COPS region. This step is supported by the development of a site evaluation and characterisation approach (Göckede et al., 2004, 2006), which combines the flux data quality approach (Foken et al., 2004) with a forward Lagrangian footprint model (Rannik et al., 2000, 2003). The approach is able to identify site-specific spatial quality structures and the spatial representivity of the measured flux data in the context of the underlying land use distribution and has been recently employed on sites of the CarboEurope network by Rebmann et al. (2005) and Göckede et al. (2008). In this study, it is used – together with an internal boundary layer evaluation procedure – in order to obtain target land use type-representative turbulent flux data sets of the required high quality usable for further analyses. The check for possible internal boundary layers, which form as a consequence of changes of the underlying surface characteristics, is implemented by using the following fetch-height relation to roughly estimate the height of the new equilibrium layer δ depending on fetch x (Raabe, 1983; Jegede and Foken, 1999) neglecting weak stability effects (Savelyev and Taylor, 2005):

$$z_a \leq \delta = 0.3\sqrt{x} \quad (1)$$

The aerodynamic measurement height z_a should be lower than δ in order to guarantee that the EC measurement takes place within the new equilibrium layer establishing over the target land use type.

2.3 Spectral analysis

Spectral analysis methods are used in this paper to study the temporal scales of the turbulence during the period of FCCs (see Sect. 3.2). Methods used are the continuous wavelet transform (CWT) and the computation of power spectra, both applied to the time series of EC raw data of the vertical wind speed, the horizontal wind speed components and the sonic temperature from 05:00 to 13:00 UTC.

To prepare data for the CWT, the time series were block averaged from the original 20 Hz raw data to a sampling frequency of 0.5 Hz in order to drastically reduce computational time of the CWT without altering the results significantly (e.g., Thomas and Foken, 2005) as the decisive scales range in the order of several seconds to a few minutes. Subsequently, all block averaged time series apart from the vertical wind speed (no trend removal necessary) have been detrended using polynomial regression. The resulting high-pass filtered time series is obtained by substracting the fitted polynomial from the block averaged time series. The residual time series is used for the calculation of the CWT using the Morlet wavelet. The CWT and plotting routine of the normalized wavelet power spectra was done by using the software package sowas (software for wavelet spectral analysis and synthesis: Maraun and Kurths, 2004; Maraun et al., 2007) implemented in the statistical computing software R. Results of a pointwise significance test (significance level: 0.95) performed by Monte Carlo simulations (1000 realizations) are indicated by black solid lines in the plots of the normalized wavelet power spectra.

The calculation of the power spectra of detrended (by polynomial regression) and tapered 20 Hz time series of the vertical wind speed, the longitudinal wind speed and sonic temperature before, during and after the period of FCCs within the time range from 05:00 to 13:00 UTC was realized by applying a fast Fourier transform (FFT) to the computed autocorrelation function. Smoothing of the raw periodogram was performed using a modified Daniell smoother window technique.

3 Results and discussion

3.1 Quality control of the turbulent flux measurements

This section presents some results of the detailed quality control effort adapted to the eddy-covariance flux data as described in Sect. 2.2.

Processed turbulent fluxes of sensible (Q_H) and latent heat (Q_E), friction velocity u_* as well as the CO_2 net ecosystem exchange *NEE* are depicted in Fig. 2 as Hovmøller-type plots where the color bar on the right side represents the calculated values with white areas indicating data failure (9.9% for each flux).

Furthermore, footprint analysis (see Sect. 2.2) were performed according to the site evaluation and characterisation approach of Göckede et al. (2004, 2006). To gain insight into the average flux contribution over the entire measurement period of the target land use type "corn" as a function of different wind sectors and stability classes, appropriate sorted data have been individually processed within the footprint analysis procedure. The results are listed in Table 1 and reveal good average flux contributions of more than 92% for all wind sectors during unstable or neutral cases. However, for stable stratification easterly and westerly sectors have to be considered critically, as flux contributions below 80% can be found, with the minimum (67%) in the 240° wind sector. Admittedly, the latter finding has to be regarded with the knowledge that the density of available data is low in the

Table 1. Average flux contribution [%] from the target land use type "corn" depending on wind sector and stability class at Fußbach. Moreover, the internal boundary layer evaluation procedure for average conditions over the entire measurement period is depicted. The internal boundary layer height δ calculated according to Eq. (1) with fetch x are listed in dependence of the 12 wind sectors distinguished. Wind sectors where δ falls below the average aerodynamic measurement height $z_a = 2.29$ m are flagged by "X".

	30°	60°	90°	120°	150°	180°	210°	240°	270°	300°	330°	360°
Average flux contribution from target land use type "corn" in %:												
Stable	92	77	82	86	86	89	86	67	73	69	84	89
Neutral	98	–	99	97	97	97	96	94	92	95	97	99
Unstable	99	100	100	100	100	99	99	99	99	99	99	100
Internal boundary layer evaluation:												
x [m]	141	83	68	84	113	102	89	59	49	66	101	162
δ [m]	3.56	2.73	2.47	2.75	3.19	3.03	2.83	2.30	2.10	2.44	3.01	3.82
z_a [m]	2.29	2.29	2.29	2.29	2.29	2.29	2.29	2.29	2.29 (X)	2.29	2.29	2.29

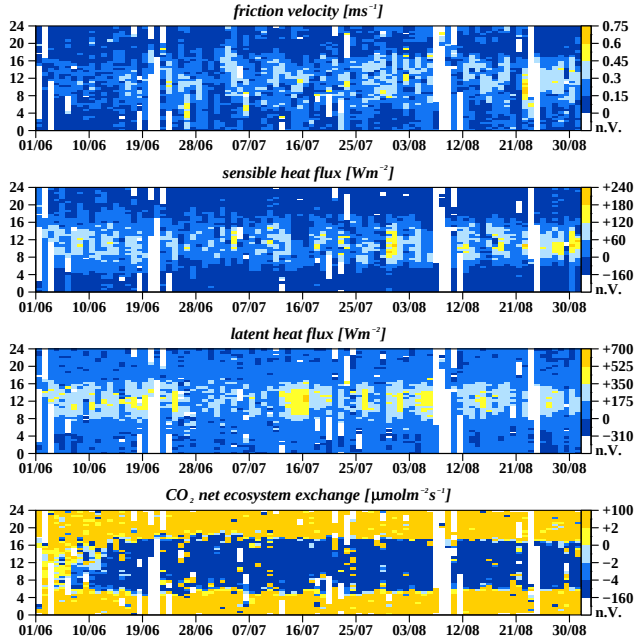

Fig. 2. Friction velocity u_* $\left[\mathrm{ms}^{-1}\right]$, sensible heat flux Q_H $\left[\mathrm{Wm}^{-2}\right]$, latent heat flux Q_E $\left[\mathrm{Wm}^{-2}\right]$ and CO_2 *NEE* $\left[\mu\mathrm{molm}^{-2}\mathrm{s}^{-1}\right]$ for the entire COPS measurement period at Fußbach. X-axis represents the day of the year, Y-axis the time of the day [UTC] and the attached color bar the calculated values, where n.V. indicates data failure.

easterly and westerly wind sectors as these do not lie within the main wind direction, thus weakening its influence on the overall assessment.

The results of the internal boundary layer evaluation of the eddy-covariance flux data as described in Sect. 2.2 are also depicted in Table 1, and are illustrative of average conditions over the entire measurement period and for the 12 wind sectors distinguished. Referring to Table 1, the 270° sector shows a greater aerodynamic measurement height z_a compared to the height of the new equilibrium layer δ, thus indicating that the flux measurements within this sector cannot be associated with the target land use type "corn" regarding average conditions over the entire measurement period. Also the data of the 240° sector should be discarded, as δ is in the same range as z_a indicating disturbed conditions.

The closure of the surface energy balance was also checked for the Fußbach site by plotting the sum of the turbulent fluxes Q_H and Q_E of each half-hourly measurement against the corresponding available energy $(-Q_S^* - Q_G)$ values, where $-Q_S^*$ is the net radiation and Q_G the ground heat flux. The heat storage in the upper soil layer for the calculation of Q_G was considered applying the "simple measurement" method after Liebethal and Foken (2007). A regression analysis revealed an average non-closure of 20.4% for the period of the entire COPS field campaign. The imbalance can primarily be attributed to the landscape heterogeneity assignable to the COPS region inducing unconsidered low-frequency flux contributions and advective flux components (Foken, 2008a; Foken et al., 2006). Indeed, large-eddy simulation studies recently revealed that turbulent organized structures (Kanda et al., 2004; Steinfeld et al., 2007) and secondary circulations (Inagaki et al., 2006) have an influence on the surface energy balance closure.

3.2 Generation of free convection at COPS IOP8b

The measurement of high-quality surface turbulent fluxes led to the detection of near-ground free convection conditions (FCCs) in the morning hours, not only at the site under investigation in this study (Fußbach), but also at other sites of the COPS energy balance and turbulence network (Eigenmann,

2008). Preliminary graphics produced in combination with routine data quality control during the COPS field phase consolidated recently observed indications (Mayer et al., 2008) that thermally-driven circulation systems may trigger FCCs in the morning hours, at times when the existing circulation system changes its previously prevailing wind direction. In the Kinzig valley a pronounced valley circulation system can frequently be observed to be generated in high-pressure situations with high solar radiation and weak synoptic forcing. At COPS IOP8b (15 July 2007) – outlined in this section as a paradigm for the generation of FCCs at Fußbach – the Sodargramm of the wind direction in Fig. 3a illustrates the cessation of the down-valley, southerly winds which prevail at night and the onset of up-valley, northerly blowing winds at about 08:30 UTC near the ground. During this transition period, a strong drop of the horizontal wind speed through the whole vertical extension of the valley atmosphere lasting from 06:50 until 08:50 UTC in the morning hours, with values smaller than $1.5\,\mathrm{ms}^{-1}$, is evident from Sodar measurements (Fig. 3b).

The occurrence of FCCs can be detected by the EC flux measurements by calculating the stability parameter ζ according to the following equation:

$$\zeta = \frac{z}{L} = -\frac{z \cdot \kappa \cdot g \cdot \left(\overline{w'\theta'_v}\right)_0}{\overline{\theta_v} \cdot u_*^3} \tag{2}$$

where z denotes the measurement height, L the Obukhov length, u_* the friction velocity, g the acceleration due to gravity, $\overline{\theta_v}$ the mean virtual potential temperature, $\left(\overline{w'\theta'_v}\right)_0$ the buoyancy flux at the surface and κ the von-Kármán constant ($\kappa \approx 0.4$). FCCs are indicated for $\zeta < -1$ (Foken, 2008b) as, according to Arya (2001), ζ is equal to the flux Richardson number R_f during unstable stratification ($R_f < 0$), which in turn is the quotient of the buoyancy term (B)

$$B = \frac{g}{\overline{\theta_v}} \cdot \left(\overline{w'\theta'_v}\right)_0 \tag{3}$$

to the shear term (S)

$$S = -\overline{u'w'} \cdot \frac{\partial \overline{u}}{\partial z} \tag{4}$$

of the turbulence kinetic energy equation. Consequently, $\zeta < -1$ indicates that buoyancy created turbulence dominates over shear created turbulence and that FCCs occur near the ground. The shear term S is the product of the momentum flux $\overline{u'w'}$ and the wind shear $\partial\overline{u}/\partial z$. Regarding the equation of ζ (Eq. 2), low values of u_* and high buoyancy fluxes will support the occurrence of FCCs. In the Kinzig valley, a powerful trigger mechanism for the occurrence of FCCs is provided by the change of the valley circulation system in the morning (Fig. 3a), which leads to a drop of the wind speed (and u_* by implication) near the ground (Fig. 3b) and thus to the domination of B over S and to $\zeta < -1$.

In Fig. 4a, the stability parameter ζ is depicted for COPS IOP8b, where the averaging period of the EC flux measurements (Fig. 4a–4f) was reduced from the standard 30 min to 5 min in order to enhance the temporal resolution. Data quality is good during the period of FCCs with quality flags after Foken et al. (2004) ranging from 1 to 3 within the 30 min data, 100% flux contribution from the target land use type "corn" and no disturbance due to internal boundary layers. Referring to Fig. 4a, FCCs with low values of ζ at 07:35–07:40 UTC correspond exactly to a 5 min duration local minimum of u_* ($0.04\,\mathrm{ms}^{-1}$) in Fig. 4c triggering the FCCs. Another period of FCCs, which can be detected from 08:10–08:40 UTC, shows stability parameter values up to $\zeta = -1.4$ and also coincides with a local minimum of u_* ($0.09\,\mathrm{ms}^{-1}$). Simultaneously, moderate values of Q_H (Fig. 4d) are found around the times of the FCCs ($54.7\,\mathrm{Wm}^{-2}$ at 08:25 UTC). Lower friction velocities u_* in general occur between 06:50 and 08:50 UTC explaining the generally small values of ζ and the occurence of FCCs during the period from 07:35 to 08:40 UTC (black dotted lines in Fig. 4a–h). In addition, Fig. 4h depicts the available energy at the ground ($-Q_S^* - Q_G$) for the portioning into Q_H (Fig. 4d) and Q_E (Fig. 4d), which can be expressed as the Bowen ratio Bo (Fig. 4f). Bo has its highest values (0.59 at 06:35 UTC) shortly before the period of FCCs demonstrating a preferred transformation of the available surface energy ($310\,\mathrm{Wm}^{-2}$ during the period of FCCs) into Q_H. The lowered values of ζ at about 18:00 UTC (see Fig. 4a) cannot be related with FCCs as values of Q_H are around zero ($-10 < Q_H < 10\,\mathrm{Wm}^{-2}$, see Fig. 4d) and data quality is very low (not shown).

Other parameters such as the ratio of the Deardorff velocity w_* (Deardorff, 1970a,b)

$$w_* = \left[\frac{g \cdot z_i}{\overline{\theta_v}} \cdot \left(\overline{w'\theta'_v}\right)_0\right]^{1/3} \tag{5}$$

to the friction velocity u_* confirm their capability to denote FCCs (see Fig. 4e), where the depth of the boundary layer z_i is determined by visual inspection of a secondary maximum in the reflectivity profiles of the Sodar measurements (Beyrich, 1997). General difficulties in z_i determination within complex terrain (Staudt, 2006; Kalthoff et al., 1998; Kossmann et al., 1998) and the high background noise of the nearby street at the Fußbach measurement site complicate the evaluation of the Sodar data. On most days, no clear secondary maximum of reflectivity can be found for the daytime boundary layer evolution, thus making the determination of z_i a rough estimate rather than an exact determination. However, Fig. 3c shows the measured reflectivity of the Sodar/RASS complex, together with the determined evolution of z_i in the morning hours between 04:00–11:40 UTC indicated as black points, thus enabling the calculation of w_* and the subsequent display of $w_* \cdot u_*^{-1}$ in Fig. 4e at the same time.

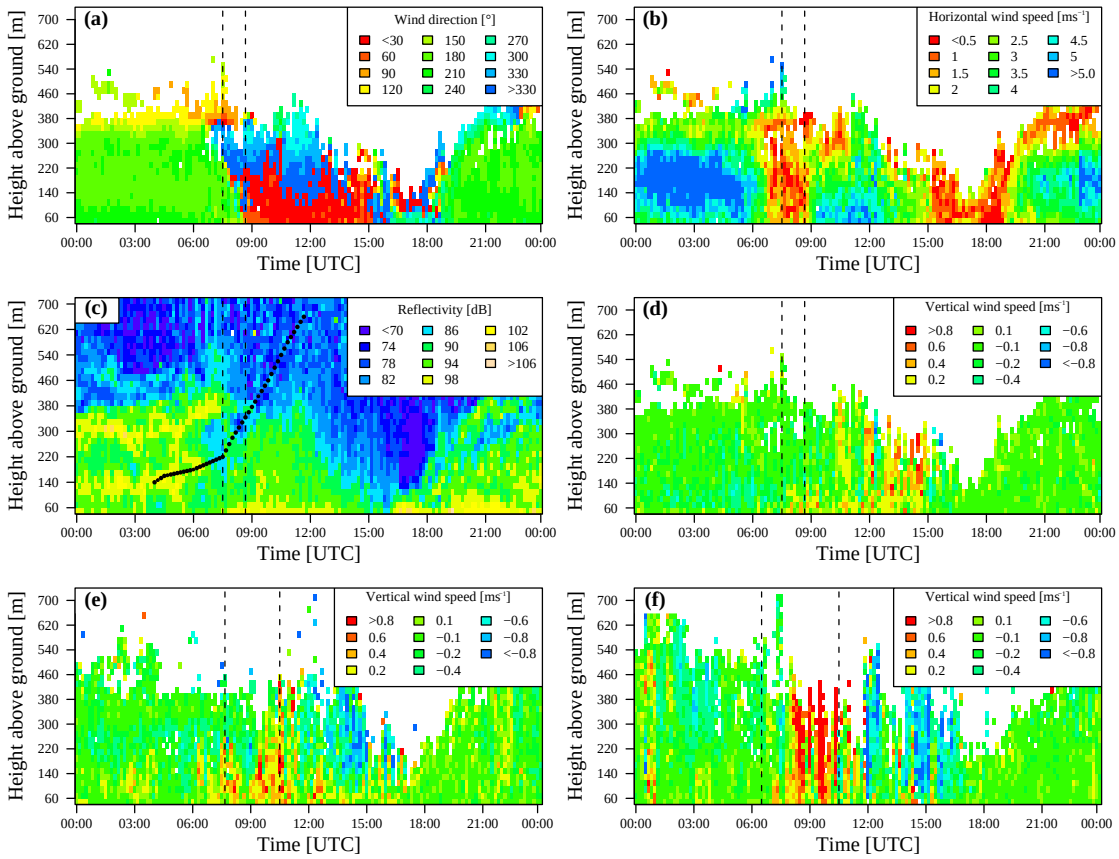

Fig. 3. Sodargramms of the wind direction $[^\circ]$ **(a)**, horizontal wind speed $\left[\mathrm{ms}^{-1}\right]$ **(b)**, reflectivity [dB] **(c)** and vertical wind speed $\left[\mathrm{ms}^{-1}\right]$ **(d)** for COPS IOP8b at Fußbach. Also plotted are the vertical wind speed $\left[\mathrm{ms}^{-1}\right]$ for COPS IOP15a **(e)** and COPS IOP15b **(f)** at Fußbach. The black dashed lines in each figure indicate the periods of FCCs in the morning hours: 07:35–08:40 UTC at IOP8b (see Fig. 4a), 07:45–10:35 UTC at IOP15a and 06:30–10:35 UTC at IOP15b. The black points in (c) represent the evolution of the boundary layer depth z_i between 04:00 and 11:40 UTC determined by visual inspection of a secondary maximum in the reflectivity profile.

Moreover, the ratio $B \cdot S^{-1}$ – calculated according to Eq. (3) and (4) – can be used directly to detect FCCs (see Fig. 4g). The wind shear $\partial\overline{u}/\partial z$, necessary for the calculation of S, was determined with the wind speeds at 4 and 9 m a.g.l. measured with the cup anemometers of an additionally installed profile mast at the corn field. Considering a canopy height of 2.31 m at COPS IOP8b results in aerodynamic measurement heights z_a of 2.46 m and 7.46 m, respectively. The remarkable minima in Fig. 4g at the times of the FCCs (07:35–08:40 UTC) underlines that the turbulence is mainly driven by buoyancy (B) rather than shear (S). The threshold of -3 (red dashed line in Fig. 4g) is chosen according to Stull (2000), which states favourable conditions for the generation of free convection for $|B| > |3 \cdot S|$.

So far, parameters indicating the occurrence of FCCs near the ground have been presented, but the impact these FCCs exert on boundary layer thermodynamics and structure has not been discussed yet.

A measure for convective activity in the ABL can be provided by our data set by the vertical wind speed measured with the Sodar/RASS complex (Fig. 3d-f). At COPS IOP8b, no increased upward vertical wind speeds can be found in the ABL during the period of FCCs (07:35–08:40 UTC, see Fig. 3d), but the onset of the first enhanced upward vertical wind speeds (0.2–0.6 ms^{-1}) can be observed close to the ground up to 140 m. However, this finding has to be considered with the knowledge that plume-like structures of rising air masses are a local phenomenon surrounded by areas of downdrafts (Stull, 1988). As the EC and Sodar/RASS measurement systems are spatially separated by about 170 m over different land use types (see Fig. 1) and the Sodar/RASS complex itself has a limited spatial and temporal resolution (10 min), it is clear that enhanced vertical wind speeds cannot be detected during each period of FCCs. On other days, however, the periods of FCCs detected close to the ground in the morning hours can be related to increased upward vertical

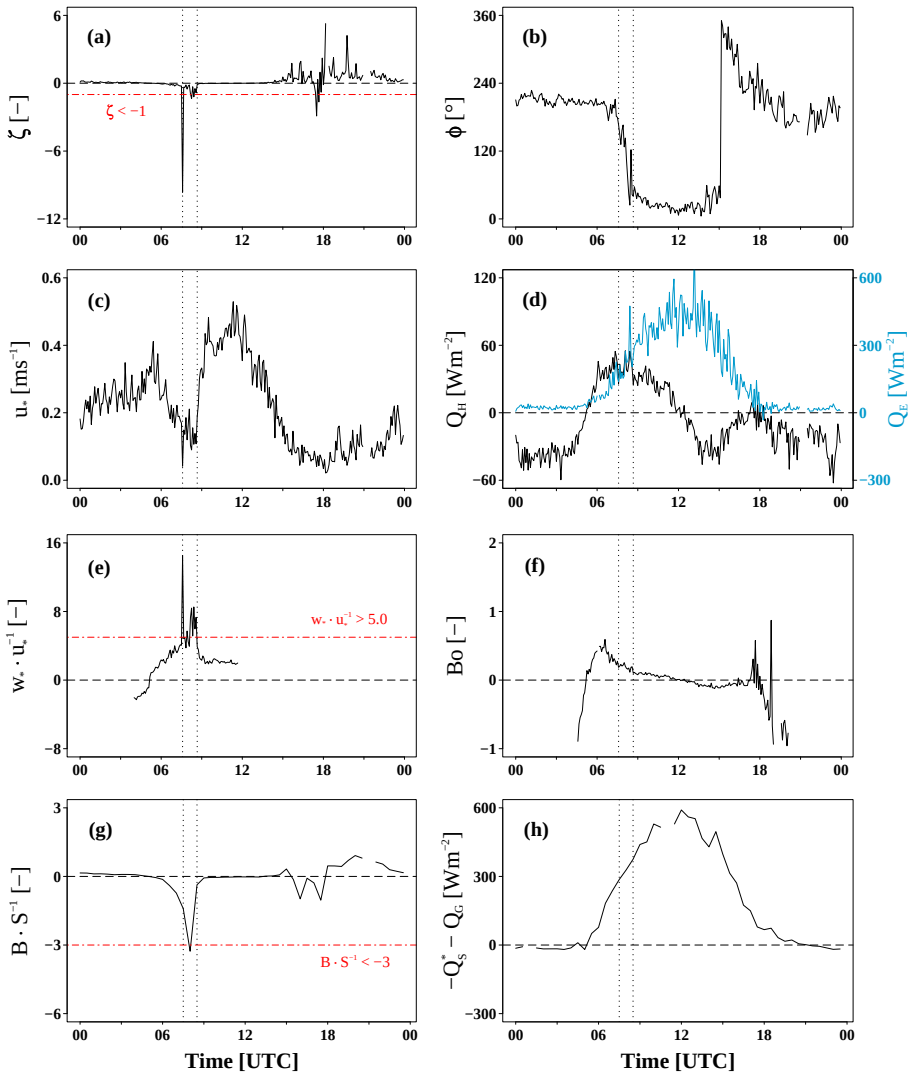

Fig. 4. Stability parameter ζ [−] **(a)**, wind direction ϕ [°] **(b)**, u_* $\left[\mathrm{ms}^{-1}\right]$ **(c)**, Q_H and Q_E $\left[\mathrm{Wm}^{-2}\right]$ **(d)**, $B \cdot S^{-1}$ [−] (a), available energy $-Q_S^* - Q_G$ $\left[\mathrm{Wm}^{-2}\right]$ (b), $w_* \cdot u_*^{-1}$ [−] (c) and Bo [−] (d) for COPS IOP8b at Fußbach. The black dotted lines in each graph indicate the period of FCCs in the morning hours (07:35 UTC to 08:40 UTC) detected by the low values of ζ.

wind speeds within the whole vertical extension of the ABL. As an example, the Sodargramms of the vertical wind speed at the high-pressure situations COPS IOP15a (12 August 2007) and IOP15b (13 August 2007) are shown in Fig. 3e and 3f, respectively, which both show strong enhanced vertical wind speeds of locally more than 0.8 ms^{-1} within the 10 min averaged values during the periods of FCCs.

Furthermore, the coherent structure of plume-like upward motions at COPS IOP8b can be assumed when regarding the turbulent time series of vertical wind speed, sonic temperature, humidity and carbon dioxide (not shown) as visual inspection of them during the period of FCCs clearly reveals ramp-like structures typical for coherent turbulent exchange (e.g., Gao et al., 1989; Bergström and Högström, 1989).

To explicitly investigate the turbulence structure during the period of FCCs at COPS IOP8b, spectral analysis of the measured high-frequency turbulent time series (see Sect. 2.3) is utilized to reveal the scales of inherent turbulent eddies. Therefore, Fig. 5a and 5b show the normalized wavelet power spectra of the vertical wind speed and sonic temperature, respectively, where the temporal section on the X-axis ranges from 05:00 to 13:00 UTC (480 min). It is obvious from the normalized wavelet power spectrum of the vertical wind speed (Fig. 5a), that during the period of FCCs (07:35–08:40 UTC) – marked by the black dotted vertical lines – a clear shift of significant areas of enhanced spectral power from high-frequency turbulence scales towards scales of lower frequency occurs. In particular, scales in the range

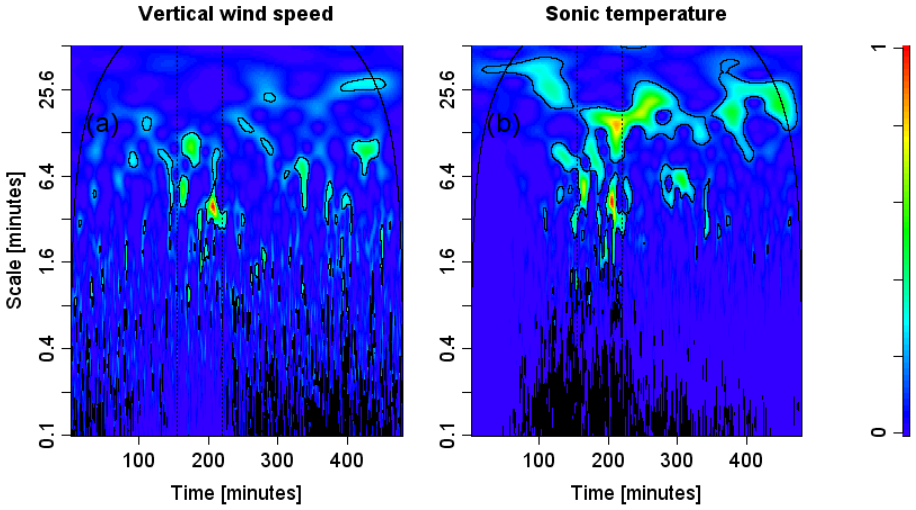

Fig. 5. Normalized wavelet power spectra of the vertical wind speed **(a)** and sonic temperature **(b)** from 05:00–13:00 UTC (480 min) for COPS IOP8b at Fußbach. The period of FCCs in the morning hours from 07:35–08:40 UTC is indicated by the black dotted vertical lines. The results of a pointwise significance test (significance level: 0.95) performed by Monte Carlo simulations (1000 realizations) are also shown in the plots marked by black solid lines. The cone of influence is visible as a black curved line in the upper part of both plots.

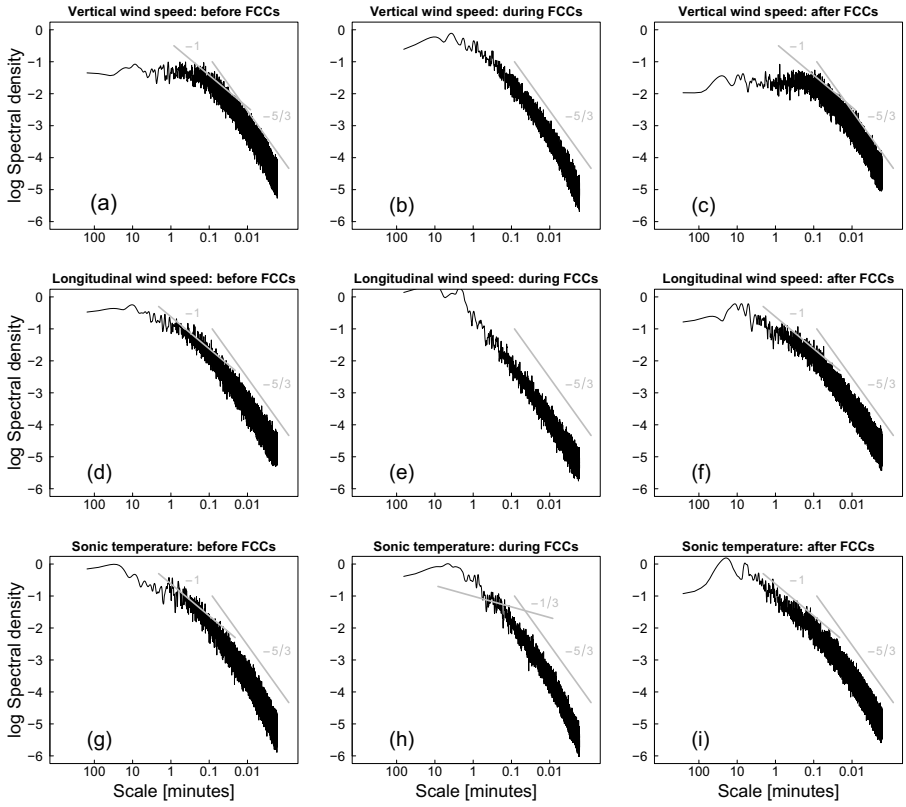

Fig. 6. Power spectra of the vertical wind speed **(a–c)**, longitudinal wind speed **(d–f)** and sonic temperature **(g–i)**, before (05:00–07:35 UTC), during (07:35–08:40 UTC) and after (08:40–13:00 UTC) the period of FCCs for COPS IOP8b at Fußbach. The chosen time periods coincide with those distinguished in Fig. 5 by the black dotted vertical lines. The gray solid lines indicate the $-5/3$, -1 and $-1/3$ power laws.

of 1 to 7 min experience an enormous gain in spectral power during the period of FCCs. These time scales can be associated with the time t_* it takes for air in plumes or thermals to cycle once between the bottom and the top of the mixed layer which is stated, e.g. in Stull (1988), to range in the order of 5 to 15 min in the case of a well developed convective boundary layer (CBL). Considering the time of occurrence of the period of FCCs early in the morning hours within a growing CBL (see Fig. 3c) which inhibits larger circulation structures, our findings seem to be in good accordance with the textbook values. In our case, the average time scale $t_* = z_i \cdot w_*^{-1}$ during the period of FCCs (07:35–08:40 UTC) – calculated with an average z_i of 285 m (see Fig. 3c) and an average w_* of $0.75\,\mathrm{ms}^{-1}$ (see Fig. 4c and 4e; values of w_* in the order of 1 to $2\,\mathrm{ms}^{-1}$ are given, e.g. in Stull, 1988) – amounts to $t_* = 6.3$ min.

Figure 5b also depicts the normalized wavelet power spectrum of the sonic temperature, which shows a slightly different behavior compared to that of the vertical wind speed (Fig. 5a) discussed above. Spectral power during the period of FCCs is also enhanced within scales in the range of 1 to 7 min (a second maximum can be found at around 13 min), but high-frequency turbulent scales are still present during the period of FCCs contrary to the finding in the normalized wavelet power spectrum of the vertical wind speed. A possible explanation might be that the highly fluctuating temperature field close to the strongly heated surface causes a non-correlation between the wind and temperature field and, consequently, a different turbulent regime within the high-frequency part of the vertical wind speed and the temperature during the period of FCCs.

Spectral characteristics of the turbulence during the period of FCCs at COPS IOP8b are further examined by plots of the computed power spectra (see Sect. 2.3) of the vertical wind speed (Fig. 6a–c), the longitudinal wind speed (Fig. 6d–f) and the sonic temperature (Fig. 6g–i), before (05:00–07:35 UTC), during (07:35–08:40 UTC) and after (08:40–13:00 UTC) the period of FCCs. All depicted power spectra clearly show Kolmogorov's $-5/3$ power law (Kolmogorov, 1941) within a subset in the inertial subrange. However, at lower frequencies, towards production scales, the shape of the spectra should depend on atmospheric stability as demonstrated, e.g. in Monin and Yaglom (1975, Chap. 8), with experimental results of Gurvich (1960, 1962) and Zubkovskii (1962), who found that wind velocity spectra satisfy the $-5/3$ power law over a certain region, but show a clear dependence on different values of the Richardson number at the lower limit of the inertial subrange. Similar experimental results have been reported, e.g. by Kaimal et al. (1972), who showed that normalized velocity and temperature spectra converge within the inertial subrange corresponding to Kolmogorov's power law, but spread out depending on ζ at the lower frequency part of the spectra. In accordance to the studies mentioned above, our computed power spectra, especially that of the vertical (Fig. 6a–c) and longitudinal (Fig. 6d–f) wind speed, experience an appreciable gain of spectral power within time scales greater than 0.5 min during the period of FCCs compared to the power spectra before and after the period of FCCs characterized by near-neutral conditions. It is obvious that the scale of maximal spectral power of the vertical wind speed during the period of FCCs (Fig. 6b), which is found at about 4 min, coincides with the time scales of maximal power observed in the normalized wavelet power spectrum of the vertical wind speed (Fig. 5a). Moreover, the study of Katul et al. (1995) is used to gain more insight into the spectral characteristics within the low-frequency part of our power spectra concerning a possible existence of a -1 power law and its deviation due to buoyancy. Katul et al. (1995) reported a -1 power law evident in the vertical and longitudinal wind speed and in the temperature power spectra during near-neutral atmospheric stratification, which can more or less be confirmed considering our power spectra before and after the period of FCCs (Fig. 6a, c, d, f, g, i) where neutral conditions are present. It has to be mentioned that the existence of a -1 power law for the vertical wind speed in the neutral case was found by Katul et al. (1995) to be only of limited extent (in accordance with our findings) and its existence is also considered to be controversial in the discussion of Katul and Chu (1998). Considering now the behavior of the low-frequency spectral characteristics during the period of FCCs, it is noticeable that the existence of a $-5/3$ power law in the inertial subrange in the case of the vertical (Fig. 6b) and longitudinal (Fig. 6e) wind speed can be extended towards the production scales, which is also stated by Katul et al. (1995) for the free convection stability regime. In the case of the temperature power spectrum Katul et al. (1995) referred to the existence of a $-1/3$ power law which can only be confirmed for a limited region, considering our temperature power spectrum (Fig. 6h). Finally, it is worthwhile to point out that our definition of the free convection regime ($\zeta < -1$) differs from that ($\zeta < -2$) used in Katul et al. (1995), so that the power laws corresponding to the case of moderately unstable conditions ($0.14 < \zeta < -1.3$) in the sense of Katul et al. (1995), i.e. a -2, a -1 and a -1 power law for the longitudinal and vertical wind speed and the temperature power spectra, respectively, may also be applied to our data, as average stability values during our period of FCCs ($\zeta = -1.3$) may also be associated with the upper edge of the moderately unstable regime of Katul et al. (1995). Nevertheless, to summarize our findings, the effect of FCCs on the spectral characteristics of the turbulence is clearly visible in our study.

3.3 FCCs during the entire COPS measurement period

Having outlined the generation of FCCs due to a change of the valley wind system in detail for COPS IOP8b within the previous section, the entire measurement period should now be regarded. At Fubach, 23 days, which make up 25% of the 92 days observed in the COPS field campaign, can be

Table 2. Mean onset and cessation times [UTC] of the up-valley wind direction and the mean times of FCCs of those days classified as "event days", with standard deviation (SD), and number (n) for the individual months (June, July, August) and for the whole COPS measurement period at Fußbach.

Onset of up-valley wind direction				Cessation of up-valley wind direction				FCCs			
Period	Mean	SD	n	Period	Mean	SD	n	Period	Mean	SD	n
June	08:01	01:14	8	June	17:36	00:55	7	June	07:33	01:08	8
July	08:03	00:37	5	July	17:23	01:35	5	July	08:14	00:51	5
August	09:06	00:46	10	August	17:56	01:10	10	August	08:48	00:42	10
whole	08:29	01:02	23	whole	17:42	01:10	22	whole	08:14	01:01	23

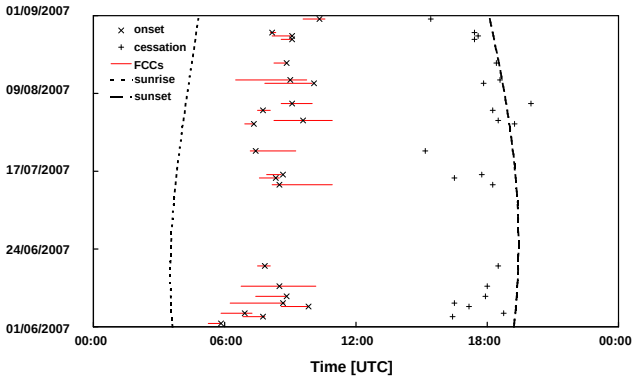

Fig. 7. Onset and cessation times of the up-valley wind direction and the corresponding periods of FCCs in the morning hours at days classified as "event days" regarding the entire COPS measurement period at Fußbach. Also depicted are the times of sunrise and sunset.

classified as "event days" coinciding with the paradigm of the generation of FCCs at COPS IOP8b outlined in Sect. 3.2. Furthermore, 19 days (21%) can be denoted as "intermittent days", as they do not exhibit a clear diurnal, persistent valley wind circulation. FCCs occur but can only be attributed to brief duration – several minutes up to a few hours – changes from down-valley to up-valley winds during the day, these sometimes not even reaching a full wind rotation of 180°. Despite the fact that most of the FCCs of these "intermittent days" seem to be triggered by short changes of wind direction of varying duration, it was decided to separate the "intermittent" from the "event days" in order to have similar flow patterns initiating the FCCs and thus a clearly structured data set. The reason for the intermittence of the valley winds is a decrease of the solar energy input, e.g. due to cloud shading. Finally, 37 days (40%) at Fußbach can be characterized as "non-event days", as FCCs do not appear. Thirteen days (14%) cannot be evaluated due to data failure.

Figure 7 shows all days classified as "event days" (23) with the onset and cessation times of the up-valley wind direction, the periods in which FCCs occurred and the times of sunrise and sunset during the entire COPS campaign. The mean onset and cessation times of the up-valley wind direction and the mean times of FCCs of those days classified as "event days", with standard deviation and number, are listed in Table 2 for the individual months and the whole measurement period. Remarkable is the adjustment of the onset of the up-valley wind direction and of the FCCs to the seasonal change of sunrise evident in the mean values of the individual months. The mean duration of the periods in which FCCs occur – depicted in Fig. 7 – is 84 min with a standard deviation of 57 min.

To clarify the difference of "event" and "intermittent days" as related to the diurnal valley wind system, persistence values P were calculated from the west-east and south-north components (u and v, respectively) and the horizontal wind speed v_h of the EC sonic anemometer following Lugauer and Winkler (2005):

$$P(t) = \frac{\sqrt{\overline{u(t)}^2 + \overline{v(t)}^2}}{\overline{v_h(t)}} \quad (6)$$

where the temporal vector mean of the horizontal wind speed is divided by the arithmetic mean of the horizontal wind speed at every time of the day. P can adopt values between 0 and 1, where 1 means that every day at that time the wind blew from the same direction. Figure 8a depicts the calculated persistence P for all days, "event days", "intermittent days" and "non-event days". Two pronounced eye-catching minima can be found the "event days", i.e. one at the times the up-valley winds start (at about 08:00 UTC) and another at the times the up-valley winds rotate back to down-valley winds (at about 18:00 UTC), indicating highly variable wind directions during these times. The P values above 0.75 for the rest of the time point to a quasi-identical flow pattern on the 23 selected "event days" at Fußbach. The small persistence values of the "intermittent days" between 06:00 and 18:00 UTC can be attributed to the non-persistence of the up-valley winds, as briefly lasting up-valley winds are interrupted by frequent rotations back to the original wind direction due to a decrease of the solar energy input (through cloud shading) which otherwise usually drives constantly blowing up-valley winds.

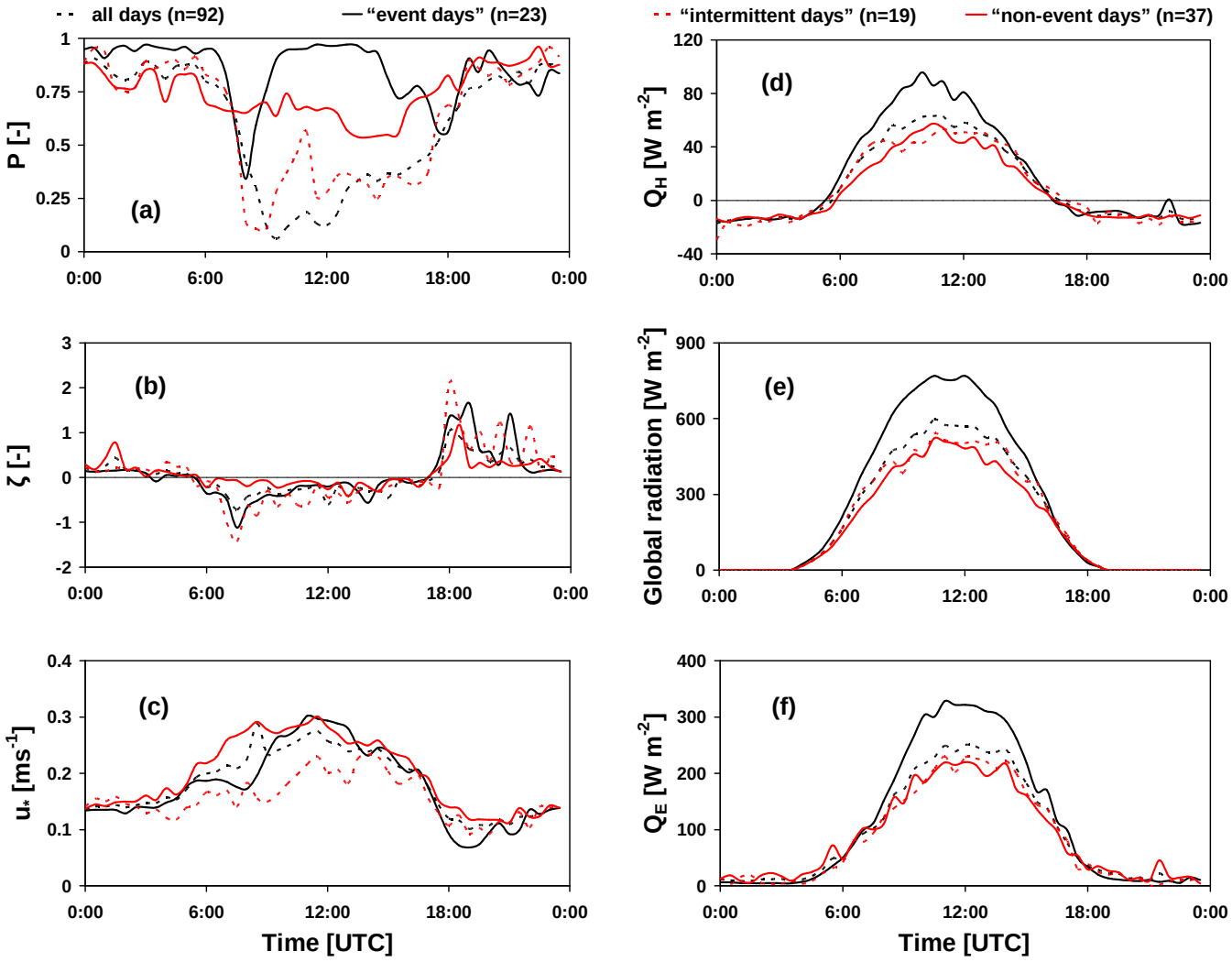

Fig. 8. Persistence P $[-]$ **(a)** and mean diurnal trends of the stability parameter ζ $[-]$ **(b)**, friction velocity u_* $\left[\mathrm{ms}^{-1}\right]$ **(c)**, sensible heat flux Q_H $\left[\mathrm{Wm}^{-2}\right]$ **(d)**, global radiation $\left[\mathrm{Wm}^{-2}\right]$ **(e)** and latent heat flux Q_E $\left[\mathrm{Wm}^{-2}\right]$ **(f)** for all days of the COPS measurement period (92), days classified as "event days" (23), "intermittent days" (19) and "non-event days" (37) at Fußbach. Thirteen days cannot be classified due to data failure.

Mean diurnal trends of ζ (Fig. 8b), u_* (Fig. 8c), Q_H (Fig. 8d), global radiation (Fig. 8e) and Q_E (Fig. 8f) of the individually classified days can be applied to characterize the FCCs. The mean values of ζ indicate the occurrence of FCCs in the morning hours at about 08:00 UTC on both "intermittent" and "event days". After this distinct minima of ζ at about 08:00 UTC (until about 12:00 UTC), the "intermittent days" show slightly lower values of ζ, indicating that the intermittence of the valley wind system causes more frequent triggering of FCCs. A clear difference in the magnitude of u_* comparing "event" and "non-event days" (see Fig. 8c) at about 08:00 UTC underlines that the drop of u_* caused by the valley wind reversal in the morning hours triggers FCCs. The generally lower values of u_* on the "intermittent days" can be explained by the non-persistence of the valley winds resulting in a continuous drop of the horizontal wind speed. Above-average values of Q_H and global radiation (Figs. 8d and 8e) can be found on the "event days", thus indicating the preferred occurrence of FCCs in clear, undisturbed weather situations with high solar radiation driving the valley winds, which act as the trigger mechanism for FCCs by providing the necessary minimum of u_* in the early morning transition period. Moreover, about 100 Wm^{-2} higher Q_E values (Fig. 8f) can be observed on the "event days" compared to the "non-event days", which also contribute, due to density effects, to the destabilization of near-ground air masses.

4 Conclusions

A comprehensive quality assurance and control effort, including footprint analysis and a check for internal boundary layers, was adapted to the EC turbulence measurements at Fußbach in order to obtain high-quality surface flux data usable for the detection ($\zeta < -1$) and description of FCCs in the Kinzig valley. FCCs were found to be triggered by a change of the local valley circulation system from down to up-valley winds in the morning hours and occurred on about half of the total 92 COPS days summing up days classified as "event" and "intermittent days". This frequent occurrence of FCCs confirms the assumption of Mayer et al. (2008) that other regions showing complex terrain – besides the alpine foreland investigated in their study – might face trigger mechanisms, such as local or mesoscale circulation systems leading to the convective release of near-ground air masses into the ABL. FCCs initiated by a change of the valley winds were also found by Hiller et al. (2008) in an alpine valley in Switzerland following their stability and data quality analysis. Unfortunately, these authors did not address these events. The large-eddy scale character of the turbulence near the ground during periods of FCCs could be confirmed by applying spectral analysis methods (see Figs. 5 and 6), thus suggesting that plume-like coherent structures of rising air masses emerge from the detected FCCs. These large-scale structures can more effectively transport quantities of heat and moisture enhanced in near-ground regions into the ABL. As enhanced surface fluxes of latent and sensible heat were found on the "event days" compared to "non-event days" (see Fig. 8) as well as increased upward vertical wind speeds in the Sodar measurements during FCCs (see Figs. 3e and 3f), a clear effect of the detected FCCs on the thermodynamic structure of the ABL is obvious. To sum up, FCCs are likely – in addition to other orographic or landscape effects – to have a non-negligible impact on ABL temperature and moisture profiles and to play a role for CI processes.

In order to directly simulate the impact of FCCs on ABL thermodynamics and on possibly subsequent cloud formation, a large-eddy simulation (LES) model will be applied for further investigations.

Acknowledgements. The project was funded within the Priority Program 1167 "Quantitative Precipitation Forecast PQP (Praecipitationis Quantitativae Predictio)" by the German Science Foundation (DFG), second and third (Fo 226/19-1) period. The authors wish to acknowledge the support and data provision by the participants of the COPS experiment and the COPS Operations Center as well as Björn Brötz for many fruitful discussions and comments. Last but not least, the authors want to thank all people which took part in the field work, especially Andrei Serafimovich, Lukas Siebicke, Katharina Staudt, Johannes Lüers and Johannes Olesch.

Edited by: G. Vaughan

References

Aubinet, M., Grelle, A., Ibrom, A., Rannik, U., Moncrieff, J., Foken, T., Kowalski, A. S., Martin, P. H., Berbiger, P., Bernhofer, C., Clement, R., Elbers, J. A., Granier, A., Grünwald, T., Morgenstern, K., Pilegaard, K., Rebmann, C., Snijders, W., Valentini, R., and Vesala, T.: Estimates of the Annual Net Carbon and Water Exchange of Forests The EUROFLUX Methodology, Adv. Ecol. Res., 30, 113–176, 2000.

Baldocchi, D., Falge, E., Gu, L. H., Olson, R., Hollinger, D., Running, S., Anthoni, P., Bernhofer, C., Davis, K., Evans, R., Fuentes, J., Goldstein, A., Katul, G., Law, B., Lee, X. H., Malhi, Y., Meyers, T., Munger, W., Oechel, W., U, K. T. P., Pilegaard, K., Schmid, H. P., Valentini, R., Verma, S., Vesala, T., Wilson, K., and Wofsy, S.: FLUXNET: A new tool to study the temporal and spatial variability of ecosystem-scale carbon dioxide, water vapor, and energy flux densities, B. Am. Meteorol. Soc., 82, 2415–2434, 2001.

Banta, R. M.: Daytime Boundary-Layer Evolution over Mountainous Terrain. Part 1: Observations of the Dry Circulations, Mon. Weather. Rev., 112, 340–356, 1984.

Banta, R. M.: The role of mountain flows in making clouds, in: Atmospheric processes over complex terrain, edited by Blumen, W., vol. 23 (45) of *Meteorological monographs*, pp. 229–283, American Meteorological Society, 1990.

Barthlott, C., Corsmeier, U., Meißner, C., Braun, F., and Kottmeier, C.: The influence of mesoscale circulation systems on triggering convective cells over complex terrain, Atmos. Res., 81, 150–175, 2006.

Bergström, H. and Högström, U.: Turbulent exchange above a pine forest. II. Organized structures., Bound.-Lay. Meteorol., 49, 231–263, 1989.

Betts, A. K., Ball, J. H., Beljaars, A. C. M., Miller, M. J., and Viterbo, P. A.: The land surface-atmosphere interaction: A review based on observational and global modeling perspectives, J. Geophys. Res.-Atmos., 101, 7209–7225, 1996.

Beyrich, F.: Mixing height estimation from sodar data – A critical discussion, Atmos. Environ., 31, 3941–3953, 1997.

Chen, F. and Avissar, R.: Impact of Land-Surface Moisture Variability on Local Shallow Convective Cumulus and Precipitation in Large-Scale Models, J. Appl. Meteorol., 33, 1382–1401, 1994.

Deardorff, J. W.: Convective Velocity and Temperature Scales for the Unstable Planetary Boundary Layer and for Rayleigh Convection, J. Atmos. Sci., 27, 1211–1213, 1970a.

Deardorff, J. W.: Preliminary Results from Numerical Integrations of the Unstable Planetary Boundary Layer, J. Atmos. Sci., 27, 1209–1211, 1970b.

Eigenmann, R.: Investigation of conditions initiating free convection using energy exchange measurements. COPS-experiment, Black Forest, 2007, Master's thesis, University of Bayreuth, Germany, 2008.

Foken, T.: The energy balance closure problem: An overview, Eco. Appl., 18, 1351–1367, 2008a.

Foken, T.: Micrometeorology, Springer, New York, 1st edn., 2008b.

Foken, T. and Wichura, B.: Tools for quality assessment of surface-based flux measurements, Agr. Forest. Meteorol., 78, 83–107, 1996.

Foken, T., Göckede, M., Mauder, M., Mahrt, L., Amiro, B. D., and Munger J. W.: Post-field data quality control, in: Handbook of Micrometeorology: A Guide for Surface Flux Measurement and

Analysis, edited by Lee, X., Massman, W., and Law, B., 181–208, Kluwer, Dordrecht, 2004.

Foken, T., Wimmer, F., Mauder, M., Thomas, C., and Liebethal, C.: Some aspects of the energy balance closure problem, Atmos. Chem. Phys., 6, 4395–4402, 2006.

Gao, W., Shaw, R. H., and Paw U, K. T.: Observation of organized structures in turbulent flow within and above a forest canopy, Bound.-Lay. Meteorol., 47, 349–377, 1989.

Göckede, M., Rebmann, C., and Foken, T.: A combination of quality assessment tools for eddy covariance measurements with footprint modelling for the characterisation of complex sites, Agr. Forest. Meteorol., 127, 175–188, 2004.

Göckede, M., Markkanen, T., Hasager, C. B., and Foken, T.: Update of a footprint-based approach for the characterisation of complex measurement sites, Bound.-Lay. Meteorol., 118, 635–655, 2006.

Göckede, M., Foken, T., Aubinet, M., Aurela, M., Banza, J., Bernhofer, C., Bonnefond, J. M., Brunet, Y., Carrara, A., Clement, R., Dellwik, E., Elbers, J., Eugster, W., Fuhrer, J., Granier, A., Grunwald, T., Heinesch, B., Janssens, I. A., Knohl, A., Koeble, R., Laurila, T., Longdoz, B., Manca, G., Marek, M., Markkanen, T., Mateus, J., Matteucci, G., Mauder, M., Migliavacca, M., Minerbi, S., Moncrieff, J., Montagnani, L., Moors, E., Ourcival, J. M., Papale, D., Pereira, J., Pilegaard, K., Pita, G., Rambal, S., Rebmann, C., Rodrigues, A., Rotenberg, E., Sanz, M. J., Sedlak, P., Seufert, G., Siebicke, L., Soussana, J. F., Valentini, R., Vesala, T., Verbeeck, H., and Yakir, D.: Quality control of CarboEurope flux data - Part 1: Coupling footprint analyses with flux data quality assessment to evaluate sites in forest ecosystems, Biogeosciences., 5, 433–450, 2008.

Gurvich, A. S.: Experimental investigation of frequency spectra of the vertical wind velocity in the atmospheric surface layer, Dokl. Akad. Nauk SSSR, 132, 806–809, 1960.

Gurvich, A. S.: Spectra of the vertical wind-velocity fluctuations and their relation to micrometeorological conditions, Atmospheric Turbulence, (Proc. In-ta Fiziki Atmosf. Akad. Nauk SSSR, No. 4), 101–136, 1962.

Hanesiak, J. M., Raddatz, R. L., and Lobban, S.: Local initiation of deep convection on the Canadian prairie provinces, Bound.-Lay. Meteorol., 110, 455–470, 2004.

Hiller, R., Zeeman, M. J., and Eugster, W.: Eddy-covariance flux measurements in the complex terrain of an Alpine valley in Switzerland, Bound.-Lay. Meteorol., 127, 449–467, 2008.

Inagaki, A., Letzel, M. O., Raasch, S., and Kanda, M.: Impact of surface heterogeneity on energy imbalance: A study using LES, J. Meteorol. Soc. Jpn., 84, 187–198, 2006.

Jegede, O. O. and Foken, T.: A study of the internal boundary layer due to a roughness change in neutral conditions observed during the LINEX field campaigns, Theor. Appl. Climatol., 62, 31–41, 1999.

Kaimal, J. C., Wyngaard, J. C., Izumi, Y., and Cote, O. R.: Spectral characteristics of surface-layer turbulence, Q. J. Roy. Meteor. Soc., 98, 563–589, 1972.

Kalthoff, N., Binder, H. J., Kossmann, M., Vogtlin, R., Corsmeier, U., Fiedler, F., and Schlager, H.: Temporal evolution and spatial variation of the boundary layer over complex terrain, Atmos. Environ., 32, 1179–1194, 1998.

Kalthoff, N., Horlacher, V., Corsmeier, U., Volz Thomas, A., Kolahgar, B., Geiss, H., Mollmann Coers, M., and Knaps, A.: Influence of valley winds on transport and dispersion of airborne pollutants in the Freiburg-Schauinsland area, J. Geophys. Res.-Atmos., 105, 1585–1597, 2000.

Kanda, M., Inagaki, A., Letzel, M. O., Raasch, S., and Watanabe, T.: LES study of the energy imbalance problem with Eddy covariance fluxes, Bound.-Lay. Meteorol., 110, 381–404, 2004.

Katul, G. G. and Chu, C. R.: A theoretical and experimental investigation of energy-containing scales in the dynamic sublayer of boundary-layer flows, Bound.-Lay. Meteorol., 98, 279–312, 1998.

Katul, G. G., Chu, C. R., Parlange, M. B., Albertson, J. D., and Ortenburger, T. A.: Low-wavenumber spectral characteristics of velocity and temperature in the atmospheric surface layer, J. Geophys. Res., 100, 14243–14255, 1995.

Kolmogorov, A. N.: Rassejanie energii pri lokolno-isotropoi turbulentnosti, Dokl. AN. SSSR., 32, 22–24, 1941.

Kossmann, M. and Fiedler, F.: Diurnal momentum budget analysis of thermally induced slope winds, Meteorol. Atmos. Phys., 75, 195–215, 2000.

Kossmann, M., Vogtlin, R., Corsmeier, U., Vogel, B., Fiedler, F., Binder, H. J., Kalthoff, N., and Beyrich, F.: Aspects of the convective boundary layer structure over complex terrain, Atmos. Environ., 32, 1323–1348, 1998.

Kottmeier, C., Kalthoff, N., Corsmeier, U., Barthlott, C., van Baelen, J., Behrendt A., Behrendt, R., Blyth, A., Coulter, R., Crewell, S., Dorninger, M., Foken, T., Hagen, M., Hauck, C., Höller, H., Konow, H., Kunz, M., Mahlke, H., Mobbs, S., Richard, E., Steinacker, R., Weckwerth, T., and Wulfmeyer, V.: Mechanisms initiating convection during the COPS experiment, Meteorol. Z., 17, 931–948, 2008.

Liebethal, C. and Foken, T.: Evaluation of six parameterization approaches for the ground heat flux, Theor. Appl. Climatol., 88, 43–56, 2007.

Lugauer, M. and Winkler, P.: Thermal circulation in South Bavaria - climatology and synoptic aspects, Meteorol. Z., 14, 15–30, 2005.

Maraun, D. and Kurths, J.: Cross Wavelet Analysis. Significance Testing and Pitfalls, Nonlinear. Proc. Geoph., 11, 505–514, 2004.

Maraun, D., Kurths, J., and Holschneider, M.: Nonstationary Gaussian Processes in Wavelet Domain: Synthesis, Estimation and Significance Testing, Phys. Rev. E., 75, 016707, doi:10.1103/PhysRevE.75.016707, 2007.

Mauder, M. and Foken, T.: Documentation and instruction manual of the Eddy covariance software package TK2, Work Report University of Bayreuth, Department of Micrometeorology, 26, ISSN: 1614-8916, 42 pp., 2004.

Mauder, M., Liebethal, C., Göckede, M., Leps, J. P., Beyrich, F., and Foken, T.: Processing and quality control of flux data during LITFASS-2003, Bound.-Lay. Meteorol., 121, 67–88, 2006.

Mayer, J. C., Staudt, K., Gilge, S., Meixner, F. X., and Foken, T.: The impact of free convection on late morning ozone decreases on an Alpine foreland mountain summit, Atmos. Chem. Phys., 8, 5941–5956, 2008.

Meißner, C., Kalthoff, N., Kunz, M., and Adrian, G.: Initiation of shallow convection in the Black Forest mountains, Atmos. Res., 86, 42–60, 2007.

Metzger, S., Foken, T., Eigenmann, R., Kurtz, W., Serafimovich, A., Siebicke, L., Olesch, J., Staudt, K., and Lüers, J.: COPS experiment, Convective and orographically induced precipitation study, 01 June 2007 – 31 August 2007, Documentation, Work Report University of Bayreuth, Department of Micrometeorology, 34,

ISSN 1614-8916, 72 pp., 2007.

Monin, A. S. and Yaglom, A. M.: Statistical Fluid Mechanics, Volume II: Mechanics of Turbulence, MIT Press, Cambridge, Massachusetts, USA, and London, England, UK, 1975.

Pielke, R. A.: Influence of the spatial distribution of vegetation and soils on the prediction of cumulus convective rainfall, Rev. Geophys., 39, 151–177, 2001.

Raabe, A.: On the relation between the drag coefficient and fetch above the sea in the case of off-shore wind in the near-shore zone, Z. Meteorol., 33, 363–367, 1983.

Rabin, R. M., Stadler, S., Wetzel, P. J., Stensrud, D. J., and Gregory, M.: Observed Effects of Landscape Variability on Convective Clouds, B. Am. Meteorol. Soc., 71, 272–280, 1990.

Rannik, U., Aubinet, M., Kurbanmuradov, O., Sabelfeld, K. K., Markkanen, T., and Vesala, T.: Footprint analysis for measurements over a heterogeneous forest, Bound.-Lay. Meteorol., 97, 137–166, 2000.

Rannik, U., Markkanen, T., Raittila, J., Hari, P., and Vesala, T.: Turbulence statistics inside and over forest: Influence on footprint prediction, Bound.-Lay. Meteorol., 109, 163–189, 2003.

Raymond, D. and Wilkening, M.: Mountain-Induced Convection under Fair Weather Conditions, J. Atmos. Sci., 37, 2693–2706, 1980.

Rebmann, C., Göckede, M., Foken, T., Aubinet, M., Aurela, M., Berbigier, P., Bernhofer, C., Buchmann, N., Carrara, A., Cescatti, A., Ceulemans, R., Clement, R., Elbers, J. A., Granier, A., Grunwald, T., Guyon, D., Havrankova, K., Heinesch, B., Knohl, A., Laurila, T., Longdoz, B., Marcolla, B., Markkanen, T., Miglietta, F., Moncrieff, J., Montagnani, L., Moors, E., Nardino, M., Ourcival, J. M., Rambal, S., Rannik, U., Rotenberg, E., Sedlak, P., Unterhuber, G., Vesala, T., and Yakir, D.: Quality analysis applied on eddy covariance measurements at complex forest sites using footprint modelling, Theor. Appl. Climatol., 80, 121–141, 2005.

Savelyev, S. A. and Taylor, P. A.: Internal boundary layers: I. Height formulae for neutral and diabatic flows, Bound.-Lay. Meteorol., 115, 1–25, 2005.

Schwitalla, T., Bauer, H.-S., Wulfmeyer, V., and Zaengl, G.: Systematic errors of QPF in low-mountain regions as revealed by MM5 simulations, Meteorol. Z., 17, 903–919, 2008.

Segal, M. and Arritt, R. W.: Nonclassical mesoscale circulations caused by surface sensible heat-flux, B. Am. Meteorol. Soc., 73, 1593–1604, 1992.

Shen, S. H. and Leclerc, M. Y.: How large must surface inhomogeneities be before they influence the convective boundary layer structure? A case study, Q. J. Roy. Meteor. Soc., 121, 1209–1228, 1995.

Staudt, K.: Determination of the atmospheric boundary layer height in complex terrain during SALSA 2005, Master's thesis, University of Bayreuth, Germany, 2006.

Steinfeld, G., Letzel, M. O., Raasch, S., Kanda, M., and Inagaki, A.: Spatial representativeness of single tower measurements and the imbalance problem with eddy-covariance fluxes: results of a large-eddy simulation study, Bound.-Lay. Meteorol., 123, 77–98, 2007.

Stull, R. B.: An introduction to boundary layer meteorology, Atmospheric sciences library, Kluwer Academic Publishers, Dordrecht, The Netherlands, 1988.

Stull, R. B.: Meteorology for scientists and engineers, Brooks/Cole, Pacific Grove, California, 2. edn., 2000.

Thomas, C. and Foken, T.: Detection of long-term coherent exchange over spruce forest using wavelet analysis, Theor. Appl. Climatol., 80, 91–104, 2005.

Whiteman, C. D.: Observations of thermally developed wind systems in mountainous terrain, in: Atmospheric processes over complex terrain, edited by Blumen, W., vol. 23 (45) of *Meteorological monographs*, 5–42, American Meteorological Society, Boston, Massachusetts, USA, 1990.

Wulfmeyer, V., Behrendt, A., Adrian, G., Althausen, D., Aoshima, F., van Baelen, J., Barthlott, C., Bauer, H. S., Blyth, A., Brandau, C., Corsmeier, U., Craig, G., Crewell, S., Dick, G., Dorninger, M., Dufournet, Y., Ehret, G., Engelmann, R., Flamant, C., Foken, T., Hauck, C., Girolamo, P. D., Graßl, H., Grzeschik, M., Handwerker, J., Hagen, M., Hardesty, R. M., Junkermann, W., Kalthoff, N., Kiemle, C., Kottmeier, C., Krauss, L., Long, C., Lelieveld, J., Madonna, F., Miller, M., Mobbs, S., Neininger, B., Pal, S., Peters, G., Radlach, M., Richard, E., Rotach, M., Russchenberg, H., Schlüssel, P., Schumann, U., Simmer, C., Steinacker, R., Turner, D., Vogt, S., Volkert, H., Weckwerth, T., Wernli, H., Wieser, A., and Wunraum, C.: Convective and Orographically-induced Precipitation Study. COPS Field Report 2.1., https://www.uni-hohenheim.de/spp-iop/documents/COPSFieldReport2.pdf, 2007.

Wulfmeyer, V., Behrendt, A., Bauer, H.-S., Kottmeier, C., Corsmeier, U., Blyth, A., Craig, G., Schumann, U., Hagen, M., Crewell, S., Di Girolamo, P., Flamant, C., Miller, M., Montani, A., Mobbs, S., Richard, E., Rotach, M. W., Arpagaus, M., Russchenberg, H., Schluessel, P., Koenig, M., Gaertner, V., Steinacker, R., Dorninger, M., Turner, D. D., Weckwerth, T., Hense, A., and Simmer, C.: The Convective and Orographically-induced Precipitation Study: A Research and Development Project of the World Weather Research Program for Improving Quantitative Precipitation Forecasting in Low-Mountain Regions, B. Am. Meteorol. Soc., 89, 1477–1486, 2008.

Zubkovskii, S. L.: Frequency spectra of the horizontal wind-velocity fluctuations in the atmospheric surface layer, Izv. Akad. Nauk SSSR, Ser. Geofiz, No. 10, 1425–1433, 1962.

Appendix C: Eigenmann et al. (2011)

Surface energy balance and turbulence network during the Convective and Orographically-induced Precipitation Study (COPS)

R. Eigenmann,[a*] N. Kalthoff,[b] T. Foken,[a] M. Dorninger,[c] M. Kohler,[b] D. Legain,[d] G. Pigeon,[d] B. Piguet,[d] D. Schüttemeyer[e] and O. Traulle[d]

[a]*Department of Micrometeorology, University of Bayreuth, Bayreuth, Germany*
[b]*Institute for Meteorology and Climate Research, Karlsruhe Institute of Technology, Karlsruhe, Germany*
[c]*Department of Meteorology and Geophysics, University of Vienna, Vienna, Austria*
[d]*Centre National de Recherches Météorologiques – Groupe d'étude de l'Atmosphère Météorologique (CNRM-GAME), Météo France – CNRS, Toulouse, France*
[e]*Meteorological Institute, University of Bonn, Bonn, Germany*
*Correspondence to: R. Eigenmann, Department of Micrometeorology, University of Bayreuth, Universitätsstrasse 30, 95440 Bayreuth, Germany.
E-mail: rafael.eigenmann@uni-bayreuth.de

Experimental data of the energy balance and the turbulence network installed during the Convective and Orographically-induced Precipitation Study (COPS) field campaign of 2007 are presented in this study. The network aims at providing continuous surface flux and other surface micrometeorological data of the required high accuracy and quality for further fundamental research. An overview of the turbulence data processing and data quality control, including footprint analysis and a check for internal boundary layers, is given. The consistently applied approach allows for a high comparability of the turbulent flux data of sensible and latent heat. The reaction of surface fluxes during the observed frontal passage during the Intensive Observation Period (IOP) 9c (20 July 2007) is presented. As surface fluxes were measured over different land-use types and at different locations within the COPS area, the effect of land use and orography on turbulent fluxes is discussed with the help of IOP 8b (15 July 2007). The flux differences between individual sites due to varying surface characteristics are often larger than the flux differences with changing altitude. The oasis effect observed for the highly evapotranspirating maize fields is found to increase the residuum of the surface energy balance. At all sites and during both IOPs the occurrence of near-ground free convection conditions (FCCs) is investigated. During the oasis effect, FCCs do not occur. Copyright © 2011 Royal Meteorological Society

Key Words: eddy-covariance; turbulent fluxes; energy balance closure; residuum; oasis effect; near-ground free convection conditions

Received 12 February 2010; Revised 27 August 2010; Accepted 31 August 2010; Published online in Wiley Online Library 2 February 2011

Citation: Eigenmann R, Kalthoff N, Foken T, Dorninger M, Kohler M, Legain D, Pigeon G, Piguet B, Schüttemeyer D, Traulle O. 2011. Surface energy balance and turbulence network during the Convective and Orographically-induced Precipitation Study (COPS). *Q. J. R. Meteorol. Soc.* **137**: 57–69. DOI:10.1002/qj.704

1. Introduction

A network of surface energy balance and turbulent flux measurement stations was set up during the comprehensive Convective and Orographically-induced Precipitation Study (COPS) field campaign (Wulfmeyer *et al.*, 2008). The campaign took place in southwestern Germany and eastern France from 1 June to 31 August 2007. It was

organized into Intensive Observation Periods (IOPs), which observed specific convective situations with a synergy of meteorological instruments (Wulfmeyer *et al.*, 2011). The aim of the COPS energy balance and turbulence network was to provide information about the temporal and spatial heterogeneity of high-quality turbulent flux values of sensible and latent heat for individual IOPs. This is important, since under weak synoptic forcing spatial inhomogeneities of surface characteristics result in inhomogeneities of turbulent fluxes of heat and moisture into the atmospheric boundary layer (ABL) and hence may determine if and where convection is initiated (e.g. Aoshima *et al.*, 2008; Kottmeier *et al.*, 2008, Behrendt *et al.*, 2011; Bennett *et al.*, 2011; Weckwerth *et al.*, 2011). An analysis of flux measurements with a more climatological focus was already performed in the COPS area within previous studies (Wenzel *et al.*, 1997). These investigations revealed a significant dependence of the energy balance components on the altitude and on the land-use types in the area of the Upper Rhine valley and the Black Forest (Kalthoff *et al.*, 1999, Wenzel and Kalthoff *et al.*, 2000). The turbulence network of the COPS campaign is comparable to that of the LITFASS-2003 experiment (Mengelkamp *et al.*, 2006), where turbulent fluxes were measured within an area of $20 \times 20\,\mathrm{km}^2$ over all relevant land-use types and were area-averaged by means of a tile approach (Avissar, 1991). The aggregated surface fluxes showed good agreement with area-integrated fluxes from long-range scintillometer and airborne measurements (Beyrich *et al.*, 2006). However, not all existing land-use types were covered with turbulence measurement stations in the case of the COPS network. Therefore, an area-averaging of fluxes based on measurements is impossible for the COPS period. More important for the COPS set-up are flux differences between the Upper Rhine valley and the mountaintops and valleys of the Black Forest and flux differences between different land-use types. Flux differences between different land-use types mainly occur due to altering surface characteristics such as albedo, emissivity, leaf area index (LAI), canopy height and structure (e.g. Munn, 1966; Oke, 1987). Different stages of vegetation development and mowing of grassland sites also lead to temporal variations of surface characteristics at a single location. The turbulent fluxes at individual locations are also influenced by differences in altitude. (Wenzel *et al.*, 1997) give theoretical considerations for the dependence of the Bowen ratio (*Bo*) on altitude. They showed that an increase or decrease of *Bo* with altitude depends on the air temperature and the relation of the temperature and humidity gradient. Observations of both an increase or decrease of *Bo* with altitude were made (e.g. Kessler, 1985). Accordingly, the first objective of this study is the investigation of flux differences due to different locations and land-use characteristics and the presentation of the data processing and quality control of the flux data. The influence of the surface fluxes on the ABL conditions and on the pre-convective environment is investigated in detail in the study of Kalthoff *et al.*, (2010). Using some stations of the COPS turbulence network, the authors focused on the relationship between soil moisture, surface fluxes, ABL conditions and convective indices. It was found that the convective indices depend on ABL conditions, which in turn are influenced by the energy transformation at the Earth's surface. However, due to a weak correlation between the surface fluxes and the ABL conditions, especially over the Black Forest, the authors concluded that advective processes also determine the ABL characteristics over the complex terrain of the COPS area.

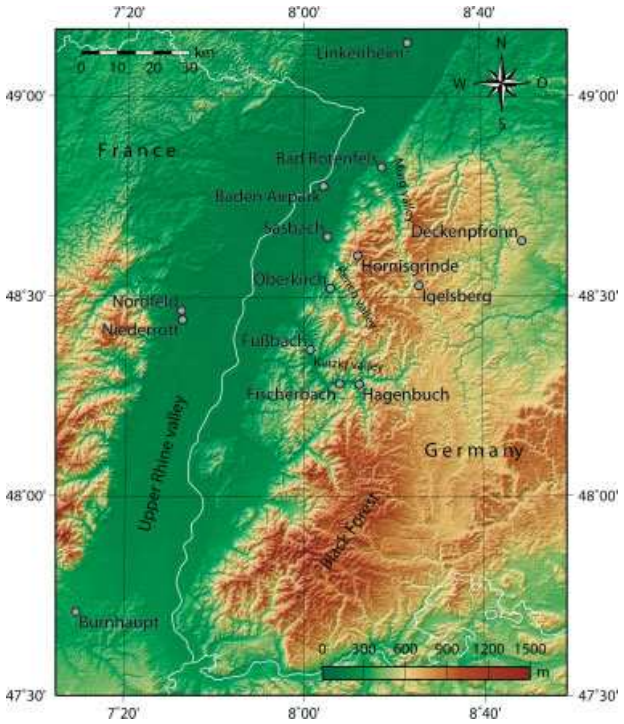

Figure 1. Topographic map of the turbulence measuring sites of the COPS field campaign (see also Table I).

The second objective of the present study is the investigation of the non-closure of the surface energy balance. A residuum of 10–30% is often found in micrometeorological field experiments (e.g. Foken *et al.*, 2010, Oncley *et al.*, 2007) and at FLUXNET sites (Wilson *et al.*, 2002). An overview of the energy balance problem is given in Culf *et al.* (2004) and Foken (2008b). The main reason for the residuum is assumed to be the landscape heterogeneity causing advective and low-frequency flux components (Foken *et al.*, 2006) and secondary circulations (Inagaki *et al.*, 2006), which are not caught by the standard eddy-covariance measurements and which transport the surplus of energy. The imbalance has important consequences for the use of surface turbulent flux data for ground truth and model validation. As the energy balance is, by definition, closed in most of the applied models, the residuum has to be considered when comparing modelled and measured flux values (e.g. Kracher *et al.*, 2009). As a first guess it is a common procedure to distribute the residuum according to the Bowen ratio (Twine *et al.*, 2000).

Moreover, the present study extends the investigation of the occurrences of near-ground free convection conditions (FCCs) of Eigenmann *et al.* (2009) in the Kinzig valley of the Black Forest to all sites in the COPS region. FCCs occur during situations of high buoyancy fluxes which coincide with very low wind speeds. Buoyancy-driven turbulence then dominates over shear-driven turbulence near the ground, which results in an effective vertical transport mechanism of heat and moisture, enhanced in near-ground regions, into upper parts of the ABL. As the dimensions of the target land-use types of most of the COPS sites are large enough ($> 250\,\mathrm{m}$) that the surface fluxes

Table I. Turbulence measuring sites of the COPS field campaign. The column 'Code' abbreviates the responsible institute (UBT: University of Bayreuth; IMK: Karlsruhe Institute of Technology; MF: Météo France; UV: University of Vienna; UBN: University of Bonn) followed by a running number. Also given are the coordinates (latitude, longitude), the altitude (metres a.s.l.) and the EC set-up (sonic anemometer, hygrometer – CSAT3: sonic anemometer by Campbell Scientific Inc., USA; USA-1: sonic anemometer by METEK GmbH, Germany; Solent R1012: sonic anemometer by Gill Instruments Ltd., UK; Young 81000: sonic anemometer by R. M. Young Company, USA; Solent HS: sonic anemometer by Gill Instruments Ltd., UK; KH20: krypton hygrometer by Campbell Scientific Inc., USA; LI-7500: open-path CO_2/H_2O gas analyzer by LI-COR Biosciences, USA). The station UV1 used the Optical Energy Balance Measurement System (OEBMS1) with a Scintillometer SLS20 system by Scintec AG, Germany instead of the EC measuring technique. The column 'Land use' indicates the target land-use type: grassland (G), maize (M), strawberry (S), fallow (F) and wheat (W). The column 'Location' sorts the stations by their location: valley (V) sites, mountaintop (T) sites, Upper Rhine (R) valley sites and sites in the lee (L) of the Black Forest.

Code	Site	Coordinates (lat., long.)	Alt.	Land use	Sonic anemometer	Hygrometer	Location
UBT1	Fußbach I [a]	48° 22′ 7.82″, 8° 1′ 21.17″	178	M	CSAT3	LI-7500	V
UBT2	Fußbach II	48° 22′ 0.88″, 8° 1′ 16.68″	180	F	USA-1	-	V
UBT3	Fischerbach [a]	48° 16′ 57.40″, 8° 7′ 56.28″	226	G	CSAT3	KH20	V
UBT4	Hagenbuch [a]	48° 16′ 54.59″, 8° 12′ 16.81″	245	G	CSAT3	LI-7500	V
IMK1	Hornisgrinde [a]	48° 36′ 12.95″, 8° 12′ 4.88″	1158	G	Solent R1012	LI-7500	T
IMK2	Baden Airpark [a]	48° 46′ 40.51″, 8° 4′ 25.20″	120	G	Solent R1012	LI-7500	R
IMK3	Linkenheim [a]	49° 8′ 9.24″, 8° 23′ 32.21″	96	W	Young 81000	-	R
IMK4	Sasbach	48° 39′ 4.20″, 8° 5′ 19.53″	133	G	Solent R1012	-	R
IMK5	Oberkirch	48° 31′ 19.15″, 8° 5′ 54.00″	203	S	Solent R1012	-	V
IMK6	Bad Rotenfels	48° 49′ 29.35″, 8° 17′ 30.55″	127	G	Solent R1012	-	V
IMK7	Igelsberg	48° 31′ 40.85″, 8° 25′ 50.35″	770	G	Solent R1012	-	T
IMK8	Burnhaupt	47° 42′ 33.52″, 7° 9′ 16.07″	299	M	Solent R1012	-	R
MF1	Niederrott [a]	48° 26′ 34.40″, 7° 32′ 38.36″	155	M	Solent HS	LI-7500	R
MF2	Nordfeld [a]	48° 27′ 58.22″, 7° 32′ 22.35″	156	M	Solent HS	LI-7500	R
UV1	Deckenpfronn [a,b]	48° 38′ 21.12″, 8° 49′ 7.86″	574	G	-	-	L
UBN1	Deckenpfronn [a]	48° 38′ 21.12″, 8° 49′ 7.86″	574	G	CSAT3	LI-7500	L

[a] Additional measurement of radiation and soil components.
[b] Not included in the data analyses of section 4 for comparability reasons.

are able to influence the structure of the ABL (Shen and Leclerc, 1995), the detected FCCs may have a strong impact on ABL characteristics and hence on the pre-convective environment in the COPS region. An impact of FCCs on vertical wind speeds (Eigenmann *et al.*, 2009) and on ozone concentrations (Mayer *et al.*, 2008) in the ABL was recently demonstrated.

Two IOPs are selected in the framework of this study: IOP 8b (15 July 2007) and IOP 9c (20 July 2007). These IOPs are chosen because the processes of convection initiation (CI) are intensively investigated and well understood (e.g. Kottmeier *et al.*, 2008; Kalthoff *et al.*, 2009; Barthlott *et al.*, 2010). The mechanisms leading to CI are very different on both days. According to Kottmeier *et al.* (2008), convection during IOP 8b is locally initiated, which means that surface fluxes and valley winds play an important role for CI, while convection during IOP 9c occurs near prefrontal convergence zones.

The article is organized as follows. Section 2 outlines the experimental set-up. Section 3 describes the processing and quality control of the turbulence data as well as the determination of the energy balance closure and the detection of FCCs. Section 4 shows and discusses the effect of land use and location on flux measurements, the energy balance closure and the occurrence of FCCs. In section 5 a summary and conclusions are given.

2. Experimental set-up

The surface energy balance and turbulence network consisted of sixteen stations set up within the heterogeneous landscape of the COPS area (see Figure 1 and Table I). The eddy-covariance (EC) measuring technique was applied in order to provide high-quality and continuous surface turbulent flux data of momentum and sensible and latent heat. Additionally, soil (Hauck *et al.*, 2011) and radiation measurements as well as standard surface meteorological data were recorded at most of the sites. Heterogeneity in the COPS region exists due to orography and due to a patchy land-use structure. Therefore, measuring sites included locations in the valleys (V) and on mountaintops (T) of the Black Forest, locations in the Upper Rhine (R) valley and locations in the lee (L) of the Black Forest (see Table I and Figure 1). Conversely, the turbulent fluxes were also measured over different land-use types (see Table I): grassland (G), maize (M), strawberry (S), fallow (F) and wheat (W). Mainly grassland sites (nine stations) and maize fields (four stations) were probed. The typical EC measuring set-up consisted of a sonic anemometer and a fast-response hygrometer according to Table I. The measurement height of all stations was in the range of 1.8–10 m, and the sampling frequency of the EC raw data amounted to 10, 20 or 32 Hz. The time stamp used was UTC (Universal Time

Table II. Flux contributions from the target land-use type (grassland), in %, dependent on wind direction sector and stability class for the station Hagenbuch (UBT4, see Table I). Average flux contributions over the entire COPS period are shown. Moreover, the internal boundary layer evaluation procedure for average conditions over the entire COPS period is presented for Hagenbuch. The height of the new equilibrium layer, δ_0, is calculated with the fetch, x, according to Eq. (1). Both variables are listed for different wind direction sectors. The flagging scheme of Table III is applied with an aerodynamic measurement height of $z_a = 2.0$ m.

Wind sector:	30°	60°	90°	120°	150°	180°	210°	240°	270°	300°	330°	360°
Flux contributions, in %, from the target land-use type (grassland):												
Stable	78	85	89	94	93	91	83	83	96	97	97	91
Neutral	94	97	95	98	99	98	96	95	99	99	100	96
Unstable	100	100	99	100	100	100	100	97	100	100	100	100
Internal boundary layer evaluation:												
x (m)	95	105	97	101	84	115	44	48	95	247	239	101
δ_0 (m)	2.9	3.1	3.0	3.0	2.8	3.2	2.0	2.1	2.9	4.7	4.6	3.0
Flag	0	0	0	0	0	0	1	0	0	0	0	0

Coordinated). All data were transformed into a common data format and transferred to the COPS data base operated by the World Data Center for Climate (WDCC) in Hamburg, Germany.

3. Turbulence data processing

3.1. TK2 processing

The EC flux data of the COPS turbulence network were processed and quality-controlled with the software package TK2 developed by the Department of Micrometeorology, University of Bayreuth (Mauder and Foken, 2004; Mauder *et al.*, 2008). Following Mauder *et al.*(2006), the processing steps and flux corrections listed below are applied to the EC raw data while running TK2.

- Calculation of averages, variances and covariances for an averaging interval of 30 min and taking into consideration the time delays between different sensors and excluding physically invalid values and spikes (Vickers and Mahrt, 1997).
- Cross-wind correction of the sonic temperature if necessary (depending on sonic anemometer type).
- Correction of oxygen cross-sensitivity for krypton hygrometers (Tanner *et al.*, 1993, van Dijk *et al.*, 2003).
- Planar fit coordinate rotation (Wilczak *et al.*, 2001).
- Correction of spectral loss due to path-length averaging, spatial separation of the sensors and the frequency dynamic effect of signals (Moore, 1986).
- Conversion of buoyancy into sensible heat flux (Schotanus *et al.*, 1983, Liu *et al.*, 2001)
- Correction for density fluctuations (WPL correction) to determine fluxes of the scalar quantities H_2O and CO_2 (Webb *et al.*, 1980; Fuehrer and Friehe, 2002; Liebethal and Foken, 2003, 2004).

The impact of these processing and flux-correction steps on flux estimates and energy balance closure is discussed in Mauder and Foken (2006).

Quality tests implemented in TK2 consist of a stationarity test and a test on the fulfilment of integral turbulence characteristics (ITC) for each turbulent flux (Foken and Wichura, 1996; Foken *et al.*, 2004). According to Foken *et al.* (2004), the final quality flag (1–9) is assigned to a specific half-hourly turbulent flux value by combining the quality flags for stationarity and ITC. Classes 1–3 can be used for fundamental research, classes 4–6 for general use such as continuously running systems and classes 7–8 for a rough orientation. Turbulent flux values marked with a quality flag of class 9 should be rejected. This information is also provided in the COPS data base at the WDCC (see section 2) as well as the information on the footprint modelling results (section 3.2) and the internal boundary evaluation (section 3.3), as described below.

3.2. Footprint modelling

In order to evaluate the spatial representativity of the measured turbulent flux data in the context of the underlying land-use distribution, a footprint model was applied to all EC flux sites of the COPS turbulence network. Following the approach of Göckede *et al.* (2004, 2006), the flux data-quality flagging scheme of Foken *et al.* (2004) is combined with the Thomson (1987) three-dimensional Lagrangian stochastic trajectory model of Langevin type (Wilson and Sawford, 1996). The parametrization follows the flow statistics and the effect of stability on the profiles used in Rannik *et al.* (2003). The approach of Göckede *et al.* (2004, 2006) allows the determination of the footprint climatology in relation to the land use (spatial representativity) and the spatial distribution of quality flags (spatial quality structure) as well as the calculation of the flux contribution of the target land-use type to the total flux measured for each half-hourly turbulent flux value. Recently, this flux data-quality evaluation approach was adapted to the sites of the CarboEurope network by Rebmann *et al.* (2005) and Göckede *et al.* (2008).

As an example, Table II shows the flux contribution from the target land-use type at the station Hagenbuch (UBT4, see Table I) for different wind direction sectors and

stability classes. The entire COPS measurement period is considered. As expected, flux contributions from the target surface increase from stable towards unstable conditions. The main wind directions (120, 150, 270 and 300°) with the highest data density (not shown) show flux contributions over 93% even under stable conditions. The lowest flux contributions are found in sectors with low data density, e.g. 78% in the 30° sector during stable conditions. Overall, the measured turbulent flux data at Hagenbuch are highly representative of the target land-use type.

3.3. Internal boundary layers

All measurements at each EC station of the COPS turbulence network were checked for the existence of internal boundary layers (IBL), which form as a result of changes in ground-surface characteristics adjacent to the tower. The exchange of energy and matter over the target land use is affected by neighbouring areas when measuring above the IBL. The following equation was used to estimate roughly the height of the new equilibrium layer, δ_0, depending on the fetch, x, for each 30° wind sector (Raabe, 1983; Jegede and Foken, 1999):

$$z_a < \delta_0 = 0.3\sqrt{x}. \quad (1)$$

The aerodynamic measurement height, z_a, is defined as the geometric height minus the zero-plane displacement. The latter can be determined with two-thirds of the canopy height (e.g. Foken, 2008a). In order to guarantee that the measurement takes place within the new equilibrium layer that establishes over the target land-use type, z_a should be lower than δ_0. Above δ_1, the measurement cannot be related to the target land-use type:

$$z_a > \delta_1 = 0.5\sqrt{x}. \quad (2)$$

Between δ_0 and δ_1, a transition area is assumed. A weak effect of stability on $\delta_{0,1}$ is neglected (Savelyev and Taylor, 2005).

For the outcome of the IBL evaluation procedure, a flagging scheme was defined depending on the relation of z_a to δ_0 and δ_1 (see Table III). This scheme was applied to each half-hourly turbulent flux value. Flux values flagged with 1 should be considered with care and flux values flagged with 2 should be rejected in any case, as the measured flux cannot be ascribed to the target land-use type.

As an example, Table II shows the results of the IBL evaluation procedure for average conditions over the entire COPS measurement period for the station Hagenbuch (UBT4, see Table I). The height of the new equilibrium layer, δ_0 (see Eq. (1)), and the fetch, x, are both given for different wind direction sectors. It can be seen that in the 210° sector the aerodynamic measurement height, $z_a = 2.0$ m, equals the height of the new equilibrium layer, $\delta_0 = 2.0$. This indicates that the flux measurement takes place at the lower edge of the transition area of the IBL and thus is flagged with 1 (see Table III).

Table III. Flagging scheme for the internal boundary layers.

Condition	Flag	Description
$z_a < \delta_0$	0	Measurement below δ_0
$\delta_0 \le z_a \le \delta_1$	1	transition area
$z_a > \delta_1$	2	Measurement above δ_1

3.4. Data selection

For the results shown in section 4, the following data selection criteria were applied; these result from the data-quality tests described in sections 3.1, 3.2 and 3.3. Only turbulent flux data with

- TK2 quality flags ≤ 6 (see section 3.1),
- flux contributions from the target land-use type $> 70\%$ (see section 3.2) and
- flags of the IBL evaluation procedure ≤ 1 (see section 3.3)

are considered further for data analysis. Due to the high landscape heterogeneity at the COPS measurement sites, we decided to allow turbulent flux data with flux contributions from the target land-use type $> 70\%$ instead of $> 80\%$ as was recommended by Göckede *et al.* (2008) as a reasonable value for representative measurements in his study above tall vegetation.

The resulting data availability after the application of these data selection criteria is shown in Table IV. Overall, most of the sites reach an adequate data availability of more than 50%. However, six stations also show very low data availability below 30%. This can be mainly attributed to data rejection due to low flux contributions from the target land-use type, either identified by the applied footprint model or by the IBL evaluation procedure. Unfavourable fetch conditions were present at these sites, as they were closely situated at the boundaries of the target land-use types, which results in an increase of the influence of neighbouring areas. At the station Linkenheim (IMK3) the large measurement height of 10 m is responsible for the failure of the IBL criteria and thus for data rejection.

3.5. Energy balance closure

A possible residuum, *res*, of the surface energy balance can be evaluated at all measuring sites of the turbulence network where additional radiation and soil measurements were carried out and both turbulent fluxes of sensible heat, Q_H, and latent heat, Q_E, were measured (see Table I). At the surface, the net radiation, Q_S^*, is transformed into Q_H and Q_E and into the ground heat flux, Q_G:

$$-Q_S^* = Q_H + Q_E + Q_G + res. \quad (3)$$

The storage of heat in the upper soil layer is included in this study within the value of Q_G and was calculated according to the 'simple measurement' method after Liebethal and Foken (2007). Other storage terms (plants, air, etc.) and photosynthesis can be neglected as they are usually very small (Foken, 2008b).

3.6. Near-ground free convection conditions

Near-ground free convection conditions can be detected with the EC measurements by calculating the stability parameter, ζ, which is the quotient of the measurement height, z, and the Obukhov length, L:

$$\zeta = \frac{z}{L} = -\frac{z\,\kappa\,g\,\left(\overline{w'\theta'_v}\right)_0}{\overline{\theta_v}\,u_*^3}. \quad (4)$$

Table IV. Number of cases, in %, for each EC station that fulfil the applied data selection criteria: flux contribution from the target land-use type (AOI = area of interest) to the total flux measured > 70%, flags of the IBL evaluation procedure ≤ 1, quality flag of the friction velocity u_* ≤ 6, quality flag of the sensible heat flux Q_H ≤ 6 and quality flag of the latent heat flux Q_E ≤ 6. Also given is the data availability (DA) in %, after the data rejection according to the previously mentioned criteria for the turbulent fluxes of u_*, Q_H and Q_E. The column 'Class' abbreviates the locations and land-use types of the sites according to Table I.

Station code	Class	AOI > 70%	IBL flag ≤ 1	flag u_* ≤ 6	flag Q_H ≤ 6	flag Q_E ≤ 6	DA u_*	DA Q_H	DA Q_E
UBT1	M,V	96	100	90	94	92	89	90	89
UBT2	F,V	74	93	91	87	–	65	61	–
UBT3	G,V	73	99	74	83	82	63	62	62
UBT4	G,V	100	100	80	90	88	80	90	88
IMK1	G,T	81	64	98	94	89	59	57	50
IMK2	G,R	86	95	96	88	86	82	74	72
IMK3	W,R	54	0	90	89	–	0	0	–
IMK4	G,R	71	29	92	84	–	26	24	–
IMK5	S,V	54	44	96	90	–	27	26	–
IMK6	G,V	59	13	96	85	–	12	12	–
IMK7	G,T	89	100	95	87	–	87	78	–
IMK8	M,R	67	81	98	87	–	66	60	–
MF1	M,R	10	22	93	90	88	10	9	9
MF2	M,R	100	100	84	90	88	84	90	87
UBN1	G,L	53	29	91	88	87	23	22	22

Here, u_* is the friction velocity, g the acceleration due to gravity, $\overline{\theta_v}$ the mean virtual potential temperature and $\left(\overline{w'\theta'_v}\right)_0$ the buoyancy flux at the surface. The von Kármán constant amounts to $\kappa = 0.4$. FCCs occur for $\zeta < -1$, as buoyancy-driven turbulence then dominates over shear-driven turbulence near the ground (e.g. Stull, 1988; see also Eigenmann *et al.*, 2009).

4. Results and discussion

First, the difference in the net radiation, Q_S^*, available for the transformation into Q_H, Q_E and Q_G at the surface (see Eq. (3)) will be highlighted for the two selected IOPs (8b and 9c, see section 1). Figure 2 shows the net radiation for IOPs 8b and 9c averaged according to the different locations distinguished in Table I. Averaging is done arithmetically, as is the case for all averages shown below. For IOP 8b, a bell-shaped course of Q_S^* is visible at the valley (V), the Upper Rhine (R) valley and mountaintop (T) sites, thus indicating a clear and sunny day with no disturbance due to cloud shading at these sites. Only the station Deckenpfronn in the lee (L) of the Black Forest shows a decrease of Q_S^* between 1430 and 1600 UTC, which can be related to convective clouds observed during IOP 8b in this area (Kalthoff *et al.*, 2009). In contrast, the reaction of the radiation components for the observed passage of a frontal structure during IOP 9c (see Kottmeier *et al.*, 2008) is clearly visible in Figure 2(b). Q_S^* is reduced by more than 250 W m^{-2} between 0830 and 1200 UTC at all locations.

4.1. Impact of a frontal passage on surface fluxes

The frontal passage observed during IOP 9c has a strong influence on the surface turbulent fluxes. However, the effect differs depending on the location of the station. Figure 3 compares averaged values of Q_H and Q_E of the valley (V) sites with those of the non-valley sites (T, R, L) for IOP 9c. Data availability at Deckenpfronn in the lee (L) of the Black Forest is very low, as many data are rejected due to the applied data selection criteria (see Table IV). In general, non-stationarity during the passage of the front increases data rejection during IOP 9c compared with other days with more stationary conditions (e.g. IOP 8b). Regarding the temporal evolution of the decline in Q_H (Q_E cannot be evaluated due to data rejection), it can be seen that the surface fluxes first diminish in the Upper Rhine (R) valley, then in the valleys (V) of the Black Forest and lastly at the mountaintop (T) sites. This corresponds with the observed direction of propagation of the front from southwest to northeast during IOP 9c (Kottmeier *et al.*, 2008). The above-mentioned temporal order can also be seen in Q_S^* (Figure 2(b)), where the further propagation of the front towards the northeast is also visible, as Q_S^* reaches its minimum half an hour later in the lee (L) of the Black Forest compared with the other locations. A strong decrease of Q_H of more than 100 W m^{-2} is visible at all sites during the frontal passage. The R sites show the lowest values of Q_S^* and Q_H, followed by the T and V sites. The reason for the highest values of Q_S^* and Q_H during the passage of the front at the V sites can be attributed to the fact that the radiative energy input by incoming long-wave radiation (not shown) is enhanced at the V sites compared with the other sites due to additional long-wave radiative fluxes from the valley sides. After the frontal passage, Q_H increases most slowly at the R sites. This can be attributed to the fact that some precipitating clouds still remain over the Upper Rhine valley, while the Black Forest area is already nearly cloud-free (see Figure 19 of Kottmeier *et al.*, 2008).

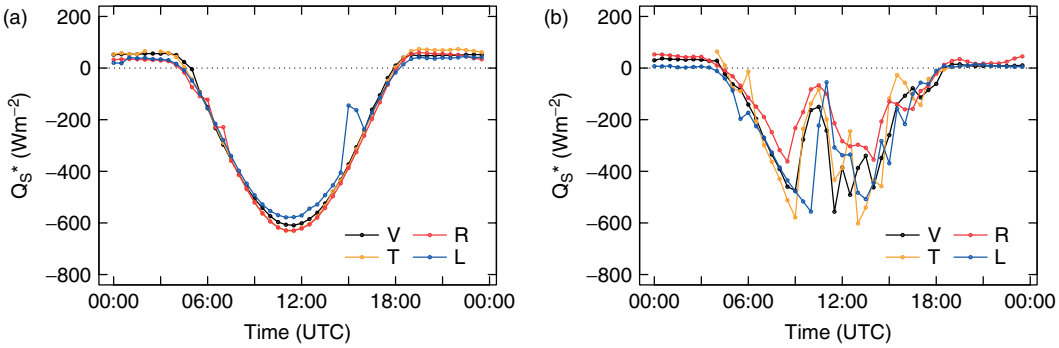

Figure 2. Surface net radiation Q_S^* during (a) IOP 8b and (b) IOP 9c, averaged according to different locations: valley (V) sites, mountaintop (T) sites, Upper Rhine (R) valley sites and sites in the lee (L) of the Black Forest (see also Table I).

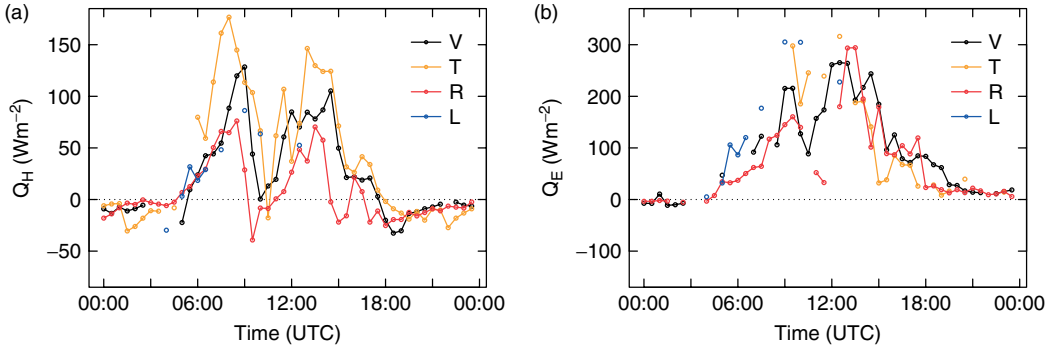

Figure 3. Surface turbulent fluxes of (a) sensible heat Q_H and (b) latent heat Q_E during IOP 9c, averaged over all valley (V) sites, mountaintop (T) sites, Upper Rhine (R) valley sites and sites in the lee (L) of the Black Forest (see also Table I).

4.2. *Effect of land use and location on surface fluxes*

The effect of land use and location of the sites on surface turbulent fluxes is investigated in this chapter. For this purpose, IOP 8b has been chosen as this day is a typical situation with weak synoptic forcing and a (nearly) spatially uniform radiative energy input (see Figure 2(a)). This allows for an optimal comparison of the influence of land use and orography on surface turbulent flux values at different sites.

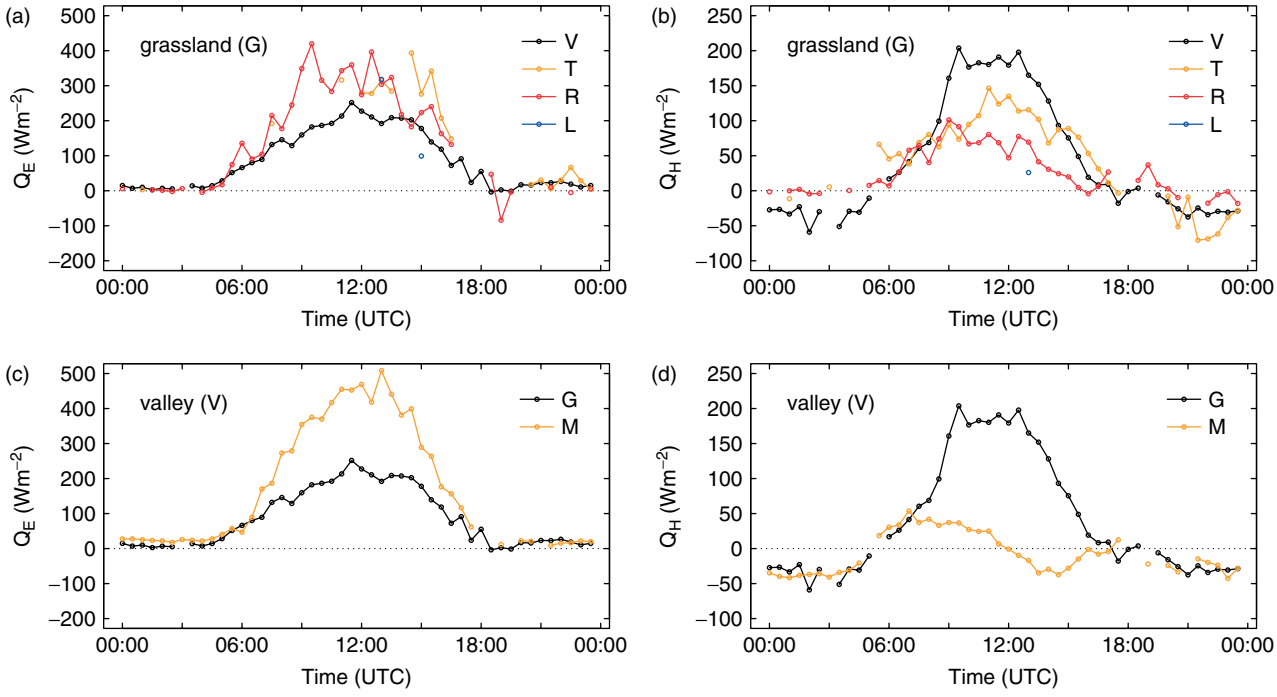

Figure 4. Surface turbulent fluxes of latent heat Q_E (panels (a) and (c)) and sensible heat Q_H (panels (b) and (d)) during IOP 8b. For daily courses (a) and (b), averaging is according to location (valley sites: V; mountaintop sites: T; Upper Rhine valley sites: R; sites in the lee of the Black Forest: L); only grassland (G) sites are considered. For daily courses (c) and (d), averaging is according to the target land-use type (G: grassland; M: maize); only valley (V) sites are taken into account.

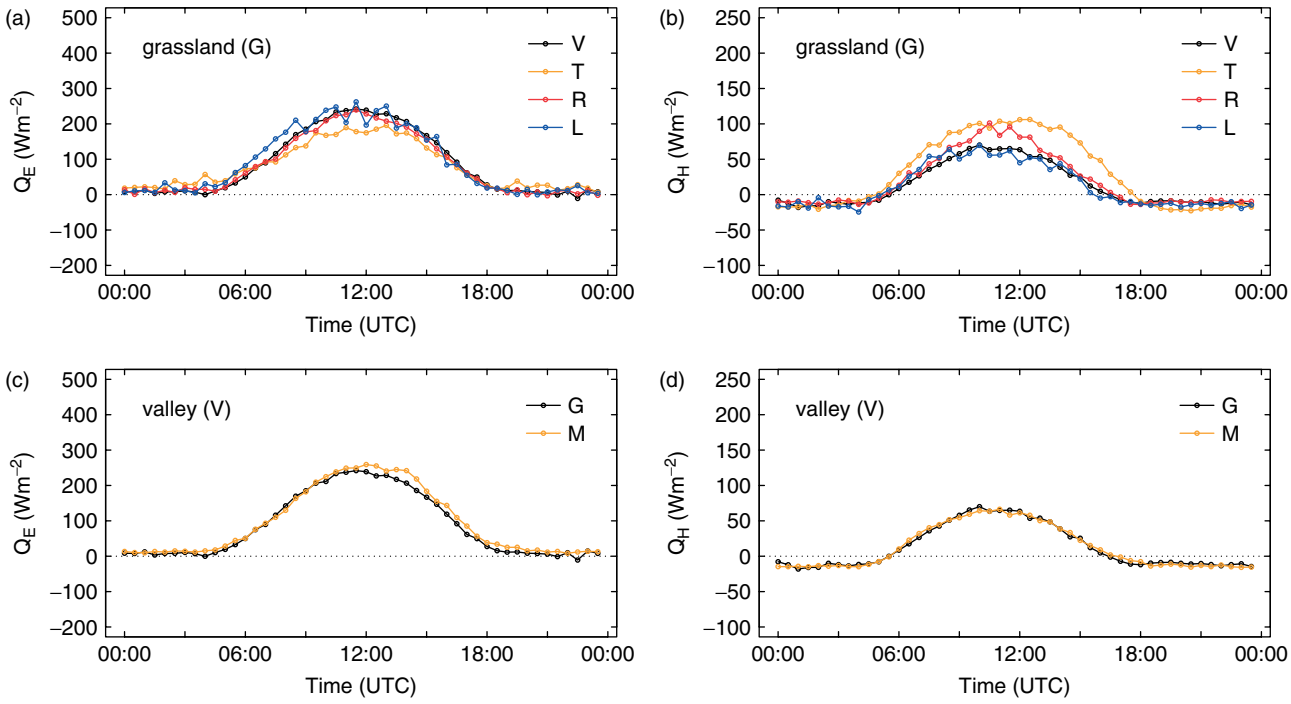

Figure 5. Same as Figure 4 but for the entire COPS measurement period.

Figure 4 shows the daily courses of Q_E and Q_H during IOP 8b averaged according to different locations (V, T, R, L) and to different target land-use types (G, M). Only target land-use types where both turbulent fluxes were measured are taken into account. In order to guarantee that the effect of land use and location is clearly separated, the daily courses averaged according to their location only consider grassland (G) sites. This type of land use is available at all locations (see Table I). Conversely, for the daily courses averaged according to their target land-use type only valley (V) sites are considered. However, it has to be mentioned that even the fluxes over the same type of land use are not comparable on a specific day, due to different surface characteristics (e.g. the grassland sites in Fischerbach and Hagenbuch were mown on 14 July). Therefore, we will also show the daily courses of Q_E and Q_H in the same way as Figure 4 but averaged over the entire COPS period (Figure 5). Daily flux differences due to changing surface characteristics within the class of grassland sites (mainly due to mowing events) are minimized by averaging over the entire COPS period, allowing the effect of orography to become visible.

Regarding Figure 4(c) and (d), the occurrence of the oasis effect (e.g. Stull, 1988) is obvious for the maize field during IOP 8b (canopy height: 2.5 m). The strong evapotranspiration results in latent cooling near the ground, while the air above the surface is still warmer. This leads to negative values of Q_H as early as around 1200 UTC (see M in Figure 4(d)). The oasis effect is a frequently occurring phenomenon. It was observed on about 46% of the days at the maize field in the Kinzig valley and on about 55% of the days at the maize fields in the Rhine valley. The oasis effect can also be expected over different land-use types, although it will not be as pronounced as over the highly evapotranspirating maize fields. The flux differences during IOP 8b between different locations (Figure 4(a) and (b)) are smaller than those that can be found for different land-use types (Figure 4(c) and (d)). However, as mentioned above, the effect of orography on flux values is barely visible on any specific day as varying surface characteristics within the same class of land-use type also have to be considered.

Therefore, Figure 5 also presents the daily courses of Q_E and Q_H averaged over the entire COPS period. Figures 5(c) and (d) show that in a long-term view the fluxes of Q_E and Q_H hardly differ between grassland and maize. Also, for the three-month COPS period values of the Bowen ratio ($Bo = Q_H/Q_E$) can be determined, which would not make much sense for a single day like IOP 8b with the occurrence of the oasis effect. The Bowen ratio at the grassland sites ($Bo = 0.26$) is slightly higher than that for maize ($Bo = 0.23$). This can be attributed to the enhanced evapotranspiration of maize during the growing period in June and July. For other land-use types, however, totally different values of *Bo* can be expected. The effect of altitude on the daily courses of Q_E and Q_H can be seen in Figure 5(a) and (b). The highest values of *Bo* can be found at the mountaintop (T) sites ($Bo = 0.56$) followed by the Upper Rhine (R) valley sites ($Bo = 0.36$), the valley (V) sites ($Bo = 0.26$) and the site in the lee (L) of the Black Forest ($Bo = 0.23$). An increase of *Bo* from the Rhine valley to the top of the Black Forest was also found by Wenzel *et al.* (1997) within a one year dataset. In general, the observed values of *Bo* in our study are in good agreement with those found in previous studies within this area (see also Kalthoff *et al.*, 1999).

To sum up, on a specific day the flux values of Q_E and Q_H are strongly determined by different types of land use and surface characteristics, while the effect of altitude plays a minor role. The spatial inhomogeneity of the transformation of radiative energy at the surface into Q_E and Q_H can be strongly influenced by the heterogeneity of surface characteristics. Therefore, on convective days with weak synoptic forcing, land-use characteristics may be decisive if and where convection is initiated. Hot spots of increased transport of heat or moisture into

Table V. Average residual $1 - b$ (%), intercept a (W m^{-2}), R^2 and the number of available half-hourly measurements of the linear regression analyses $Q_H + Q_E = a + b(-Q_S^* - Q_G)$ at each EC station with additional radiation and soil measurements (see Table I). Also given are the sensor types for the radiation and soil heat flux measurements – CM24, CM14: pyranometer/albedometer by Kipp & Zonen, the Netherlands; DD-PIR: double direction precision infrared radiometer by Eppley Laboratory, Inc., USA; CNR1: net radiometer by Kipp & Zonen, the Netherlands; CG3: pyrgeometer by Kipp & Zonen, the Netherlands; HFP01SC, HFP01: heat flux plates by Hukseflux Thermal Sensors, the Netherlands; RIMCO HP3: heat flux plate by McVan Instruments, Australia; CN3: heat flux plate by Carter-Scott Design, Victoria, Australia.

Station code	Class	Residual	Intercept	R^2	Number of cases	Radiation sensor(s)	Soil heat flux plate
UBT1	M,V	21	5.2	0.86	3322	CM24/DD-PIR	HFP01SC
UBT3	G,V	30	−3.6	0.82	1705	CNR1	RIMCO HP3
UBT4	G,V	17	11.6	0.89	3206	CNR1	HFP01SC
IMK1	G,T	24	30.3	0.86	1290	CM14/CG3	CN3
IMK2	G,R	26	12.0	0.88	1929	CM14/CG3	CN3
MF1	M,R	36	11.0	0.87	106	CNR1	HFP01
MF2	M,R	24	17.4	0.89	1073	CNR1	HFP01
UBN1	G,L	26	13.1	0.93	622	CNR1	HFP01

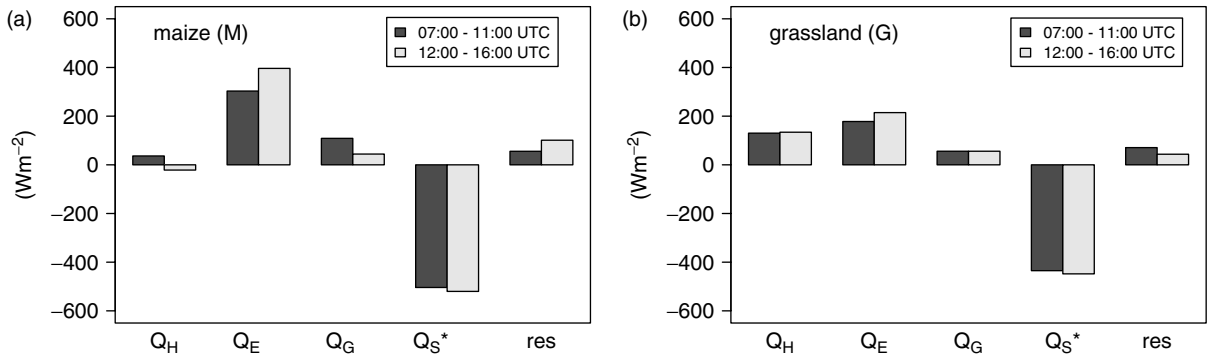

Figure 6. Sensible heat flux Q_H, latent heat flux Q_E, ground heat flux Q_G, net radiation Q_S^* and the residuum, *res*, of the surface energy balance (see Eq. (3)), at stations (a) Fußbach I and (b) Hagenbuch (see Table I) for IOP 8b. Average values for the time periods from 0700–1100 UTC (black) and 1200–1600 UTC (grey) are given. The target land-use types at Fußbach I and Hagenbuch are maize (M) and grassland (G), respectively.

the ABL may form. However, it should be mentioned that slope and valley winds, which frequently occur in the Black Forest (Kossmann and Fiedler, 2000; Kalthoff *et al.*, 2000), as well as secondary circulations (Barthlott *et al.*, 2006) may redistribute the surface-initiated heat and moisture distribution in the ABL and thus may modulate the local forcing of convection initiation by surface fluxes.

4.3. *Energy balance closure*

Regarding the entire COPS measurement period, the residuum of the surface energy balance (see section 3.5) ranges between 17% and 36% at the sites within the COPS region (see Table V). This is comparable with the range reported by e.g. Mauder *et al.* (2006) for different agricultural sites (residuum: 20–30%) during the LITFASS-2003 experiment. The residuum of 36% at the station Niederrott (MF1) should be considered with care, as only 106 half-hourly measurements were available for the determination of the residuum (see Table V).

Furthermore, it is found that the oasis effect at the maize fields during IOP 8b has important consequences for the daily course of the non-closure of the surface energy balance. To make this finding clear, two stations of the Kinzig valley (Fußbach I: UBT1 and Hagenbuch: UBT4; see Table I) are selected to investigate the residuum, *res*, of the energy balance (see Eq. (3)) over the target land-use types maize (UBT1) and grassland (UBT4). At the chosen maize field the oasis effect appears to be very strong, with negative values of Q_H shortly after midday (see Figure 4(d)). Therefore, a strong influence of the oasis effect on *res* can also be expected. Moreover, the two selected stations are located within the same orographic feature (Kinzig valley), are comparable in field size and show similar average residuals during the entire COPS period (see Table V). The latter suggests a similar heterogeneity of the local landscape at both sites, which is assumed to be the main reason for the observed residuum (see section 1). All the above-mentioned reasons result in an optimal comparison of the two sites and allow a proper investigation of the effect of land use on the residuum on a specific day (IOP 8b). For two time periods of equal length before (0700–1100 UTC) and after (1200–1600 UTC) midday (maximum net radiation at 1130 UTC: see Figure 2(a)), average values of Q_H, Q_E, Q_G, Q_S^* and *res* are calculated. Figure 6 shows the results for Fußbach I and Hagenbuch with the target land-use types maize (M) and grassland (G), respectively. The two time periods appear to be comparable, as the average value of Q_S^* available for transformation into Q_H, Q_E and Q_G only differs by about 3% between the two time periods at both sites. The oasis effect

is clearly visible at the maize field, as it shows positive values of Q_H before midday and negative values after midday. At the grassland site, however, the same positive value of Q_H is found during both time periods and no oasis effect occurs. The difference between the values of Q_E before and after midday is 2.5 times higher at the maize field (93 W m^{-2}) than at the grassland site (37 W m^{-2}), indicating enhanced evapotranspiration. At the maize field, Q_G is 1.5 times higher before midday compared with the time period after midday, while at the grassland site Q_G is equal in both periods. The lowered values of Q_G at the maize field after midday may partly be attributed to the oasis effect, during which the energy for the enhanced evapotranspiration is provided not only by a negative Q_H but also by a reduced Q_G. Also, the applied correction of the measured soil heat flux with the heat storage between the heat flux plate and the ground according to Liebethal and Foken (2007) may contribute to an enhancement of the values of Q_G at the maize field before midday. The soil temperature gradient between just below the surface and the depth of the installed heat flux plate are used for the correction. As soil temperatures at larger depths react more slowly to radiation, the soil temperature gradients (and thus Q_G) are larger in the morning than in the afternoon. Although the maize field had a canopy height of 2.5 m, the spacing between individual plants was large enough that radiation could still easily reach the ground. However, at the ground of the maize field there was bare soil, in contrast to the grassland site, which was characterized by a much denser vegetation structure. This leads to higher soil temperature gradients and thus to higher values of Q_G at the maize field before midday. The residuum, *res*, can be seen to increase by 82% from 56 W m^{-2} before midday to 101 W m^{-2} after midday at the maize field. This contrasts with the grassland site, which shows 38% lower values of the residuum after midday (44 W m^{-2}) when compared with the period before midday (71 W m^{-2}).

The enhanced residuum after midday at the maize field may be explained by an intensification of advection during the oasis effect. The strong latent cooling of the surface leads to more advective flux components directed towards the target land-use type. As these advective flux components are not caught by the EC system, the residuum increases. Following the idea of Foken (2008b) and Foken *et al.* (2010), energy transported by advection over a heterogeneous landscape can also be transferred to energy within larger eddies, not seen by the EC system, at significant heterogeneities and roughness changes of the land surface. The higher residuum before midday at the grassland site may be explained by enhanced advective flux components due to stronger temperature gradients between adjacent land-use types and the grassland in the morning hours, which are reduced in the time period after midday.

4.4. *Free convection conditions*

On both selected IOPs (see section 1), the EC measurements at the different sites were investigated with regard to the occurrence of FCCs (see section 3.6). The following points can be made.

(1) Similarly to (Eigenmann *et al.*, 2009), FCCs occur during IOP 8b at all valley (V) sites in the morning due to a change of the valley circulation system. IOP 8b is a day with undisturbed incoming radiation (see Figure 2(a)). Accordingly, at all sites in the Kinzig, Rench and Murg valleys, strong thermally induced up-valley winds can be found on this day (not shown). During the period of wind direction change from down- to up-valley winds in the morning hours (0600–0930 UTC), the friction velocity u_* (and also shear) is significantly reduced, while the buoyancy flux, $\left(\overline{w'\theta'_v}\right)_0$, is already large enough. Referring to Eq. (4), low values of u_* and simultaneously large values of $\left(\overline{w'\theta'_v}\right)_0$ will lead to $\zeta < -1$ and to a dominance of buoyancy over shear. These are the situations in which FCCs are detected close to the ground at the measurement height of the EC system. As might have been expected, no FCCs are observed during IOP 9c at the valley (V) sites. Thermally driven valley winds do not occur during IOP 9c (not shown), thus inhibiting periods of low shear during the change of valley wind direction in the morning hours. Moreover, stronger wind speeds (not shown) are generally present during IOP 9c due to the frontal passage leading to an enhancement of shear and to the non-occurrence of FCCs on this day at the valley (V) sites.

(2) At the mountaintop (T) sites of the Black Forest (Hornisgrinde and Igelsberg), no FCCs are observed on both days under investigation (IOP 8b and 9c). Enhanced wind speeds at the mountaintops (not shown) are the reason for the mainly neutral conditions near the ground at these two sites during the entire daytime period.

(3) In the Upper Rhine (R) valley and in the lee (L) of the Black Forest (Deckenpfronn), FCCs occur in the morning hours during both IOPs. A reduction of u_* and shear and a dominance of buoyancy can be observed during periods of low wind speeds. Even in IOP 9c, FCCs occur before the passage of the frontal structure. The reasons for the low wind speed periods are complex and probably bound to an interaction of local and mesoscale flow features.

(4) For IOP 8b only, FCCs are also detected in the Upper Rhine (R) valley and at Deckenpfronn (L) during midday and in the afternoon due to periods of low values of u_* (not shown). These periods may be attributed to local circulations, which break down and re-establish. During midday and in the afternoon, no FCCs occur in the valleys (V) and at the mountaintop (T) sites of the Black Forest due to enhanced wind speeds.

(5) The statement about the occurrence of FCCs during midday and afternoon in the Upper Rhine (R) valley made under point (4) is restricted to stations with grassland (G) being the target land-use type (Sasbach, Baden Airpark). The maize (M) fields in the Upper Rhine (R) valley (Niederrott, Nordfeld and Burnhaupt le Bas) do not show FCCs at these times. This can be explained by the appearance of the oasis effect in the early afternoon at the maize fields, leading to negative values of Q_H (e.g. Figure 4(d)). Figure 7 shows the daily course of the stability parameter, ζ, from 0700–1600 UTC during IOP 8b averaged over the maize (M) fields and over the grassland (G) sites in the Upper Rhine (R) valley. It can be seen that ζ is occasionally lower than -1 for both land-use types in the morning hours until 1030 UTC. However, from 1100 – 1600 UTC ζ only reaches -1 over the

grassland sites, where the oasis effect does not occur. Consequently, a strong influence of the target land-use type on the occurrence of FCCs is evident.

5. Summary and conclusions

A comprehensive data set of surface turbulent fluxes was collected during the COPS experiment of summer 2007. Uniformly applied data processing and quality-control steps allow for a high comparability of the flux data measured over different land-use types and locations within the COPS region. In the present study, IOPs 8b and 9c are chosen in order to highlight some typical features of turbulent fluxes.

The turbulent fluxes of sensible heat, Q_H, and latent heat, Q_E, strongly decrease during the passage of a frontal structure during IOP 9c. Although data rejection is enhanced because of non-stationary conditions on this day, the decline of Q_H due to a reduction of the net radiation, Q_S^*, is visible at different locations. The times of the decrease of Q_H at different locations follow the direction of propagation of the observed front.

IOP 8b is used to study the influence of the location and land-use type on surface turbulent fluxes. On a specific day with weak synoptic forcing, flux differences of Q_H and Q_E between different land-use types but also between sites with the same type of land use are found. For the latter, different surface characteristics, e.g. due to mowing of the grassland sites or different stages of vegetation development, are relevant. Flux differences of Q_H and Q_E between individual sites due to different surface characteristics are often larger than the flux differences with changing altitude. Therefore, the spatial distribution of land-use characteristics and thus the spatial inhomogeneity of turbulent fluxes of heat and moisture into the ABL may be strongly decisive if and where convection is initiated on a specific day with weak synoptic forcing. A modulation of the atmospheric temperature and moisture fields by thermally driven wind systems in the complex terrain of the Black Forest has to be considered. Averaging the fluxes over the entire COPS period minimizes temporal flux differences due to mowing and vegetation development within the class of grassland sites, allowing the effect of altitude to become visible. Higher Bowen ratios are found at the top of the mountains and lower values in the valleys.

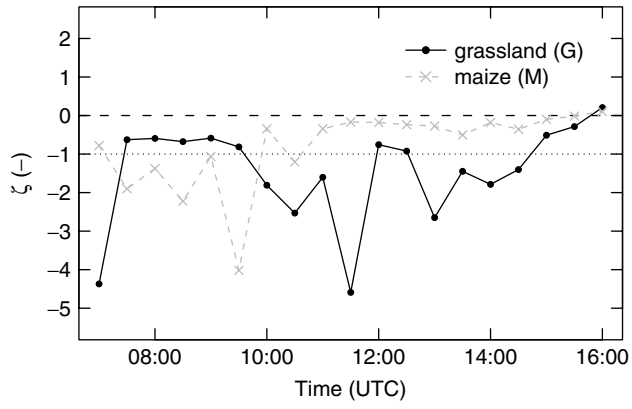

Figure 7. Stability parameter ζ from 0700–1600 UTC during IOP 8b averaged over the maize (M) fields and over the grassland (G) sites in the Upper Rhine (R) valley (see Table I).

The oasis effect, which frequently occurs over the highly evapotranspirating maize fields, is found to influence the non-closure of the surface energy balance. With the onset of the oasis effect shortly after midday, the residuum of a certain maize field in IOP 8b increases by 82%. Enhanced advective flux components during the oasis effect not caught by the EC measuring system are assumed to be the reason for the increase of the residuum.

During the oasis effect, near-ground free convection conditions cannot be observed. Nevertheless, FCCs are found at all sites of the Rench, Murg and Kinzig valleys in the Black Forest in the morning hours during IOP 8b. Recently, Eigenmann *et al.* (2009) showed for the Kinzig valley that FCCs can be found on about 50% of the days in the COPS period. Furthermore, the present study reveals that FCCs do not occur at the mountaintop sites of the Black Forest during IOPs 8b and 9c, but that FCCs are detected during both IOPs at the Upper Rhine valley sites.

Acknowledgements

The authors are grateful to the German Science Foundation (DFG), which funded the Priority Program 1167 and the COPS project. The first author was also funded by the DFG (Fo 226/19-1). Moreover, this work was supported by the French National Research Agency (ANR) (ANR-06-BLAN-0018-01) and by Météo France. We thank all participants of the COPS experiment and the COPS Operations Center for their support and data provision as well as NASA for making available the SRTM3 V2 topographical data used in Figure 1. Last but not least, the authors thank all colleagues, farmers and land owners who contributed to a successful realization of the energy balance and turbulence network during the COPS field campaign. Special thanks go to Stefan Metzger for his work during the experiment at the measuring sites of the University of Bayreuth.

References

Aoshima F, Behrendt A, Bauer H-S, Wulfmeyer V. 2008. Statistics of convection initiation by use of Meteosat rapid scan data during the Convection and Orographically-induced Precipitation Study (COPS). *Meteorol. Z.* **17**: 921–930.

Avissar R. 1991. A statistical–dynamical approach to parameterize subgrid-scale land-surface heterogeneity in climate models. *Surv. Geophys.* **12**: 155–178.

Barthlott C, Schipper JW, Kalthoff N, Adler B, Kottmeier C, Blyth A, Mobbs S. 2010. Model representation of boundary-layer convergence triggering deep convection over complex terrain: A case study from COPS. *Atmos. Res.* **95**: 172–185.

Behrendt A, Pal S, Aoshima F, Bender M, Blyth A, Corsmeier U, Cuesta J, Dick G, Dorninger M, Flamant C, Di Girolamo P, Gorgas T, Huang Y, Kalthoff N, Khodayar S, Mannstein H, Träumner K, Wieser A, Wulfmeyer V. 2011. Observation of convection initiation processes with a suite of state-of-the-art research instruments during COPS IOP 8b. *Q. J. R. Meteorol. Soc.* **137**(S1): 81–100, DOI: 10.1002/qj.758.

Bennett LJ, Blyth AM, Burton RR, Gadian AM, Weckwerth TM, Behrendt A, Di Girolamo P, Dorninger M, Lock S-J, Smith VH, Mobbs SD. 2011. Initiation of convection over the Black Forest mountains during COPS IOP15a. *Q. J. R. Meteorol. Soc.* **137**(S1): 176–189.

Beyrich F, Leps JP, Mauder M, Bange J, Foken T, Huneke S, Lohse H, Lüdi A, Meijninger WML, Mironov D, Weisensee U, Zittel P. 2006. Area-averaged surface fluxes over the LITFASS region based on eddy-covariance measurements. *Boundary-Layer Meteorol.* **121**: 33–65.

Culf AD, Foken T, Gash JHC. 2004. 'The energy balance closure problem'. In *Vegetation, Water, Humans and the Climate: A New Perspective on an Interactive System, Global Change – the IGBP Series*, Kabat P (ed). Springer: Berlin; pp 159–166.

Eigenmann R, Metzger S, Foken T. 2009. Generation of free convection due to changes of the local circulation system. *Atmos. Chem. Phys.* **9**: 8587–8600.

Foken T. 2008a.. *Micrometeorology*. Springer: Heidelberg.

Foken T. 2008b.. The energy balance closure problem: An overview. *Ecol. Appl.* **18**: 1351–1367.

Foken T, Wichura B. 1996. Tools for quality assessment of surface-based flux measurements. *Agric. Forest Meteorol.* **78**: 83–105.

Foken T, Göckede M, Mauder M, Mahrt L, Amiro BD, Munger JW. 2004. 'Post-field data quality control'. In *Handbook of Micrometeorology: A Guide for Surface Flux Measurement and Analysis*, Lee X, Massman W, Law B (eds). Kluwer: Dordrecht, pp 181–208.

Foken T, Wimmer F, Mauder M, Thomas C, Liebethal C. 2006. Some aspects of the energy balance closure problem. *Atmos. Chem. Phys.* **6**: 4395–4402.

Foken T, Mauder M, Liebethal C, Wimmer F, Beyrich F, Leps JP, Raasch S, DeBruin HAR, Meijninger WML, Bange J. 2010. Energy balance closure for the LITFASS-2003 experiment. *Theor. Appl. Climatol.* **101**: 149–160.

Fuehrer PL, Friehe CA. 2002. Flux corrections revisited. *Boundary-Layer Meteorol.* **102**: 415–457.

Göckede M, Rebmann C, Foken T. 2004. A combination of quality assessment tools for eddy covariance measurements with footprint modelling for the characterisation of complex sites. *Agric. Forest Meteorol.* **127**: 175–188.

Göckede M, Markkanen T, Hasager CB, Foken T. 2006. Update of a footprint-based approach for the characterisation of complex measurement sites. *Boundary-Layer Meteorol.* **118**: 635–655.

Göckede M, Foken T, Aubinet M, Aurela M, Banza J, Bernhofer C, Bonnefond JM, Brunet Y, Carrara A, Clement R, Dellwik E, Elbers J, Eugster W, Fuhrer J, Granier A, Grünwald T, Heinesch B, Janssens IA, Knohl A, Koeble R, Laurila T, Longdoz B, Manca G, Marek M, Markkanen T, Mateus J, Matteucci G, Mauder M, Migliavacca M, Minerbi S, Moncrieff J, Montagnani L, Moors E, Ourcival JM, Papale D, Pereira J, Pilegaard K, Pita G, Rambal S, Rebmann C, Rodrigues A, Rotenberg E, Sanz MJ, Sedlak P, Seufert G, Siebicke L, Soussana JF, Valentini R, Vesala T, Verbeeck H, Yakir D. 2008. Quality control of CarboEurope flux data – Part 1: Coupling footprint analyses with flux data quality assessment to evaluate sites in forest ecosystems. *Biogeosciences* **5**: 433–450.

Hauck C, Barthlott C, Krauß L, Kalthoff N, Schädler G, Kottmeier C. 2011. Soil moisture variability and its influence on convective precipitation over complex terrain. *Q. J. R. Meteorol. Soc.* **137**(S1): 42–56, DOI: 10.1002/qj.766.

Inagaki A, Letzel MO, Raasch S, Kanda M. 2006. Impact of surface heterogeneity on energy imbalance: A study using LES. *J. Meteorol. Soc. Jpn* **84**: 187–198.

Jegede OO, Foken T. 1999. A study of the internal boundary layer due to a roughness change in neutral conditions observed during the LINEX field campaigns. *Theor. Appl. Climatol.* **62**: 31–41.

Kalthoff N, Fiedler F, Kohler M, Kolle O, Mayer H, Wenzel A. 1999. Analysis of energy balance components as a function of orography and land use and comparison of results with the distribution of variables influencing local climate. *Theor. Appl. Climatol.* **62**: 65–84.

Kalthoff N, Adler B, Barthlott C, Corsmeier U, Mobbs S, Crewell S, Träumner K, Kottmeier C, Wieser A, Smith V, Di Girolamo P. 2009. The impact of convergence zones on the initiation of deep convection: A case study from COPS. *Atmos. Res.* **93**: 680–694.

Kalthoff N, Kohler M, Barthlott C, Adler B, Mobbs SD, Corsmeier U, Träumner K, Foken T, Eigenmann R, Krauß L, Khodayar S, Girolamo PD. 2010. The dependence of convection-related parameters on surface and boundary layer conditions over complex terrain. *Q. J. R. Meteorol. Soc.*, DOI: 10.1002/qj.686.

Kessler A. 1985. *Heat balance climatology*. Elsevier: Amsterdam.

Kottmeier C, Kalthoff N, Barthlott C, Corsmeier U, van Baelen J, Behrendt A, Behrendt R, Blyth A, Coulter R, Crewell S, DiGirolamo P, Dorninger M, Flamant C, Foken T, Hagen M, Hauck C, Höller H, Konow H, Kunz M, Mahlke H, Mobbs S, Richard E, Steinacker R, Weckwerth T, Wieser A, Wulfmeyer V. 2008. Mechanisms initiating convection during the COPS experiment. *Meteorol. Z.* **17**: 931–948.

Kracher D, Mengelkamp HT, Foken T. 2009. The residual of the energy balance closure and its influence on the results of three SVAT models. *Meteorol. Z.* **18**: 647–661.

Liebethal C, Foken T. 2003. On the significance of the Webb correction to fluxes. *Boundary-Layer Meteorol.* **109**: 99–106.

Liebethal C, Foken T. 2004. On the significance of the Webb correction to fluxes. Corrigendum. *Boundary-Layer Meteorol.* **113**: 301.

Liebethal C, Foken T. 2007. Evaluation of six parameterization approaches for the ground heat flux. *Theor. Appl. Climatol.* **88**: 43–56.

Liu HP, Peters G, Foken T. 2001. New equations for sonic temperature variance and buoyancy heat flux with an omnidirectional sonic anemometer. *Boundary-Layer Meteorol.* **100**: 459–468.

Mauder M, Foken T. 2004. '*Documentation and instruction manual of the eddy covariance software package TK2*', Work Report University of Bayreuth, Dept. of Micrometeorology, 26, 42 pp. University of Bayreuth: Bayreuth; ISSN 1614-8916.

Mauder M, Foken T. 2006. Impact of post-field data processing on eddy covariance flux estimates and energy balance closure. *Meteorol. Z.* **15**: 597–609.

Mauder M, Liebethal C, Göckede M, Leps JP, Beyrich F, Foken T. 2006. Processing and quality control of flux data during LITFASS-2003. *Boundary-Layer Meteorol.* **121**: 67–88.

Mauder M, Foken T, Clement R, Elbers JA, Eugster W, Grünwald T, Heusinkveld B, Kolle O. 2008. Quality control of CarboEurope flux data – Part 2: Inter-comparison of eddy-covariance software. *Biogeosciences* **5**: 451–462.

Mayer JC, Staudt K, Gilge S, Meixner FX, Foken T. 2008. The impact of free convection on late morning ozone decreases on an Alpine foreland mountain summit. *Atmos. Chem. Phys.* **8**: 5941–5956.

Mengelkamp HT, Beyrich F, Heinemann G, Ament F, Bange J, Berger F, Bösenberg J, Foken T, Hennemuth B, Heret C, Huneke S, Johnsen KP, Kerschgens M, Kohsiek W, Leps JP, Liebethal C, Lohse H, Mauder M, Meijninger W, Raasch S, Simmer C, Spiess T, Tittebrand A, Uhlenbrock J, Zittel R. 2006. Evaporaton over a heterogeneous land surface – The EVA-GRIPS project. *Bull. Am. Meteorol. Soc.* **87**: 775–786.

Moore CJ. 1986. Frequency response corrections for eddy correlation systems. *Boundary-Layer Meteorol.* **37**: 17–35.

Munn RE. 1966. *Descriptive micrometeorology*. Academic Press: New York.

Oke TR. 1987. *Boundary layer climate*. Methuen: London.

Oncley SP, Foken T, Vogt R, Kohsiek W, DeBruin HAR, Bernhofer C, Christen A, van Gorsel E, Grantz D, Feigenwinter C, Lehner I, Liebethal C, Liu H, Mauder M, Pitacco A, Ribeiro L, Weidinger T. 2007. The Energy Balance Experiment EBEX-2000. Part I: Overview and energy balance. *Boundary-Layer Meteorol.* **123**: 1–28.

Raabe A. 1983. On the relation between the drag coefficient and fetch above the sea in the case of off-shore wind in the near-shore zone. *Z. Meteorol.* **33**: 363–367.

Rannik Ü, Markkanen T, Raittila J, Hari P, Vesala T. 2003. Turbulence statistics inside and over forest: Influence on footprint prediction. *Boundary-Layer Meteorol.* **109**: 163–189.

Rebmann C, Göckede M, Foken T, Aubinet M, Aurela M, Berbigier P, Bernhofer C, Buchmann N, Carrara A, Cescatti A, Ceulemans R, Clement R, Elbers JA, Granier A, Grünwald T, Guyon D, Havránková K, Heinesch B, Knohl A, Laurila T, Longdoz B, Marcolla B, Markkanen T, Miglietta F, Moncrieff J, Montagnani L, Moors E, Nardino M, Ourcival JM, Rambal S, Rannik Ü, Rotenberg E, Sedlak P, Unterhuber G, Vesala T, Yakir D. 2005. Quality analysis applied on eddy covariance measurements at complex forest sites using footprint modelling. *Theor. Appl. Climatol.* **80**: 121–141.

Savelyev SA, Taylor PA. 2005. Internal boundary layers: I. Height formulae for neutral and diabatic flows. *Boundary-Layer Meteorol.* **115**: 1–25.

Schotanus P, Nieuwstadt FTM, DeBruin HAR. 1983. Temperature measurement with a sonic anemometer and its application to heat and moisture fluxes. *Boundary-Layer Meteorol.* **26**: 81–93.

Shen S, Leclerc MY. 1995. How large must surface inhomogeneities be before they influence the convective boundary layer structure? A case study. *Q. J. R. Meteorol. Soc.* **121**: 1209–1228.

Stull RB. 1988. *An Introduction to Boundary Layer Meteorology*, Atmospheric Sciences Library. Kluwer Academic Publishers: Dordrecht.

Tanner BD, Swiatek E, Greene JP. 1993. 'Density fluctuations and use of the krypton hygrometer in surface flux measurements'. In *Management of Irrigation and Drainage Systems: Integrated Perspectives*, Allen RG (ed). American Society of Civil Engineers: New York, USA, pp 945–952.

Thomson DJ. 1987. Criteria for the selection of stochastic models of particle trajectories in turbulent flows. *J. Fluid Mech.* **180**: 529–556.

Twine TE, Kustas WP, Norman JM, Cook DR, Houser PR, Meyers TP, Prueger JH, Starks PJ, Wesely ML. 2000. Correcting eddy-covariance flux underestimates over a grassland. *Agric. Forest Meteorol.* **103**: 279–300.

van Dijk A, Kohsiek W, DeBruin HAR. 2003. Oxygen sensitivity of krypton and Lyman-alpha hygrometers. *J. Atmos. Ocean. Tech.* **20**: 143–151.

Vickers D, Mahrt L. 1997. Quality control and flux sampling problems for tower and aircraft data. *J. Atmos. Ocean. Tech.* **14**: 512–526.

Webb EK, Pearman GI, Leuning R. 1980. Correction of flux measurements for density effects due to heat and water-vapor transfer. *Q. J. R. Meteorol. Soc.* **106**: 85–100.

Weckwerth TM, Wilson JW, Hagen M, Emerson TJ, Grebe L. 2011. Radar climatology of the COPS region. *Q. J. R. Meteorol. Soc.* **137**(S1): 31–41.

Wenzel A, Kalthoff N. 2000. Method for calculating the whole-area distribution of sensible and latent heat fluxes based on climatological observations. *Theor. Appl. Climatol.* **66**: 139–160.

Wenzel A, Kalthoff N, Fiedler F. 1997. On the variation of the energy balance components with orography in the Upper Rhine Valley. *Theor. Appl. Climatol.* **57**: 1–9.

Wilczak JM, Oncley SP, Stage SA. 2001. Sonic anemometer tilt correction algorithms. *Boundary-Layer Meteorol.* **99**: 127–150.

Wilson JD, Sawford BL. 1996. Review of Langrangian stochastic models for trajectories in the turbulent atmosphere. *Boundary-Layer Meteorol.* **78**: 191–210.

Wilson K, Goldstein A, Falge E, Aubinet M, Baldocchi D, Berbigier P, Bernhofer C, Ceulemans R, Dolman H, Field C, Grelle A, Ibrom A, Law BE, Kowalski A, Meyers T, Moncrieff J, Monson R, Oechel W, Tenhunen J, Valentini R, Verma S. 2002. Energy balance closure at FLUXNET sites. *Agric. Forest Meteorol.* **113**: 223–243.

Wulfmeyer V, Behrendt A, Bauer HS, Kottmeier C, Corsmeier U, Blyth A, Craig G, Schumann U, Hagen M, Crewell S, Di Girolamo P, Flamant C, Miller M, Montani A, Mobbs S, Richard E, Rotach MW, Arpagaus M, Russchenberg H, Schlüssel P, König M, Gärtner V, Steinacker R, Dorninger M, Turner DD, Weckwerth T, Hense A, Simmer C. 2008. The convective and orographically-induced precipitation study: A Research and Development Project of the World Weather Research Program for improving quantitative precipitation forecasting in low-mountain regions. *Bull. Am. Meteorol. Soc.* **89**: 1477–1486.

Wulfmeyer V, Behrendt A, Kottmeier C, Corsmeier U, Barthlott C, Craig G, Hagen M, Althausen D, Aoshima F, Bauer HS, Bennett L, Blyth A, Brandau C, Crewell S, Dick G, Di Girolamo P, Dorninger M, Dufournet Y, Ehret G, Engelmann R, Flamant C, Foken T, Gorgas T, Grzeschik M, Handwerker J, Hauck C, Höller H, Junkermann W, Kalthoff N, Kiemle C, Klink S, König M, Krauss L, Long CN, Madonna F, Mobbs S, Neininger B, Pal S, Peters G, Pigeon G, Radlach M, Richard E, Rotach MW, Russchenberg H, Schwitalla T, Smith V, Steinacker R, Trentmann J, Turner DD, van Baelen J, Vogt S, Volkert H, Weckwerth T, Wernli H, Wieser A, Wirth M. 2011. The Convective and Orographically-Induced Precipitation Study (COPS): the scientific strategy, the field phase, and research highlights. *Q. J. R. Meteorol. Soc.* **137**(S1): 3–30, DOI: 10.1002/qj.752.

Appendix D: Zhou et al. (2011)

Theor Appl Climatol (2011) 105:217–228
DOI 10.1007/s00704-010-0393-5

ORIGINAL PAPER

The study of near-ground free convection conditions at Nam Co station on the Tibetan Plateau

Degang Zhou · Rafael Eigenmann · Wolfgang Babel · Thomas Foken · Yaoming Ma

Received: 18 May 2010 / Accepted: 6 December 2010 / Published online: 1 January 2011

Abstract This study investigates the near-ground free convection conditions (FCCs) based on eddy covariance (EC) measurements at Nam Co station near the Nam Co Lake on the Tibetan Plateau (TP). The spatial and temporal structure of EC measurements at this station is evaluated by using the comprehensive software package TK2 together with a footprint model. The obtained high-quality turbulent flux data are used to study the occurrence of FCCs, which can be detected with the EC system by calculating the stability parameter. Two types of generation of FCCs can be identified. (1) During the wind direction change of a diurnal thermally forced land-lake circulation system in the morning, strongly reduced wind speeds and simultaneously high buoyancy fluxes lead to a period of dominance of buoyancy over shear, and hence, to the occurrence of FCCs. (2) On days with the appearance of clouds, the land-lake circulation is weakened or reversed, dependent on the temperature gradients between the land and the Nam Co Lake. During the period of adaptation of the land-lake breeze to the alternating situation of heating differences, wind speeds decrease and buoyancy again dominates over shear near the ground. These are the situations where FCCs are also detected during the entire day at Nam Co station. The investigation of FCCs regarding the whole measurement period shows that FCCs can be mainly attributed to case (1) during the non-monsoon period, while FCCs are generated by both mechanisms (1 and 2) during the monsoon season. An impact of the FCCs on the near-ground profiles of air temperature and humidity is demonstrated. The FCCs are assumed to play an important role for the land surface-atmosphere exchange processes and the atmospheric boundary layer (ABL) conditions on the TP by providing an effective transport mechanism of near-ground air mass characteristics into upper parts of the ABL.

D. Zhou (✉)
Centre for Monsoon System Research, Institute of Atmospheric Physics, Chinese Academy of Sciences,
P.O. Box 2718, No. 6, Bei'ertiao, Haidian district,
Beijing 100190, China
e-mail: degangzhou@163.com

R. Eigenmann · W. Babel · T. Foken
Department of Micrometeorology, University of Bayreuth,
Universitätsstrasse 30,
95440, Bayreuth, Germany

Y. Ma
Institute of Tibetan Plateau Research,
Chinese Academy of Sciences,
P.O. Box 2871, Beijing 100085, China

1 Introduction

The Tibetan Plateau (TP) is the largest and highest plateau in the world. Because of the topographic feature of the TP, the underlying surface absorbs a large amount of solar radiation and undergoes dramatic diurnal and seasonal changes of surface heating and water fluxes. Such energy and water cycles on the TP play an important role in the Eastern Asian Monsoon circulation (e.g., Ye and Gao 1979). Several large field experiments such as GAME-Tibet and CAMP-Tibet were carried out to investigate the land surface-atmosphere exchange processes on the TP, whose findings are reported in many studies (e.g., Yang et al. 2002, 2004; Ma et al. 2002, 2005; Zuo et al. 2005). The terrain on the TP consists of a lot of different land use types such as lake, glacier, alpine steppe, bare soil, and wetland with different scales. As a consequence, there are complex interactions between different types of land use and the atmosphere, which affect the development of thermally induced circulations and water and energy cycles (Whiteman

1990; Segal and Arritt 1992; Li et al. 2006; Lu et al. 2008), and the occurrence of large thermal convective cells (Chen et al. 2002). In general, land surface-atmosphere interactions are highly decisive for the local occurrence and timing of the initiation of convection, cloud formation, and precipitation (e.g., Hanesiak et al. 2004; Chen and Avissar 1994; Rabin et al. 1990; Banta 1990; Raymond and Wilkening 1980).

Following the study of Eigenmann et al. (2009), the present study aims at the investigation of near-ground free convection conditions (FCCs) in experimental data at Nam Co Station for Multisphere Observation and Research, Chinese Academy of Sciences (hereinafter Nam Co station). FCCs observed at ground level may result in an effective, vertical transport of near-ground air mass characteristics into upper parts of the atmospheric boundary layer (ABL). An impact of the FCCs on the vertical wind speeds in the ABL measured with a Sodar and on ozone concentrations at a mountain summit was recently demonstrated by Eigenmann et al. (2009) and Mayer et al. (2008), respectively. Both authors detected FCCs with the help of an eddy covariance (EC) system by calculating the stability parameter from directly measured turbulent flux data. In the present study, the same approach will be applied to detect FCCs at Nam Co station. As the EC data are used for the detection of FCCs, this study will also give a short introduction in the EC data processing and EC data quality including footprint analysis at Nam Co station. A more detailed quality assessment of EC data at Nam Co station can be looked up in Metzger et al. (2006). The preconditions for the occurrence of FCCs are periods of high buoyancy fluxes which coincide with a strong decrease of the wind speed. Buoyancy then dominates over shear within turbulence production near the ground. In the case of Eigenmann et al. (2009), the drop of the wind speed was initiated by a change of the diurnal valley circulation system in the Kinzig valley, Black Forest, southwestern Germany. The nighttime down-valley winds cease and up-valley winds slowly build up in the morning, leading to the low wind speeds during the period of wind direction change in the Kinzig valley. Similar findings were reported by Mayer et al. (2008). These authors found that ozone drop events on a mountain summit in the Alpine foreland of southern Germany can be attributed to the occurrence of FCCs, which effectively transport ozone-free air masses from the nearby valley towards the measuring site at the mountain top. In their study, the low wind speed period in the morning, which triggers the occurrence of FCCs, is caused by a change of the wind direction of a mesoscale circulation system known as Alpine Pumping (Lugauer and Winkler 2005). Similar mechanisms leading to FCCs are assumed to occur at Nam Co station on the TP. A numerical simulation of the ABL flow characteristics in the region of the Nam Co station by Lu et al. (2008) recently indicated that local circulation systems near Nam Co station include a wind circulation between a nearby mountain range and its foreland as well as a smaller scale circulation induced by the inhomogeneity of thermal forcing between the large Nam Co Lake and the grasslands. This land-lake circulation system is expected to trigger FCCs at Nam Co station. In general, the FCCs are assumed to play an important role for the land surface-atmosphere exchange processes on the TP similar to the findings in other study areas as described above.

The article is organized as follows. Section 2 introduces the field measurements at Nam Co station. Section 3 outlines some typical features of EC data quality by applying a footprint model, and Section 4 presents the findings of the investigation of FCCs at Nam Co station. Conclusions are given in Section 5.

2 Field measurements at Nam Co station

Nam Co station (30.773 N, 90.963 E, 4,745 m a.s.l.) was established by the Institute of Tibetan Plateau Research, Chinese Academy of Sciences in August 2005. The station is located at 1 km distance southeast of Nam Co Lake, which is the second largest saline lake on the TP (Guan et al. 1984). Moreover, the station is situated 15 km north-northwest of a mountain range (Nyainqentanglha Mountain) oriented from west-southwest to east-northeast with an altitude of up to 5,700 m a.s.l. Figure 1 shows the position of the Nam Co station and the distribution of the land use. A small inner lake oriented from west-southwest to east-northeast is located 300 m northwestern, and a 52-m meteorological tower 40 m northeastern of the EC flux site. Furthermore, a solar panel, the station main building, and another building are located 70 m, 90 m, and 105 m about 10° west by south of the flux site, respectively. The terrain is slightly inclined with the altitude dropping by about 1 m on a 250-m distance along the direction from the flux site to the inner lake. The dominating land use class is alpine steppe, referred to as grass(−) in Fig. 1, with a canopy height not exceeding 5 cm. A small portion of grass is higher and denser, which is named grass(+). To sum up, the canopy at Nam Co station can be considered as rather homogenous.

The 52-m meteorological tower was set up to observe the lower boundary layer with wind speed, air temperature, and relative humidity measurements in five levels (1 m, 2 m, 4 m, 10 m, and 20 m), and wind direction measurements in three levels (1 m, 2 m, and 20 m). Additionally, pressure and precipitation were measured as well as the soil temperature and the soil moisture content in six levels (0 cm, 10 cm, 20 cm, 40 cm, 80 cm, and 160 cm). The averaging interval of all these measurements was 10 min.

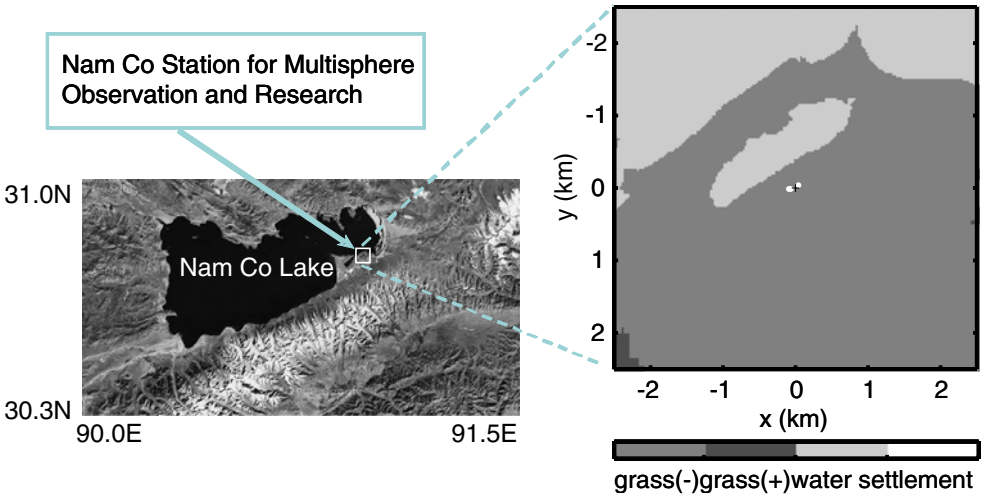

Fig. 1 Position and land use map of Nam Co station. The land uses at Nam Co station include short grass, referred to as grass(−), denser grass, referred to as grass(+), water, and settlement

The EC flux site was equipped with a CSAT3 (Campbell Scientific, Inc.) sonic anemometer and a LI-7500 (LI-COR Biosciences) open-path H_2O/CO_2 gas analyzer at a height of 3 m. The sampling frequency was 10 Hz. Additionally, upward and downward components of long wave (Kipp & Zonen CG3) and shortwave radiation (Kipp & Zonen CM3) were measured with an averaging interval of 30 min. All measurements are available for about 7 months from 21 March 2007 to 21 October 2007. However, data failure occurred from 20 April to 24 May due to instrument malfunction.

3 Data processing and quality control of turbulence measurements

The turbulent flux measurements at Nam Co station were carried out with the EC method. This method is one of the best measurement techniques currently available for the determination of material and energy fluxes between the atmosphere and the underlying surface (Moncrieff 2004), although some general problems are still present, e.g., the widespread shortfall of the sum of sensible and latent heat flux measured by this method as compared to the available energy (e.g., Aubinet et al. 2000; Foken 2008a). The EC method has become by now a widely accepted tool for the determination of mass and energy fluxes applied by several flux networks such as Ameriflux, CARBOEUROFLUX and Asia Flux, overall coordinated within FLUXNET (Baldocchi et al. 2001). Moreover, the focus of flux observations has shifted progressively from ideal and homogeneous sites to sites within complex and heterogeneous terrain (e.g., Schmid 2002). In general, the adoption of the EC method is based on the assumption that certain statistical and meteorological requirements are fulfilled (e.g., Massman and Lee 2002; Foken and Wichura 1996) and that the equipment is working reliably. With the development of the quality control and site characterization procedure including footprint investigations (e.g., Foken et al. 2004; Mauder et al. 2006; Göckede et al. 2004, 2006, 2008), site-specific spatial quality structures and the spatial representativeness of the measured fluxes can be identified, given that the underlying land use distribution is available. This approach improves our understanding of the flux measurements and survey in complex terrain and is also applied to the EC flux data at Nam Co station within the present study.

The turbulent flux data were post-processed with the comprehensive software package TK2 developed at the Department of Micrometeorology, University of Bayreuth (Mauder and Foken 2004; Mauder et al. 2008). The software comprises all state of the art flux corrections and post-field quality control including tests for steady state and integral turbulence characteristics (Foken and Wichura 1996; Foken et al. 2004). Planar fit rotation according to Wilczak et al. (2001) was done for six periods, P1 to P6, due to changes in vegetation structure and large-scale meteorological conditions. The start time and end time of these periods, and the momentum roughness length of grass (−) derived from Monin–Obukhov similarity theory during these periods are reported in Table 1. Here, P1, P2, and P6 are periods during the non-monsoon period, P4 and P5 periods during the inner-monsoon period, and P3, a period during the transition of both.

Figure 2 shows the diurnal and seasonal variations of the sensible heat flux, the latent heat flux, the friction velocity, u_*, as well as the wind direction for the entire measurement period at Nam Co station. The results indicate that the sensible heat flux dominates the energy transfer from the Earth's surface into the atmosphere before monsoon. However, with the start of the monsoon period in July, the values of the sensible heat flux decrease and latent heat dominates the turbulent energy exchange at the surface until the retreat of monsoon in October. The friction velocity is usually small during the night and increases in

Table 1 The start time and end time of the planar fit periods P1 to P6 distinguished for the processing of turbulent flux data at Nam Co station in 2007. The momentum roughness length, z_{0m}, of grass(−) during each period is also given

Period	P1	P2	P3	P4	P5	P6
Start time	22 Mar	25 May	21 Jun	29 Jul	20 Aug	18 Sept
End time	20 Apr	19 Jun	26 Jul	17 Aug	17 Sept	21 Oct
z_{0m} (mm)	3.9	3.8	5.3	7.3	6.0	4.0

the daytime. A diurnal circulation system present at Nam Co station becomes visible regarding the wind direction in Fig. 2d. Winds coming from northwest to southwest prevail in the daytime, while easterly to southerly winds dominate at night. During non-monsoon, the diurnal circulation is superimposed by a southwesterly flow, while during monsoon, an increased southeasterly component is obvious.

Footprint analyses according to Göckede et al. (2004, 2006) in combination with the data quality flagging scheme of Foken et al. (2004) were performed with a forward Lagrangian footprint model (Rannik et al. 2003; Göckede et al. 2005). Detailed terrain data were used for the land use distribution. Metzger et al. (2006) already investigated the temporal and spatial quality distribution of turbulent flux data at Nam Co station. Their results indicated that the general poor data quality of the sensible heat flux might be attributed to the occurrence of organized structures or mesoscale flow patterns in the boundary layer at the site. In this study, only a short overview of the results of the quality control effort applied on the turbulent flux data shall be given in the following.

Footprint calculations were performed in all periods, P1 to P6. The momentum roughness lengths of the lake and of the settlement were set constant to 0.002 m and 0.5 m, respectively, and the momentum roughness length of grass (+) was set to double the value of grass(−) in each period as listed in Table 1. The resolution of the land use map used for the footprint calculations amounts to 20 m (see Fig. 1). In the following, only the footprint analysis results of the period P5 are presented. The results in the other periods are similar and not discussed within this study. Moreover, the quality flagging scheme according to Rebmann et al. (2005) is used for all following figures, with flags ranging from 1 (good data quality) to 5 (poor data quality). Figure 3 shows the spatial distribution of the quality flags of the friction velocity during the period P5 as related to the footprint climatology. It can be seen that during unstable and neutral stratifications, quality ratings within the 5% effect level ring mostly consist of classes 1 and 2, which means that the data are suitable for fundamental research. However, during stable stratification, quality flags sometimes degrade to class 3 or 4. In the case of the footprint analyses of the sensible heat flux (not shown), most of the quality flags are rated as 1 or 2 during unstable stratification, while during neutral and stable stratifications, quality flags degrade even to 5.

The reason for the poor quality ratings (flag 5) of the friction velocity during the day and during the night is obviously different. Eighty-one percent of the bad values rated as 5 among the nighttime data can be related to bad integral turbulence characteristics. This means that there is a big deviation of the friction velocity from statistical

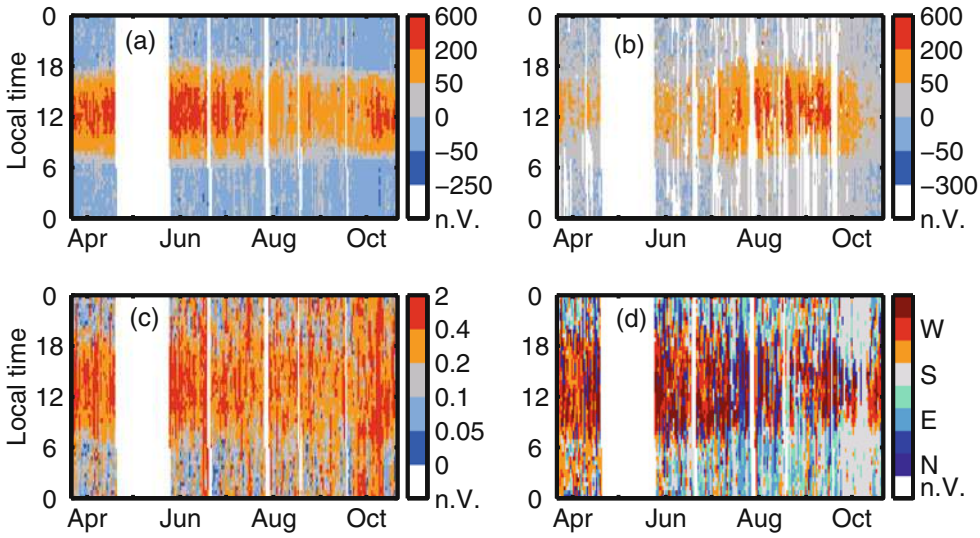

Fig. 2 The diurnal variations of **a** the sensible heat flux (W m^{-2}), **b** the latent heat flux (W m^{-2}), **c** the friction velocity, u_* (m s^{-1}), and **d** the wind direction over the entire measurement period at Nam Co station. The values of the variables are *color-coded* (values of the variables are gray-coded for the printed version)

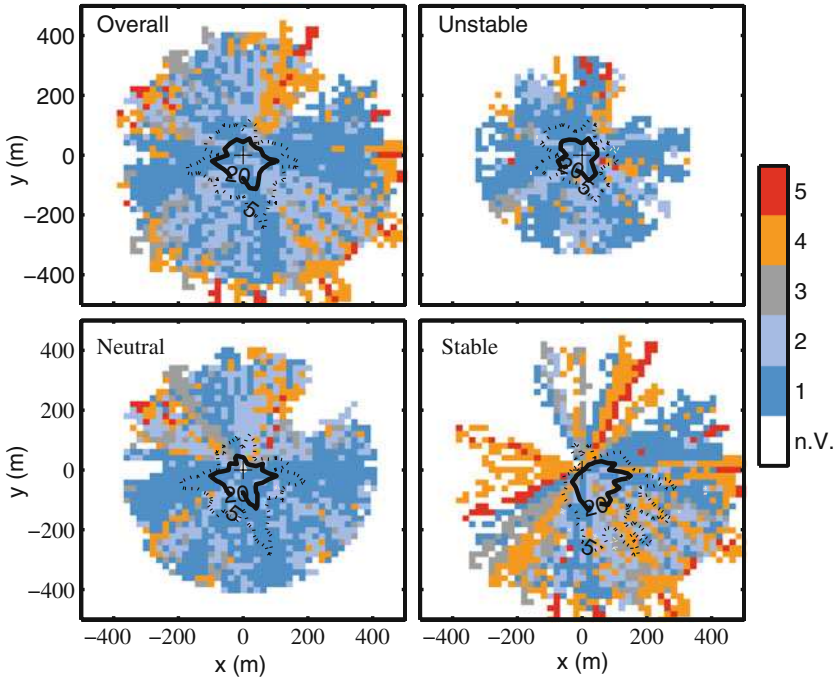

Fig. 3 Spatial distribution of quality flags of the friction velocity as related to footprint climatology depending on atmospheric stratification at Nam Co station. The flux site is indicated by the central, *black* (white in the printed version) *crosshair*, whereas quality flags (1–5) after Rebmann et al. (2005) are distinguished according to the color bar. *Black* (white in the printed version) *contour lines* display the 5% (*dotted*) and 20% (*solid*) effect level rings of the measurements

similarity characteristics under strong stable stratification, which might be related to the occurrence of intermittency or gravity waves. On the contrary, 68% of the bad values rated as 5 among the daytime data can be attributed to stationarity problems.

Regarding the spatial distribution of quality flags, the bad-rated measurements in the western and northeastern upwind sector can be explained by the influence of the station building and the meteorological tower on the measurements. As the effect of a slightly inclined terrain is eliminated by the planar fit rotation and the bad quality ratings indeed do not concentrate on a certain sector, the poor quality flags within other sectors than the western and northeastern cannot be attributed to the local topography. Consequently, this implies that instationarity is the reason for the bad quality ratings in the other sectors in the daytime, which is caused by changing mesoscale or local flow patterns.

Moreover, the surface energy imbalance was investigated at Nam Co station. For example, the average non-closure during the period P5 reaches 31%. This value is similar to those found in previous studies on the TP (Tanaka et al. 2001; Yang et al. 2004). The soil heat flux in the present study is calculated by using six layers of soil temperature and soil moisture content and applying the thermal diffusion equation and correction method according to Yang and Wang (2008). In the present literature of the energy balance closure discussion (e.g., Foken et al. 2010; Foken 2008a; Culf et al. 2004), the landscape heterogeneity, which induces advective and low-frequency flux components (e.g., Foken et al. 2006), and secondary circulations (e.g., Inagaki et al. 2006), which may transport the surplus of energy not caught by the standard EC measurements, are considered to mainly cause the residuum of the surface energy balance. In summary, the terrain features at Nam Co station are predestinated to induce thermally driven circulations, thus, influencing the non-closure of the surface energy balance.

4 Near-ground free convection conditions

4.1 The detection of FCCs

FCCs occur in the atmosphere if the buoyancy term dominates over the shear term within the turbulence kinetic energy equation (e.g., Stull 1988). The buoyancy term (B),

$$B = \frac{g}{\overline{\theta_v}} \cdot \left(\overline{w'\theta_v'}\right)_0, \tag{1}$$

consists of the product of the buoyancy parameter, $g \cdot \overline{\theta_v}^{-1}$, and the buoyancy flux at the surface, $\overline{w'\theta_v'}$. The buoyancy parameter is the quotient of the acceleration due to gravity, g, and the mean virtual potential temperature, $\overline{\theta_v}$. The shear term (S),

$$S = -\overline{u'w'} \cdot \frac{\partial \overline{u}}{\partial z}, \tag{2}$$

is the product of the momentum flux, $\overline{u'w'}$, and the wind shear, $\partial\overline{u}/\partial z$. The quotient of B and S can also be expressed as the flux Richardson number R_f (e.g., Stull

1988). During unstable stratification ($R_f < 0$), R_f equals the stability parameter (e.g., Ayra 2001),

$$\zeta = \frac{z}{L} = -\frac{z \cdot \kappa \cdot g \cdot \left(\overline{w'\theta_v'}\right)_0}{\overline{\theta_v} \cdot u_*^3}, \quad (3)$$

where z denotes the measurement height, L the Obukhov length, κ the von-Kármán's constant, and u_* the friction velocity. Consequently, by calculating the stability parameter, ζ, from directly measured EC turbulent flux data, free convection conditions can be detected for $\zeta < -1$ (e.g., Foken 2008b). Regarding Eq. 3, the fulfillment of $\zeta < -1$ for the occurrence of FCCs requires that high buoyancy fluxes coincide with small values of u_* at the same time.

In the following sections, the averaging interval of the EC flux data is reduced from 30 min to 5 min in order to get a better insight into the temporal structure of the FCCs. Therefore, it should be kept in mind that the depicted turbulent fluxes do not include spectral energy from eddies of larger scales. Moreover, the investigation of FCCs is restricted to days with no precipitation during the day and to time periods when the sensible heat flux exceeds the threshold of 20 Wm^{-2}. This threshold seems to be reasonable for the criteria of high buoyancy fluxes required for the occurrence of FCCs according to Eq. 3. Low values of u_* occur at Nam Co station during the wind direction change of a land-lake wind circulation system between the Nam Co Lake and the grassland, which dominates the local flow structure at the measuring site (see e.g. Lu et al. 2008). Hence, the change of the thermally induced circulation is able to cause the occurrence of FCCs at Nam Co station. Two types of processes leading to the low wind speed periods in combination with a wind direction change of the circulation system, and consequently to the occurrence of FCCs, can be distinguished and are presented in the next section.

4.2 The types of generation of FCCs

4.2.1 Generation of FCCs due to a change of the diurnal circulation system

The first type of generation of FCCs is similar to the case detected by Eigenmann et al. (2009) in the Kinzig valley, Black Forest, southwestern Germany, where FCCs appear in the morning hours during the change of the diurnal valley circulation system from down to up-valley winds. Typical for this type of generation of FCCs is that the drop of the horizontal wind speed, which is together with high buoyancy fluxes a precondition for the occurrence of FCCs (see Eq. 3), is caused by the wind direction change of a diurnal circulation system in the morning after sunrise. This diurnal circulation system is forced by solar heating on fair weather days. The low wind speeds occur during the wind direction change when the previously prevailed wind ceases and winds from another direction start to build up according to the thermal forcing.

At Nam Co station, a diurnal circulation system can be observed on many fair weather days as shown in Fig. 4. Regarding the wind statistics for the entire measurement period, it can be confirmed that a thermally induced, land-lake wind circulation between Nam Co Lake and the grassland near the station is dominating the local wind regime at Nam Co station (see also Fig. 1). During the daytime (Fig. 4a), the frequent occurrence of a lake breeze is obvious from the high frequency of winds coming from northwestern directions (7.3%). Higher frequencies can also be found in the west-southwestern sector. On the contrary, during the night (Fig. 4b), a land breeze with south-southeastern wind directions dominates the flow regime. A diurnal land-lake wind circulation at Nam Co site was also recently confirmed by the numerical simulations of Lu et al. (2008).

Figure 5 gives an example for the occurrence of FCCs on 29 June 2007. Each 5-min value, where the stability parameter, ζ, is lower than -1, is marked by gray dotted lines in Fig. 5a. It is obvious that FCCs are present during the time from 0625 to 0740 hours local time (in this study, local time corresponds to local solar time=Beijing time −2 h) in the morning. At this time, after sunrise, the sensible and latent heat flux (Fig. 5b) are already large enough, but the friction velocity, u_* (0.11 ms^{-1}), and the horizontal wind speed are still very small (Fig. 5c), so that FCCs are triggered according to Eq. 3. The small values of u_* and the horizontal wind speed can be related to the change of the wind direction (Fig. 5e) from southeast to northwest during the onset of the lake breeze. The downward solar radiation in Fig. 5d indicates fair weather conditions on this day, which force the diurnal circulation system. Finally, the data quality flags of u_*, ranging from 1 (good data quality) to 5 (low data quality) according to Rebmann et al. (2005), are depicted in Fig. 5f for half-hour intervals. Note that the quality flags of u_* during the daytime are good (flag 1). However, during the FCCs from 0630 to 0730 hours, the flags degrade to 3 due to stationarity problems.

4.2.2 Generation of FCCs due to the adaption of the land-lake wind circulation system to surface heating differences during cloud cover

The second type of generation of FCCs is closely related to the appearance of clouds during the entire daytime. Clouds frequently occur during the monsoon period at Nam Co site and decrease the direct solar radiation which reaches the surface. As a consequence, the lake breeze between the Nam Co Lake and the grassland at Nam Co station, which normally builds up in the daytime on undisturbed radiation days (see

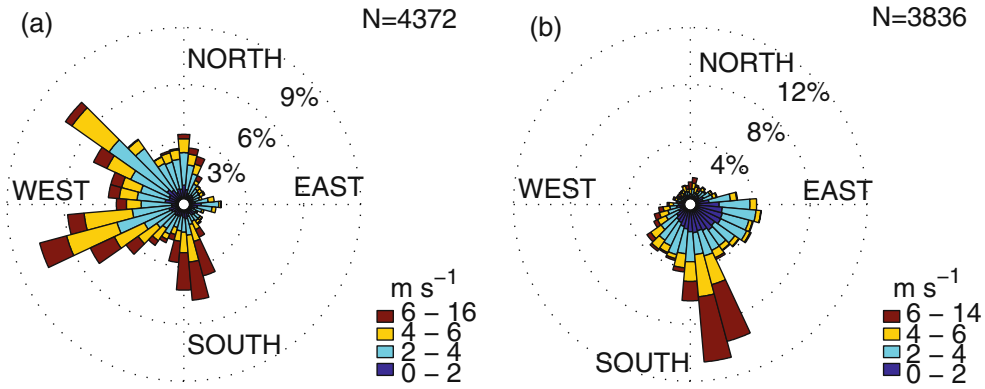

Fig. 4 Wind statistics at Nam Co station during the entire measurement period **a** during the daytime and **b** during the night

Fig. 5d, e), is weakened or even a reversal can be observed. The cloud shading leads to a strong and fast drop of the surface temperature over the grassland, while the lake surface temperature only experiences a small decrease due to the high heat capacity of water. During the period of weakening or reversal of the circulation system, horizontal wind speeds and shear are reduced, and buoyancy dominates the production of turbulence, thus leading to the occurrence of FCCs. If the reversal of the circulation system (land breeze) occurs during cloud shading, FCCs can also be triggered at the time the land breeze shifts back again to a lake breeze shortly after the disappearance of clouds. At these times, temperature gradients and wind speeds are lowered again, buoyancy dominates over shear and FCCs occur.

Figure 6 depicts a typical case on 23 August 2007 with several periods of FCCs marked by the gray dotted lines in Fig. 6a. The latent heat flux generally exceeds the sensible heat flux on that day (Fig. 6b). The periods of FCCs coincide with periods of small values of the friction velocity (Fig. 6c). The daily course of the downward solar radiation (Fig. 6d) shows the appearance of clouds in the daytime with a minimum of 174 Wm^{-2} at 1200 hours. At 1200 hours, a reversal of the circulation system is obvious from Fig. 6e. From 1100 to 1140 hours, the surface skin temperature and the air temperature at 2 m height at Nam Co station decreases by 3.5 K and 0.8 K, respectively, while the air temperature above the lake can be assumed to show only some small and slow changes. As a consequence, the lake breeze circulation is weakened. Winds come from the Nam Co Lake (western directions) until 1205 hours, shift to a land breeze (eastern, southeastern directions) until 1425 hours, and rotate back to wind directions coming from the lake (north, northwestern directions) afterwards. The surface skin temperature and the air temperature again increase by 11.1 K

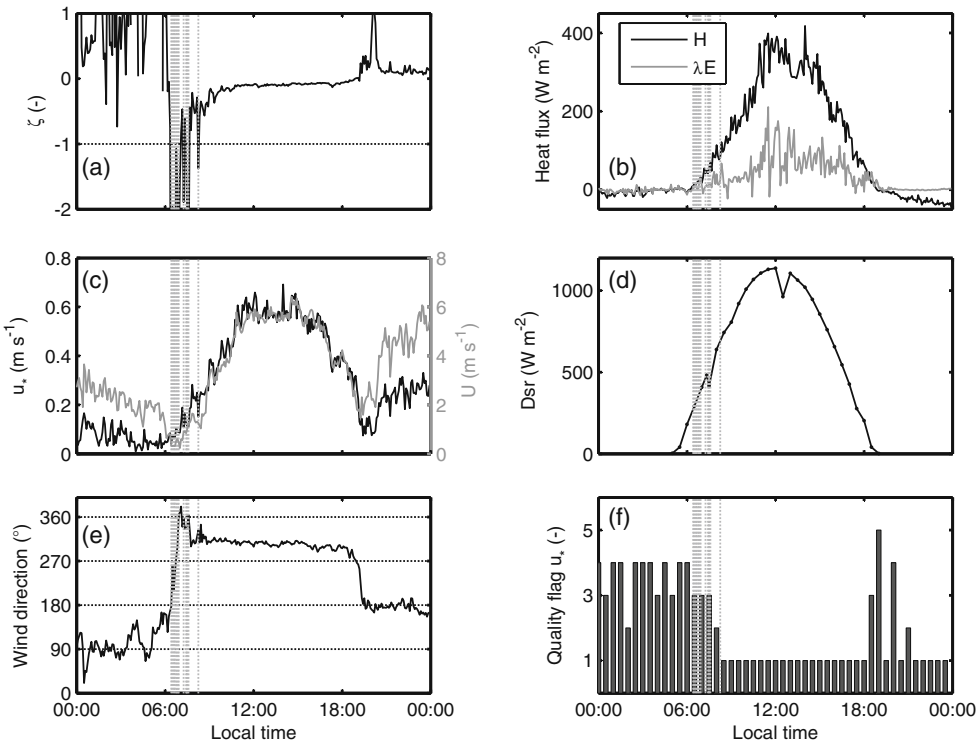

Fig. 5 Daily courses of **a** the stability parameter, **b** the sensible and latent heat flux (W m^{-2}), **c** the friction velocity and the horizontal wind (m s^{-1}), **d** the downward solar radiation (W m^{-2}), **e** the wind direction, and **f** the quality flags of the friction velocity on 29 June 2007. The periods of FCCs are indicated by the *gray dotted lines* in each plot

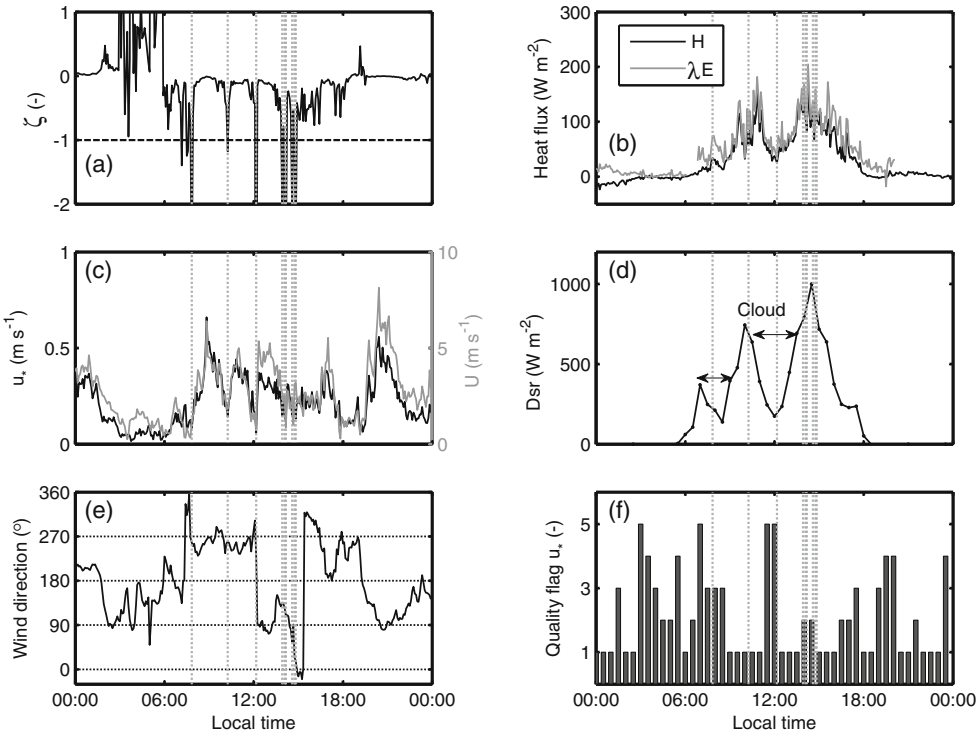

Fig. 6 Daily courses of **a** the stability parameter, **b** the sensible and latent heat flux (W m^{-2}), **c** the friction velocity and the horizontal wind (m s^{-1}), **d** the downward solar radiation (W m^{-2}), **e** the wind direction, and **f** the quality flags of the friction velocity on 23 August 2007. The periods of FCCs are indicated by the *gray dotted lines* in each plot

and by 3.8 K from 1300 to 1440 hours, respectively. During the reversal of the lake breeze to winds coming from the land (1205 hours) and during the repeated onset of the lake breeze (1400–1500 hours), FCCs are detected (see Fig. 6a). These FCCs are triggered by the periods of low wind speeds and u_* (Fig. 6c), which come along with the cessation and the onset of the lake breeze. Furthermore, the two periods of FCCs at 0750 and 1015 hours can also be related to cloud cover periods (see Fig. 6d) and to a weakening of the prevailing circulation system. The quality flags of u_* are shown in Fig. 6f. During the FCCs at 0750 hours and noon, data quality is poor (flag 3 and 5, respectively). At 0750 hours, the poor data quality can be attributed to stationarity problems, while at noon, stationarity problems together with bad integral turbulence characteristics are found. During the other periods of FCCs on this day, data quality is rather good (mainly flags 1 and 2).

The second type of generation of FCCs is quite different to the first type, as the appearance of clouds determines the occurrence of FCCs during the day. On some days, FCCs can be attributed to both types of generation. The distribution of FCCs during the entire measurement period is addressed in Section 4.4.

4.3 Impact of FCCs on near-ground boundary layer conditions

The impact of the FCCs on the boundary layer conditions near the surface is investigated with the help of the measurements of the meteorological tower. The results are exemplarily shown for 29 June 2007, already described in Section 4.2. Figure 7 shows the horizontal wind speed, the air temperature, and the specific humidity from 0530 to 0830 hours in five levels of the meteorological tower as well as the averaged profiles of these quantities before, during, and after the period of FCCs. During the period of FCCs, a strong collapse of the horizontal wind speed (Fig. 7a) can be observed, and also, the vertical gradient of the horizontal wind speed decreases compared to the time periods before and after FCCs (Fig. 7b). The surface skin temperature shows an increasing trend (Fig. 7c). It is lower than the air temperature until 0650 hours, but exceeds it from 0700 hours onwards. From 0650 to 0700 hours, the air temperature is consistent with the surface skin temperature. Together with the vertical gradient of the air temperature which is nearly zero during FCCs (Fig. 7d), this finding points to a strong vertical mixing of the air temperature during this time. The specific humidity shows an increasing trend during the FCCs (Fig. 7e). Again, the vertical gradient of specific humidity (Fig. 7f) is small during the FCCs, which implies an effective transport and mixing of specific humidity into upper parts of the ABL.

In summary, it is obvious that FCCs have an impact on near-ground ABL moisture and temperature profiles. Heated air masses are animated to ascend in convective pulse-like motions, which result in vertically uniform values of the air temperature, humidity, and the wind speed. Consequently, near-ground air mass characteristics are effectively trans-

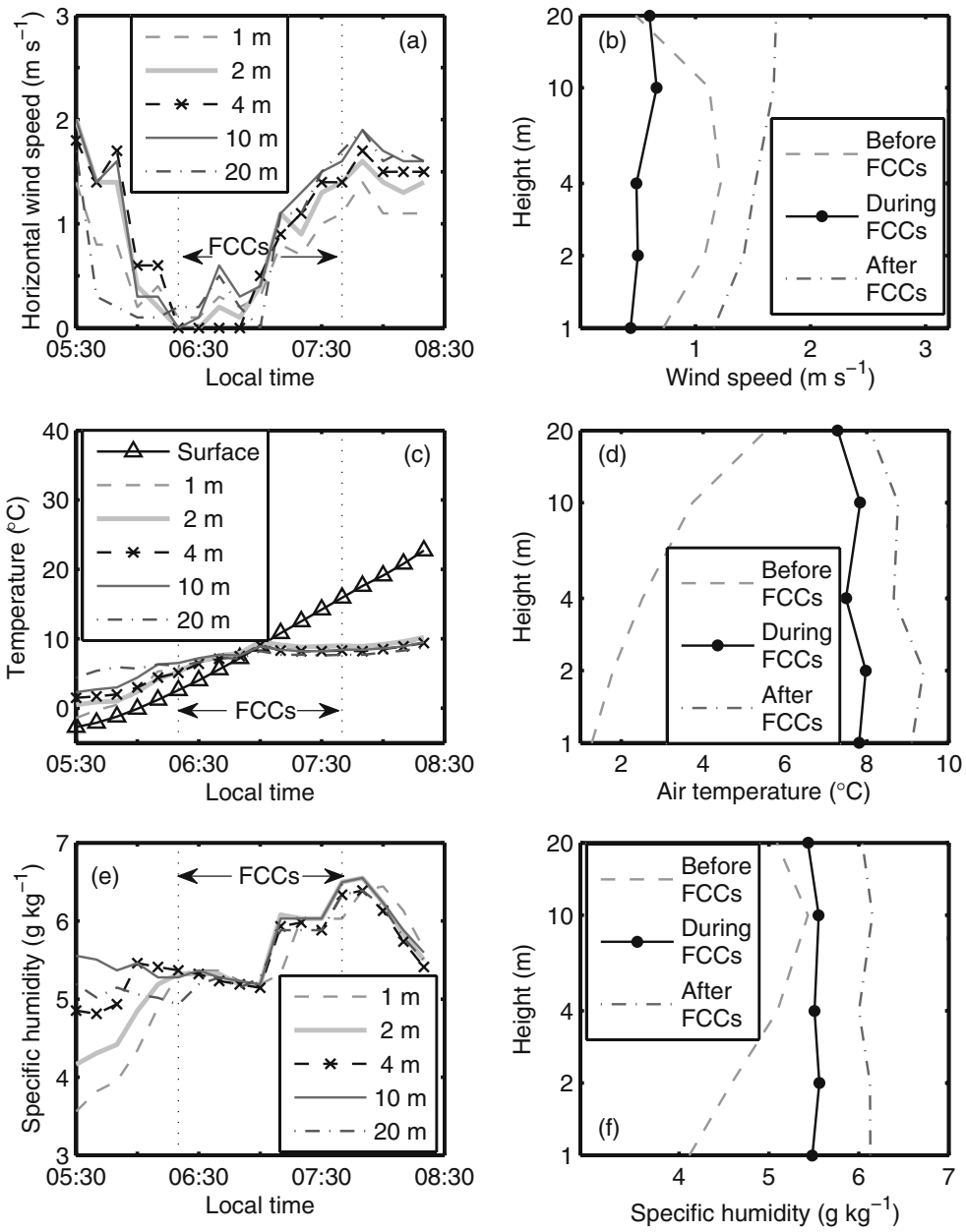

Fig. 7 **a** Horizontal wind speed, **c** air temperature and **e** specific humidity from 0530 to 0830 hours measured in five levels of the meteorological tower at Namco station on 29 June 2007. The period of FCCs (0620–0740 hours) is indicated by the *dashed*, *vertical lines*. Also depicted are the averaged, vertical profiles of **b** the horizontal wind speed, **d** the air temperature, and **f** the specific humidity for the time periods before (0530–0620 hours), during (0620–0740 hours), and after (0740–0830 hours) FCCs

ported into upper parts of the ABL. This process influences the conditions of the ABL, e.g., temperature and moisture profiles, and hence, plays an important role for the land surface-atmosphere exchange processes on the TP.

4.4 The distribution of FCCs during the entire measurement period

Regarding the entire measurement period, 67 days (39.6%) with FCCs can be observed. Time periods with precipitation and sensible heat fluxes below the threshold of 20 $W m^{-2}$ are excluded (see Section 4.1). Figure 8 shows the distribution of FCCs during the entire measurement period and the corresponding frequencies in the course of the day as a histogram. The results indicate that FCCs during the non-monsoon period mainly occur in the morning hours. Referring to Fig. 8b, the maximum value of occurrences of FCCs (117) can be found in the time period from 0730 to 0830 hours. On the contrary, during the monsoon period, the distribution of the FCCs is bimodal, with one peak in the morning with 74 occurrences of FCCs in the time from 0830 to 0930 hours, and another peak in the afternoon with 70 occurrences of FCCs in the time from 1330 to 1430 hours. The FCCs in the afternoon during monsoon have a close relationship with cloud cover as shown in Section 4.2. Fujinami et al. (2005) investigated the cloud cover frequency for high clouds during the monsoon on the southern TP, and showed that cloud cover frequency in the afternoon was

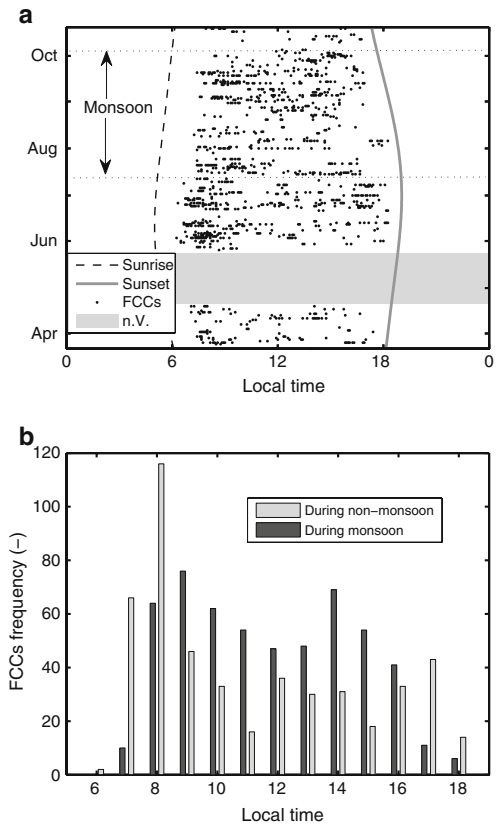

Fig. 8 **a** The distribution of FCCs during the entire measurement period and **b** the corresponding frequencies in the course of the day as a *histogram*

higher than in the morning in the latitudinal zone where Nam Co station is located. Such cloud cover frequency is consistent with the mode of the distribution of FCCs in the afternoon. To sum up, more FCCs can be triggered in the afternoon during monsoon than during non-monsoon.

5 Conclusions

The quality of turbulent flux measurements at Nam Co station was assessed by using the turbulence data processing software TK2 together with a forward Lagrangian footprint model. Hence, high-quality flux data sets were obtained for the investigation of near-ground FCCs, which can be detected by calculating the stability parameter with EC measurements. The results indicate that during FCCs, the quality of the turbulent fluxes is often degraded compared to the other daytime values (see e.g., Fig. 6f). These bad-rated data are detected by the standard quality evaluation procedure. However, we have to bear in mind that the poor ratings are caused by FCCs which are a typical phenomenon within a convective boundary layer in the daytime (e.g., Stull 1988). Consequently, the poor-rated data should not be rejected for further analysis. In contrast, the quality evaluation procedure should routinely indicate that the bad quality ratings can be related to the occurrence of FCCs and consider them in the flag calculation.

Two types of generation of FCCs at Nam Co station are identified. It is found that FCCs are either generated in the morning during the reversal of a thermally forced diurnal land-lake wind circulation system or occur during the whole daytime due to the adaption of the land-lake wind circulation system to surface heating differences in combination with cloud cover periods. In both cases, a low wind speed period is induced during the change of the circulation system, which leads to a dominance of buoyancy over shear, and thus, to the occurrence of FCCs. The second type of generation of FCCs, which is related to the appearance of clouds, more frequently occurs at Nam Co station compared to other sites without a nearby lake (see Eigenmann et al. 2009; Mayer et al. 2008). As the nearby Nam Co Lake more or less retains its surface temperature during cloud cover periods due to the high heat capacity of water, while a strong drop of the surface temperature over the grassland can be observed simultaneously, a reversal of the local circulation at Nam Co station is facilitated. The decrease of the surface temperature over the grassland could be also reinforced as the diffuse radiation components are reduced compared to lowland sites due to the topographical characteristics of the TP. Consequently, more FCCs are generated at Nam Co station due to cloud shading periods compared to e.g., the Kinzig valley, where FCCs are mainly triggered in the morning due to the wind direction change of the diurnal valley circulation system.

The distribution of FCCs at Nam Co station regarding the entire measurement period indicates that during non-monsoon, FCCs mostly occur in the morning, while during the monsoon period, the frequency distribution of FCCs has two peaks, one in the morning and another in the afternoon. In the case of the afternoon peak, a strong relation to cloud cover frequency is identified.

An impact of FCCs on near-ground boundary layer conditions is obvious from the profiles of meteorological values of a nearby tower with measurement heights up to 20 m. During FCCs, vertically uniform values of the air temperature, humidity, and the wind speed are observed indicating an effective, vertical transport of near-ground air mass characteristics into upper parts of the ABL. To sum up, an impact of FCCs on near-ground ABL moisture and temperature profiles can be confirmed for Nam Co station. Hence, FCCs seem to play an important role for the land surface-atmosphere exchange processes on the TP.

In the future, the measuring setup at Nam Co station should include boundary layer profiling as well as modeling techniques, such as Large Eddy Simulation, in order to further investigate the local circulation structure at Nam Co station and the impact of FCCs on ABL conditions.

Acknowledgements This paper was realized under the auspices of the National Natural Science Foundation of China (40825015), the Chinese National Key Program for Developing Basic Sciences (2010CB951701), and EU-FP7 CEOP-AEGIS(212921). The authors wish to acknowledge the support and data provision by the participants of Nam Co Monitoring and Research Station for Multi-sphere Interactions. The visit of the first author at Bayreuth was funded by the German Science Foundation (DFG) within the Priority Program SPP 1372 and the Chinese Academy of Science. The contribution of the University of Bayreuth to this study was funded within the DFG projects FO 226/18-1 and FO 226/19-1.

References

Aubinet M, Grelle A, Ibrom A, Rannik Ü, Moncrieff J, Foken T, Kowalski AS, Martin PH, Berbigier P, Bernhofer C, Clement R, Elbers J, Granier A, Grünwald T, Morgenstern K, Pilegaard K, Rebmann C, Snijders W, Valentini R, Vesala T (2000) Estimates of the annual net carbon and water exchange of forests: the EUROFLUX methodology. Adv Ecol Res 30:113–175

Ayra SP (2001) Introduction to micrometeorology. Academic, San Diego

Baldocchi D, Falge E, Gu L, Olson R, Hollinger D, Running S, Anthoni P, Bernhofer C, Davis K, Evans R, Fuentes J, Goldstein A, Katul G, Law B, Lee X, Malhi Y, Meyers T, Munger W, Oechel W, KT PU, Pilegaard K, Schmid HP, Valentini R, Verma S, Vesala T, Wilson K, Wofsy S (2001) FLUXNET: a new tool to study the temporal and spatial variability of ecosystem-scale carbon dioxide, water vapor, and energy flux densities. Bull Am Meteorol Soc 82:2415–2434

Banta RM (1990) The role of mountain flows in making clouds. In: Blumen W (ed) Atmospheric processes over complex terrain, chap 9. Meteorological monographs, 23(45). American Meteorological Society, Boston, pp 229–283, 23(45)

Chen F, Avissar R (1994) Impact of land-surface moisture variability on local shallow convective cumulus and precipitation in large-scale models. J Appl Meteorol 33:1382–1401

Chen Z, Zhou M, Qian F, Li S, Su L et al (2002) Convection activities in the atmospheric boundary layer over the western plateau of China (in Chinese). J Appl Meteorol Sci 13:142–145

Culf AD, Foken T, Gash JHC (2004) The energy balance closure problem. In: Kabat P et al (eds) Vegetation, water, humans and the climate: a new perspective on an interactive system. Springer, Berlin, pp 159–166

Eigenmann R, Metzger S, Foken T (2009) Generation of free convection due to changes of the local circulation system. Atmos Chem Phys 9:8587–8600

Foken T (2008a) The energy balance closure problem: an overview. Ecol Appl 18:1351–1367

Foken T (2008b) Micrometeorology. Springer, Heidelberg

Foken T, Göckede M, Mauder M, Mahrt L, Amiro BD, Munger JW (2004) Post-field data quality control. In: Lee X, Massman W, Law B (eds) Handbook of micrometeorology: a guide for surface flux measurement and analysis. Kluwer, Dordrecht, pp 181–208

Foken T, Mauder M, Liebethal C, Wimmer F, Beyrich F, Leps JP, Raasch S, DeBruin HAR, Meijninger WML, Bange J (2010) Energy balance closure for the LITFASS-2003 experiment. Theor Appl Climatol. doi:10.1007/s00704-009-0216-8

Foken T, Wichura B (1996) Tools for quality assessment of surface-based flux measurements. Agric For Meteorol 78:83–105

Foken T, Wimmer F, Mauder M, Thomas C, Liebethal C (2006) Some aspects of the energy balance closure problem. Atmos Chem Phys 6:4395–4402

Fujinami H, Nomura S, Yasunari T (2005) Characteristics of diurnal variations in convection and precipitation over the southern Tibetan Plateau during summer. SOLA 1:49–52

Göckede M, Foken T, Aubinet M, Aurela M, Banza J, Bernhofer C, Bonnefond JM, Brunet Y, Carrara A, Clement R, Dellwik E, Elbers J, EugsterW FJ, Granier A, Grünwald T, Heinesch B, Janssens IA, Knohl A, Koeble R, Laurila T, Longdoz B, Manca G, Marek M, Markkanen T, Mateus J, Matteucci G, Mauder M, Migliavacca M, Minerbi S, Moncrieff J, Montagnani L, Moors E, Ourcival JM, Papale D, Pereira J, Pilegaard K, Pita G, Rambal S, Rebmann C, Rodrigues A, Rotenberg E, Sanz MJ, Sedlak P, Seufert G, Siebicke L, Soussana JF, Valentini R, Vesala T, Verbeeck H, Yakir D (2008) Quality control of CarboEurope flux data—part 1: coupling footprint analyses with flux data quality assessment to evaluate sites in forest ecosystems. Biogeosciences 5:433–450

Göckede M, Markkanen T, Hasager CB, Foken T (2006) Update of a footprint-based approach for the characterization of complex measurement sites. Bound Lay Meteorol 118:635–655

Göckede M, Markkanen T, Mauder M, Arnold K, Leps JP, Foken T (2005) Validation of footprint models using natural tracer measurements from a field experiment. Agric For Meteorol 135:314–325

Göckede M, Rebmann C, Foken T (2004) A combination of quality assessment tools for eddy covariance measurements with footprint modelling for the characterisation of complex sites. Agric For Meteorol 127:175–188

Guan Z, Chen C, Ou Y et al (1984) Rivers and lakes of Xizang province (in Chinese). Science Press, Beijing

Hanesiak JM, Raddatz RL, Lobban S (2004) Local initiation of deep convection on the Canadian prairie provinces. Bound Lay Meteorol 110:455–470

Inagaki A, Letzel MO, Raasch S, Kanda M (2006) Impact of surface heterogeneity on energy imbalance: a study using LES. J Meteorol Soc Jpn 84:187–198

Li M, Dai Y, Ma Y, Zhong L, Lu S (2006) Analysis on structure of atmospheric boundary layer and energy exchange of surface layer over Mount Qomolangma region (in Chinese with English abstract). Plateau Meteorol 25:807–813

Lugauer M, Winkler P (2005) Thermal circulation in South Bavaria—climatology and synoptic aspects. Meteorol Z 14:15–30

Lu Y, Ma Y, Li M, Yang X (2008) Numerical simulation of typical atmospheric boundary layer characteristics over lake Namco region, Tibetan Plateau in summer (in Chinese with English abstract). Plateau Meteorol 27:733–740

Ma Y, Fan S, Ishikawa H, Tsukamoto O, Yao T, Koike T, Zuo H, Hu Z, Su Z (2005) Diurnal and inter-monthly variation of land surface heat fluxes over the central Tibetan Plateau area. Theor Appl Climatol 80:259–273

Ma Y, Tsukamoto O, Wang J, Ishikawa H, Tamagawa I (2002) Analysis of aerodynamic and thermodynamic parameters over the grassy marshland surface of Tibetan Plateau. Prog Nat Sci 12:36–40

Massman WJ, Lee X (2002) Eddy covariance flux corrections and uncertainties in long-term studies of carbon and energy exchanges. Agric For Meteorol 113:121–144

Mauder M, Foken T (2004) Documentation and instruction manual of the eddy covariance software package TK2. Work Report University of Bayreuth, Department of Micrometeorology, Print: ISSN 1614-8916, pp 42

Mauder M, Foken T, Clement R, Elbers JA, Eugster W, Grünwald T, Heusinkveld B, Kolle O (2008) Quality control of CarboEurope flux data—part 2: inter-comparison of eddy-covariance software. Biogeosciences 5:451–462

Mauder M, Liebethal C, Göckede M, Leps JP, Beyrich F, Foken T (2006) Processing and quality control of flux data during LITFASS-2003. Bound Lay Meteorol 121:67–88

Mayer JC, Staudt K, Gilge S, Meixner FX, Foken T (2008) The impact of free convection on late morning ozone decreases on an Alpine foreland mountain summit. Atmos Chem Phys 8:5941–5956

Metzger S, Ma Y, Markkanen T, Göckede M, Li M, Foken T (2006) Quality assessment of Tibetan Plateau eddy covariance measurements utilizing footprint modeling. Adv Earth Sci 21:1260–1267

Moncrieff J (2004) Surface turbulent fluxes. In: Kabat P, Claussen M, Dirmeyer PA, Gash JHC, Bravo de Guenni L, Meybeck M, Pielke RA Sr, Vörösmarty CJ, Hutjes RWA, Lütkemeier S (eds) Vegetation, water, humans and the climate: a new perspective on an interactive system. Springer, Berlin

Rabin RM, Stadler S, Wetzel PJ, Stensrud DJ, Gregory M (1990) Observed effects of landscape variability on convective clouds. Bull Am Meteorol Soc 71:272–280

Rannik Ü, Markkanen T, Raittila J, Hari P, Vesala T (2003) Turbulence statistics inside and over forest: influence on footprint prediction. Bound Lay Meteorol 109:163–189

Raymond D, Wilkening M (1980) Mountain-induced convection under fair weather conditions. J Atmos Sci 37:2693–2706

Rebmann C, Göckede M, Foken T, Aubinet M, Aurela M, Berbigier P, Bernhofer C, Buchmann N, Carrara A, Cescatti A, Ceulemans R, Clement R, Elbers JA, Granier A, Grünwald T, Guyon D, Havránková K, Heinesch B, Knohl A, Laurila T, Longdoz B, Marcolla B, Markkanen T, Miglietta F, Moncrieff J, Montagnani L, Moors E, Nardino M, Ourcival JM, Rambal S, Rannik Ü, Rotenberg E, Sedlak P, Unterhuber G, Vesala T, Yakir D (2005) Quality analysis applied on eddy covariance measurements at complex forest sites using footprint modelling. Theor Appl Climatol 80:121–141

Schmid HP (2002) Footprint modeling for vegetation atmosphere exchange studies: a review and perspective. Agric For Meteorol 113:159–183

Segal M, Arritt RW (1992) Nonclassical mesoscale circulations caused by surface sensible heat-flux gradients. Bull Amer Meteorol Soc 73:1593–1604

Stull RB (1988) An introduction to boundary layer meteorology. Kluwer Academic Publishers, Dordrecht

Tanaka K, Ishikawa H, Hayashi T, Tamagawa I, Ma Y (2001) Surface energy budget at Amdo on the Tibetan Plateau using GAME/Tibet IOP98 data. J Meteorol Soc Jpn 79:505–517

Whiteman CD (1990) Observations of thermally developed wind systems in mountainous terrain. In: Blumen W (ed) Atmospheric processes over complex terrain, chap 2. Meteorological monographs, 23(45). American Meteorological Society, Boston, pp 5–42

Wilczak JM, Oncley SP, Stage SA (2001) Sonic anemometer tilt correction algorithms. Bound Lay Meteorol 99:127–150

Yang K, Koike T, Fujii H, Tamagawa K, Hirose N (2002) Improvement of surface flux parameterizations with a turbulence-related length. Q J R Meteorol Soc 128:2073–2088

Yang K, Koike T, Ishikawa H, Ma Y (2004) Analysis of the surface energy budget at a site of GAME/Tibet using a single-source model. J Meteorol Soc Jpn 82:131–153

Yang K, Wang J (2008) A temperature prediction-correction method for estimating surface soil heat flux from soil temperature to moisture data. Sci China Ser D 51:721–729

Ye D, Gao Y (1979) The meteorology of the Qinghai-Xizang Plateau (in Chinese). Science Press, Beijing

Zuo H, Hu Y, Li D, Lu S, Ma Y (2005) Seasonal transition and its boundary characteristics in Amdo area of Tibetan Plateau. Prog Nat Sci 15:239–245

Appendix E: Brötz et al. (2013)

Early-morning flow transition in a valley in low-mountain terrain

Björn Brötz · Rafael Eigenmann · Andreas Dörnbrack · Thomas Foken · Volkmar Wirth

Received: date / Accepted: date

Abstract This study investigates the evolution of the early-morning boundary layer in a low-mountain valley in south-western Germany during the Convective and Orographically induced Precipitation Study (COPS) in summer 2007. A subset of 23 fair weather days of the campaign was selected to study the transition of the boundary-layer flow in the early morning. The typical valley atmosphere in the morning hours was characterized by a stable temperature stratification and a pronounced valley wind system. During the reversal period - named as low wind period - of the valley wind system (duration of 1-2 hours), the horizontal wind was very weak and the conditions for free convection were fulfilled close to the ground. Ground-based Sodar observations of the vertical wind showed enhanced values of upward motion, and the corresponding statistical properties differ from those observed under windless convective conditions over flat terrain. Large-eddy simulations of the boundary-layer transition in the valley were conducted. Statistical properties of the simulated flow agree with the observed quantities. Spatially coherent turbulence structures are present in temporal as well as in ensemble mean analysis. Thus, the complex orography forms coherent convective structures at predictable, specific locations during the early-morning low wind situations. These coherent updraughts - found in both the Sodar observations and the simulation - lead to a flux counter to the gradient of the stably stratified valley atmosphere and reach up to the heights of the surrounding ridges. Furthermore, the energy balance in the surface layer in the low wind periods is closed. However, it becomes unclosed after the onset of the valley wind. The partition into the sensible and the latent heat fluxes indicates that

B. Brötz · V. Wirth
University of Mainz, Institute for Atmospheric Physics, 55099 Mainz, Germany

Present address of B. Brötz:
Deutsches Zentrum für Luft- und Raumfahrt, Institut für Physik der Atmosphäre, Oberpfaffenhofen, Germany
E-mail: Bjoern.Broetz@dlr.de

A. Dörnbrack
Deutsches Zentrum für Luft- und Raumfahrt, Institut für Physik der Atmosphäre, Oberpfaffenhofen, Germany

R. Eigenmann · T. Foken
University of Bayreuth, Department of Micrometeorology, 95440 Bayreuth, Germany

T. Foken
Bayreuth Center of Ecology and Environmental Research (BayCEER), 95440 Bayreuth, Germany

missing flux components of sensible heat are the main reason for the unclosed energy balance in the considered situations. This result supports previously published investigations on the energy balance closure.

Keywords Convection in a valley · Coherent structures · Large-eddy simulation · Energy balance closure · COPS

1 Introduction

Turbulent fluxes of heat, moisture, and momentum in the atmospheric boundary layer are of key importance both for the evolution of the boundary layer itself and for the overlying free atmosphere. The accurate knowledge of the magnitude and the vertical profiles of these fluxes and their reliable parametrization are essential for both numerical weather prediction and climate simulations, respectively. Sophisticated micrometeorological instrumentation and analysis techniques have successfully been applied in order to determine fluxes over flat and homogeneous terrain.

However, the determination of these fluxes above complex terrain, i.e. mountainous and/or with heterogeneity in land use, remains a challenging task (Foken, 2008; Mahrt, 2010). The boundary layer in complex terrain is characterized by orographically (Defant, 1949; Whiteman, 1990; Whiteman, 2000; Zardi and Whiteman, 2013) or thermally induced (Segal and Arritt, 1992) wind systems. In a convective boundary layer over flat surfaces quasi-stationary turbulence structures evolve (Schmidt and Schumann, 1989). Over heterogeneous surfaces (Dörnbrack and Schumann, 1993; Walko et al., 1992) coherent structures with surface-scale dependent length scales develop, especially in the lower part of the boundary layer. These flow structures can potentially modify the turbulent fluxes from valleys, thus potentially modifying the evolution of the mountainous boundary layer as a whole. Rotach et al. (2008) and Weigel et al. (2007) investigated the exchange processes in an alpine valley and found strong dependencies of the turbulent fluxes on orography and stratification in the mountainous boundary layer. Mayer et al. (2008) investigated an observed anomaly in the chemical composition of air at a mountain station. This anomaly was traced back to fluxes through the stably stratified valley atmosphere that were released during the reversal of the thermally driven wind system in the morning.

Over homogeneous terrain a strong influence of coherent turbulent structures, i.e. persistent quasi-stationary patterns of turbulent motion, on the turbulent fluxes was shown in several studies (Raasch and Harbusch, 2001; Kanda et al., 2004; Inagaki et al., 2006). In particular, the interpretation of micrometeorological measurements in complex terrain requires the comprehensive knowledge about how turbulence is organized at the observational site and its surrounding. This leads to the guiding questions for this study: (i) How does the convective boundary layer in a typical low-mountain valley get organized in the early morning hours after sunrise? (ii) How does an along-valley wind in the morning change the convective structures? (iii) To what extent is the vertical transport in the valley affected? (iv) How are micrometeorological flux measurements at a specific location affected by complex terrain? To address these questions, large-eddy simulations (LES) were conducted. The results of the simulations are compared to observations.

A unique dataset obtained during the field phase of COPS constitutes the basis of this study (see Eigenmann et al., 2009). The field campaign of summer 2007 in the low-mountain region of south-western Germany and eastern France, i.e. Black Forest and Vosges mountains, is well described in the literature (e.g. Wulfmeyer et al., 2011). The objective of the

campaign is to understand the influence of the orography of a low-mountain range on precipitation. Several surface flux measurement stations were installed throughout the respective region during the campaign (Eigenmann et al., 2011; Kalthoff et al., 2011). In addition, ground-based Sodar/RASS instruments were installed on some of these stations. Our study uses data from one of these sites where a full energy balance station and a Sodar/RASS operated simultaneously. The site Fußbach is located in the Kinzig valley, which is a typical low-mountain valley of the region with a pronounced valley wind system developing on fair weather days in summer.

In micrometeorological field experiments the energy balance is often not closed (e.g. Oncley et al., 2007; Foken et al., 2010). Although many uncertainties are connected with the determination of the components of the energy balance (Mahrt, 2010), strong indications exist that the residual occurs due to transport by large-scale eddies or secondary circulations which are not captured by the eddy-covariance method (e.g. Mauder and Foken, 2006; Foken, 2008; Foken et al., 2010, 2011; Stoy et al., 2013). As these secondary circulations are mainly associated with the buoyancy flux, the partitioning of the residual according to the buoyancy flux ratio approach, proposed by Charuchittipan et al. (2013), appears to be appropriate to close the energy balance. The buoyancy flux ratio approach partitions the residual according to the buoyancy flux ratio instead of the usually used Bowen ratio (Twine et al., 2000). Thus, a larger fraction of the residual would be attributed to the sensible heat flux with the buoyancy flux ratio approach. Also the COPS energy balance site Fußbach of this study shows an average residual of 21% during the entire field campaign (see Eigenmann et al., 2011).

The remainder of this article is organized as follows. Section 2 describes the data and the methods applied, in particular the numerical model and its set-ups. Section 3 presents the results and the discussion of them. The conclusions are given in Sect. 4.

2 Methods and data

2.1 Observational data

The data used in this study were obtained by observations conducted during the COPS experiment in the low-mountain terrain of the Kinzig valley. Turbulence data were measured at a height of 2 m above the valley surface and friction velocity u_*, sensible heat Q_H and latent heat Q_E were calculated with the eddy-covariance method (EC) (Foken et al., 2012). An averaging time of 30 min was used for the EC. Contributions to the fluxes with a time scale exceeding these 30 min cannot be captured. The geographical location of the site Fußbach was 48° 22′ 7.8″ N, 8° 1′ 21.2″ E, 178 m a.s.l. (the position is marked in Fig. 3). The local time is UTC+1 hour. Details about the site and the measurement set-up can be found in Metzger et al. (2007) and Eigenmann et al. (2009, 2011). Close to the turbulence station, a Sodar/RASS system measured vertical profiles of wind components and virtual temperature. Moreover, the remaining components of the energy balance, net radiation Q_S^*, and soil heat flux Q_G, were measured at the EC site. An overview of the data processing, quality control, and flux characteristics of the turbulent data as well as the calculation of the energy balance is given in Eigenmann et al. (2011).

The study of Eigenmann et al. (2009) identified 23 days during the three-month COPS campaign with free convective conditions based on the EC measurements in the early-morning hours. Free convective conditions were identified by the stability parameter $\zeta = zL^{-1}$ for $\zeta < -1$, where L is the Obukhov length. These periods were characterized by low

horizontal wind due to the reversal of the valley wind system from down-valley winds to up-valley winds. The mean time of the occurrence of the free convective situations on these 23 days is 0815 UTC with a standard deviation of 1 hour.

The vertical wind speed w derived from the Sodar observations was analysed for the identified low wind periods. In the remainder of the article this period of low wind will be referred to as p_1 and the subsequent period of up-valley wind will be referred to as p_2. In order to make the individual days comparable, each Sodar sample of w was normalized with the Deardorff convective velocity w_* (Deardorff, 1970). The measurement height z was normalized with the height of the boundary layer z_i. Surface buoyancy fluxes for the calculation of w_* were derived from the EC measurements and values of z_i were determined by a secondary maximum in the reflectivity profiles of the Sodar measurements as described in Eigenmann et al. (2009) and suggested by Beyrich (1997). After that, histograms of ww_*^{-1} were calculated for three characteristic heights of $zz_i^{-1} = 0.25, 0.50$ and 0.75.

2.2 Simulations

2.2.1 Numerical Model

The numerical simulations were conducted by means of the multiscale geophysical flow solver EULAG (Smolarkiewicz et al., 1997; Prusa et al., 2008). EULAG solves the non-hydrostatic, anelastic equations of motion, here written in an extended perturbational form (Smolarkiewicz and Margolin, 1997):

$$\nabla \cdot (\rho_b \mathbf{v}) = 0, \tag{1}$$

$$\frac{D\mathbf{v}}{Dt} = -\nabla\pi' - \mathbf{g}\frac{\Theta'}{\Theta_b} + \mathbf{M} + \mathbf{D} + \mathbf{F} - \alpha\,\mathbf{v}', \tag{2}$$

$$\frac{D\Theta'}{Dt} = -\mathbf{v}\cdot\nabla\Theta_e + \mathscr{H} - \beta\,\Theta'. \tag{3}$$

$$\frac{De}{Dt} = \mathscr{S} \tag{4}$$

The set of anelastic equations (1)-(4) describes the anelastic mass continuity equation (1), the three components of the momentum equation (2), and the thermodynamic equation (3), respectively. The equation (4) for the subgrid-scale (SGS) turbulent kinetic energy (TKE) e completes the system of equations. In (1)-(4), the operators ∇ and $\nabla\cdot$ symbolize gradient and divergence, while $D/Dt = \partial/\partial t + \mathbf{v}\cdot\nabla$ is the material derivative, and $\mathbf{v}$ is the physical velocity vector. The vector representing the gravitational acceleration $\mathbf{g} = (0,0,-g)^T$ occurs in the buoyancy term of Equ. (2). The quantities $\rho_b(z)$ and $\Theta_b(z)$ refer to the basic states, prescribed hydrostatic reference profiles usually employed in the anelastic approximated equations (Clark and Farley, 1984).

In addition to the horizontally homogeneous basic state, a more general ambient (environmental) state is denoted by the subscript $_e$. The corresponding variables may vary in the horizontal directions and they have to satisfy Equ. (1)-(3); see Prusa et al. (2008) for a discussion of ambient state and its benefits. The primed variables $\mathbf{v}'$ and Θ' appearing in Equ. (2)-(3) correspond to deviations from the environmental variables $\mathbf{v}_e$ and Θ_e. The quantity π' in the linearized pressure gradient term in Equ. (2) denotes a density normalized pressure deviation.

The terms proportional to α and β denote wave absorbing devices used at the upper boundary of the computational domain. The source terms $\mathbf{D}$ and $\mathscr{H}$ not explicitly stated

in Equ. (2) and (3) symbolize the viscous dissipation of momentum and the diffusion of heat, respectively. **F** symbolizes an additional forcing for specified simulations, see below. The formulation of the TKE production and dissipation term hidden in $\mathscr{S}$ and the applied parameters follow the description of Sorbjan (1996).

The quantity **M** denotes metric forces due to the curvilinearity of the underlying physical system. In the present work, a non-orthogonal terrain-following system of coordinates $(\bar{x},\bar{y},\bar{z}) = (x,y,H(z-h)/(H-h))$ is used which assumes a model depth H and an irregular lower boundary $h(x,y)$ (Gal-Chen and Somerville, 1975; Smolarkiewicz and Margolin, 1993; Wedi and Smolarkiewicz, 2004). The explicit formulation of the transformed system of equations can be found in Prusa and Smolarkiewicz (2003) or, more recently, in Kühnlein et al. (2012). In symbolic form, the resulting system of motion for the prognostic variables $\Psi = u,v,w,\Theta,e$ can be written as a flux-form Eulerian conservation law

$$\frac{\partial}{\partial t}(\rho^*\Psi) + \nabla\cdot(\mathbf{v}\rho^*\Psi) = \rho^* F^{\Psi} \tag{5}$$

where $\rho^* = \rho_b G$, with G as the Jacobian of the transformation. A finite difference approximation of Equ. (5) is

$$\Psi^{n+1} = MPDATA\left(\Psi^n + 0.5\Delta t F^{\Psi}\Big|^n, \mathbf{v}^{n+\frac{1}{2}}, \rho^*\right) + 0.5\Delta t\rho^* F^{\Psi}\Big|^{n+1} \tag{6}$$

where MPDATA[1] stands for the non-oscillatory forward-in-time (NFT) advection transport scheme described in Smolarkiewicz and Margolin (1998). The elliptic equation for pressure is solved iteratively with a Krylov-sub space solver, see Thomas et al. (2003). Both elements are integral part of the EULAG and are fundamental for the stability of the code and the reliability of the results.

2.2.2 Simulation strategy

Among the broad range of applications documented in literature, EULAG was successfully applied to atmospheric boundary-layer flows (see Smolarkiewicz et al., 2007; Piotrowski et al., 2009). For the questions investigated in this paper, the set-up was chosen in the following way.

The numerical simulations are conducted in a domain of $(L_x, L_y, H) = (7680\,\text{m}, 7680\,\text{m}, 2430\,\text{m})$ with a regular grid size of $\Delta x = \Delta y = \Delta z = 30\,\text{m}$. For a simulation of 2.5 h physical time, 30 000 timesteps with $\Delta t = 0.3\,\text{s}$ are necessary. The height $h(x,y)$ of the lower boundary is taken from the ASTER digital topographic data set (NASA Land Processes Distributed Active Archive Center NASA LP DAAC, 2001) in a $30\,\text{m}\times 30\,\text{m}$ regular resolution. In all simulations shown here the computational domain is periodic in the horizontal directions. To enable this periodicity the topography was smoothly relaxed within a frame around the actual region of interest. Due to the complex orography and the low inversion layer height the width of the frame could be chosen to be 300 m.

For all simulations an anelastic basic state with a background stratification $N = 0.01\,\text{s}^{-1}$ is used according to Clark and Farley (1984), resulting in exponentially decreasing ρ_b and increasing Θ_b-profiles.

To investigate the guiding questions of this study, two different simulation set-ups were designed. First, idealized simulations of an evolving convective boundary layer (CBL) over flat terrain $h(x,y) = 0$ were conducted and they are denoted by *S*, and, secondly, the CBL

[1] MPDATA stands for Multidimensional Positive-Definite Advection Transport Algorithm

Table 1 Set-ups for the simulations in this study

name	terrain	stratification below z_i	z_i, (m)	wind forcing	dx, (m)
*S*1	flat	neutral	800	off	20
*S*2	flat	–	0	off	20
*R*1	complex	neutral	800	off	30
*R*2	complex	–	0	on (during p2)	30

was simulated over realistic topography $h(x,y)$ and these simulations are denoted by *R*, see Table 1.

All simulations were initialized with a resting fluid, and two different ambient potential temperature profiles $\Theta_e(z)$ were applied to distinguish between an early mixed layer with a capping inversion layer at $z_i = 800$ m (Simulations *S*1 and *R*1) and a stably stratified ambient state covering the whole depth of the computational domain (simulations *S*2 and *R*2):

$$\text{Simulations } S1 \text{ and } R1: \quad \Theta_e = \begin{cases} \Theta_0 & \text{for} \quad h \le z < z_i \\ \Theta_0 \left(1 + \frac{N^2}{g}(z - z_i)\right) & \text{for} \quad z_i \le z \le H \end{cases} \tag{7}$$

$$\text{Simulations } S2 \text{ and } R2: \quad \Theta_e = \Theta_0 \left(1 + \frac{N^2}{g} z\right) \qquad \text{for} \quad h \le z \le H \tag{8}$$

White noise with an amplitude of $0.001\,\mathrm{m\,s^{-1}}$ was added to the initial vertical wind field in order to initiate convective motions. For the ensemble runs analysed in Section 3.2, eight independent realizations were simulated using the set-up *R*1. For this purpose, the random generator was seeded differently at the initial time for each realization. Because the three wind components are zero before adding the noise, the random disturbance is 100 % of the absolute value of the wind vector. This ensures that the eight realizations are statistically independent. The numerical simulations were conducted for a dry atmosphere. At the surface a sensible heat flux $Q_H = 0.05\,\mathrm{K\,m\,s^{-1}}$ was specified in all runs. The homogeneous heating can be justified because flux differences between different types of land surfaces turned out to be negligible in the observed early-morning situations (see Eigenmann et al., 2011). The effect of orographic shading is not taken into account. Orographically-induced flows (valley winds, upslope flows, etc.) are expected to mainly dominate the properties of the CBL in the valley at this time of the day.

During the night-day-transition, the along-valley winds are part of a mountain plain circulation between a mountain massive and an adjacent plane, in our case the Black Forest and the Upper Rhine Valley, respectively. Due to the small computational domain, the effect of this meso-scale circulation on the flow in the valley is modelled by an additional dynamical forcing $\mathbf{F} = (0, -v_0(z)\tau^{-1}, 0)$ for the meridional wind component v, where $\tau = t_{\mathrm{end}} - t_{\mathrm{beg}}$ is the period when the forcing is applied. The reference profile for the horizontal wind speed $v_0(z)$ was derived from the Sodar observations. In the simulation *R*2 the additional forcing $\mathbf{F}$ is applied. The period from $t = 0$ to t_{beg} represents the observed low wind period p_1. The period from t_{beg} to the end of the simulation represents the up-valley wind period p_2. In the remainder of the article two simulation times referred to as t_1 for a time in p_1 and t_2 for a time in p_2 are chosen in order to compare differences in the simulated periods p_1 and p_2.

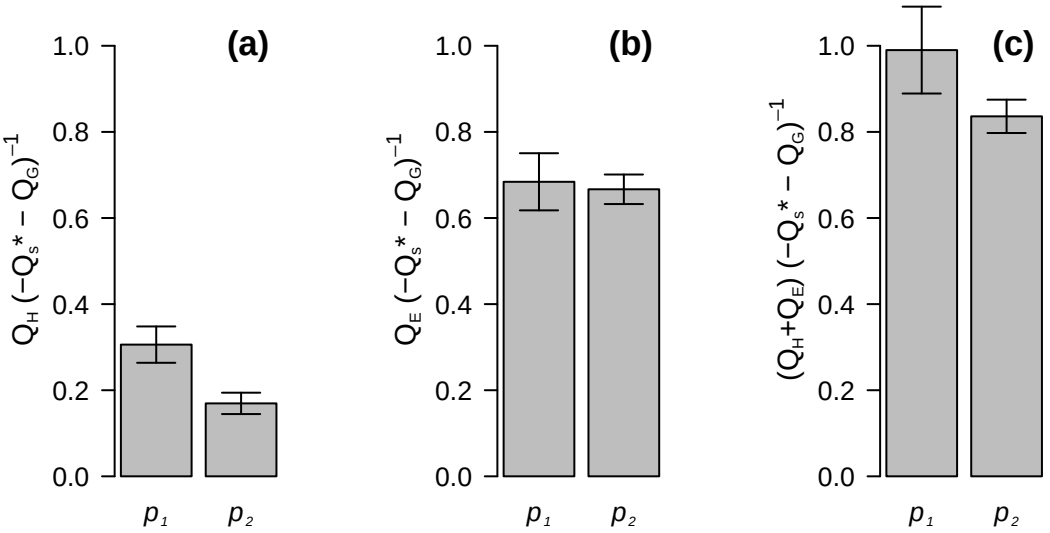

Fig. 1 Bar plots of the mean of the fluxes of Q_H (a), Q_E (b) and the sum of both (c) normalized with the available energy $-Q_S^* - Q_G$ during the low wind speed period p_1 and the first 2 hours of p_2. Average values for the 23 selected days at the Fußbach site are given for both periods. Also shown are the 95% confidence intervals which indicate significant differences in the mean values for (a) and (c).

3 Results and Discussion

3.1 Modification of the energy balance by the valley wind

To analyse the effect of the valley wind on the energy balance of the EC flux measurements, the selected periods p_1 and p_2 are analysed separately. Figure 1 shows the mean of the fluxes Q_H and Q_E and the sum of both normalized with the available energy $-Q_S^* - Q_G$ during the low wind speed period p_1 and the first 2 hours of p_2. This interval was chosen in order to make the data basis of both periods comparable. A closed energy balance means that the ratio of the sum of the turbulent fluxes $Q_H + Q_E$ and the available energy $-Q_S^* - Q_G$ is equal to one. Altogether, the energy balance is closed in p_1, while in p_2 a residual of 16% occurs on average (see Fig. 1c). The latter value is close to the average residual of 21% found during the entire COPS campaign at this site (see Eigenmann et al., 2011).

Regarding Fig. 1a and b, the relative flux contributions missing in period p_2 compared to period p_1 have exactly the proportions of the buoyancy flux ratio. The buoyancy flux ratio would distribute about 85% of the residual to Q_H and 15% to Q_E for a typical Bowen ratio of about 0.45 in the observed early-morning situations. As such, Fig. 1 supports the application of the buoyancy flux ratio approach (see Charuchittipan et al., 2013) for the correction of the energy balance. The missing flux components in period p_2 are assumed to be transported within buoyancy-driven secondary circulations not captured by the EC measurements (e.g. Foken, 2008). The transfer of the missing energy into the secondary circulation mainly happens at significant surface heterogeneities which can be found over complex terrain. Advection-dominated processes (also not captured by the EC) probably lead to the transport of the missing energy to these heterogeneities. As wind speeds vanish in period p_1, no energy is transferred into secondary circulations and the energy balance is closed. However, the along-valley wind in period p_2 leads to missing advective flux components and thus to the observed residual in this period.

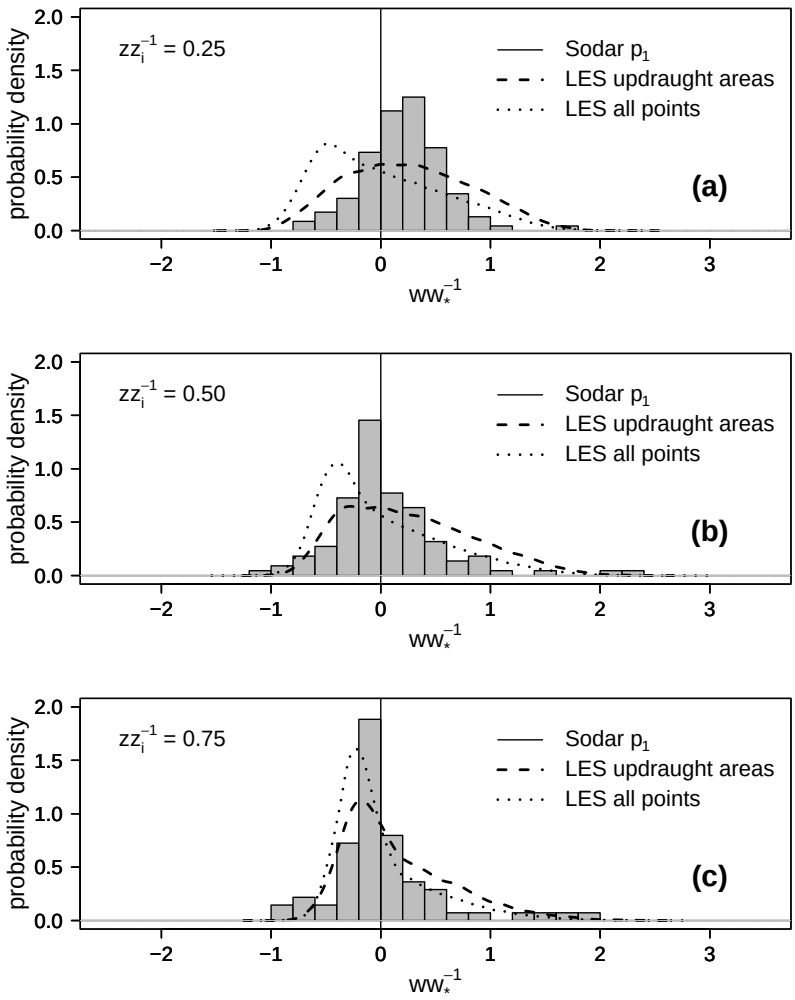

Fig. 2 Probability densities of the normalized vertical wind speed ww_*^{-1} for three heights ($zz_i^{-1} = 0.25, 0.5, 0.75$). Histograms are derived from Sodar observations at the Fußbach site during the low wind speed periods p_1 on the 23 selected days, while curves are derived from the simulation *S*2. The dotted curve shows the probability density function (pdf) for all points in the horizontal plane, the dashed curve shows the pdf for the conditionally sampled updraught areas only.

The finding discussed above also supports the choice of a constant heat flux forcing for the transient simulation *R*2 (see Sect. 2.2). The same relative forcing by Q_H is achieved for both periods p_1 and p_2 by adding (for simplification) 100% of the residual to Q_H. In this way, the forcing of period p_1 can also be used for period p_2. Moreover, no significant relative flux differences of Q_E exist in both periods (see Fig. 1b). Thus, for the questions addressed in this study, it appears to be appropriate to concentrate on dry model runs.

3.2 Coherent structures in the valley imposed by surrounding orography

In order to investigate the early-morning CBL evolution inside the valley, Sodar data from the morning period p_1 of the selected days were chosen to create the histograms of the normalized vertical wind ww_*^{-1} (see Fig. 2). The observed distributions of this study deviate strongly from probability density functions (pdfs) observed over flat, homogeneous environments as reported by many studies (e.g. Deardorff and Willis, 1985; Stull, 1988). In these

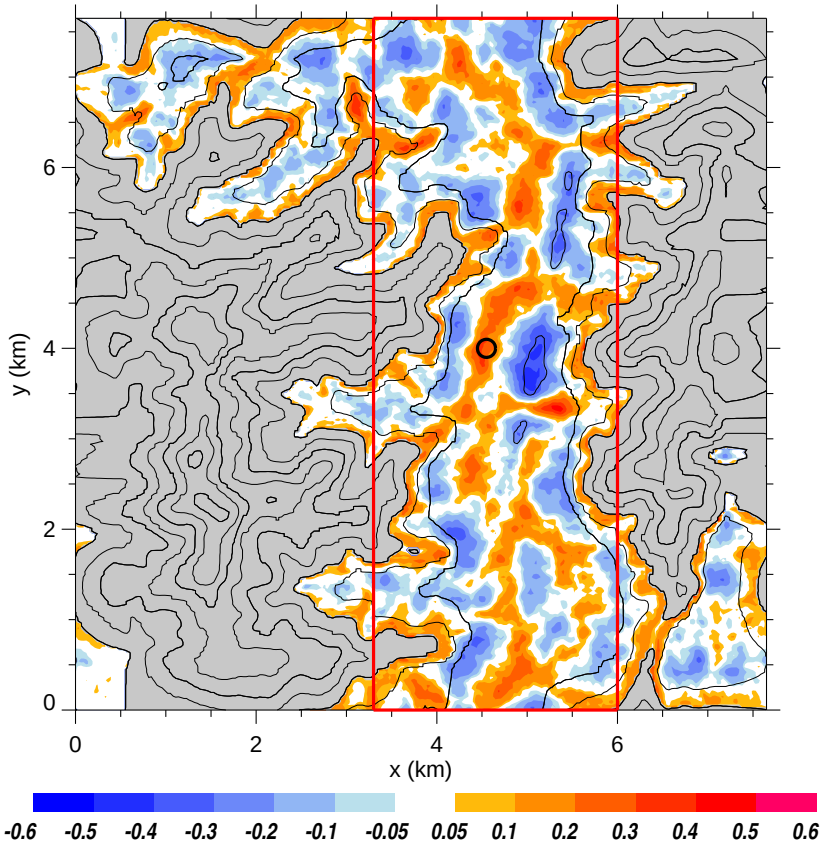

Fig. 3 Ensemble and time mean of the vertical wind speed in m s^{-1} at 300 m a.s.l. for simulation *R*1 (colour-coded). Black solid lines mark the orography in steps of 50 m. Grey contours mark intersection with the orography. The red frame represents the section of the valley shown in Fig. 5. The position of the Sodar is indicated by the black circle.

studies the pdfs are right-skewed and show a negative maximum. Especially in the lower part of the boundary layer ($zz_i^{-1} = 0.25$) the maximum of the observed distribution at Fußbach site is shifted towards weak positive values instead of the weak negative values known from literature. Also the observed histogram is far less skewed at this height. To find the cause of this behaviour, idealized simulations of a CBL are carried out (Simulation *S*1 and *S*2, described in Sect. 2.2).

To gain confidence in the simulations the well known pdfs of the vertical wind in a convective boundary layer are calculated for the simulated data of set-up *S*1. Very good agreement with the published values is found (not shown). Moreover, the simulation results show the well-known spoke patterns of coherent convective motion known from numerous numerical studies (e.g. Schmidt and Schumann, 1989). The data from the simulation of set-up *S*2 is then used to create the pdfs for a CBL with growing mixed layer, see Fig. 2 (situation more close to observation period p_1). In this set-up, spoke patterns evolve in the simulated boundary layer that grow slightly in size as the inversion layer height grows in time. A conditional sampling is applied to obtain the pdfs of the coherent updraught areas.

The resulting pdfs resemble the properties of the histograms from the Sodar data (see Fig. 2). The maximum and the skewness of the pdfs of the conditionally sampled updraught areas match well with those of the histograms of the observational data for all heights. Only the absolute numbers of the probability density do not fully match. A possible explanation

for this is that the Sodar instrument averages over a certain volume, so that the probability density of values around zero gets increased. This effect becomes larger with height.

We interpret these findings as follows: It is well known that coherent convective motions evolve in a CBL which remain quasi-stationary in space and time (see e.g. Stull, 1988). This means that the location where a possible Sodar instrument is located will remain under an updraught or a downdraught area for a long time. As a consequence, it is very likely that a Sodar measurement will capture only the statistical properties of a part of the velocity spectrum. The fact that the result from Fig. 2 stems from a composite over 23 periods with similar overall conditions suggests the hypothesis that the Sodar instrument was preferentially located at an updraught region.

To verify this hypothesis, an ensemble of eight large-eddy simulations was carried out with realistic topography at the lower boundary (simulation *R*1) and different initial noise seeding for *w* (see Sect. 2.2.2). Figure 3 shows the ensemble and time mean of the vertical wind speed at 300 m a.s.l. (approximately 130 m above the valley floor). Although we applied both a temporal mean and an ensemble mean to the simulated data, coherent patterns of the CBL flow field inside the valley remain. This mean flow field has a larger amplitude than its analogue from simulations over flat terrain. We interpret this finding as follows: The surrounding ridges impose coherent convective motions to the valley flow at specific locations during the early-morning p_1 periods. Their positions relative to the ridges persist in contrast to the changing locations of the coherent structures in the flat CBL simulation. The position of the observational site is marked by a black circle in Fig. 3 and shows that the site is located in an updraught region.

3.3 Vertical transport in the early-morning valley atmosphere

Spectral analysis of the EC measurements in the valley showed an increase of spectral power within turbulent scales of a few minutes during the low wind speed period p_1 in the morning (see Eigenmann et al., 2009). These time scales could be related to the presence of large coherent vertical structures (e.g. plumes or updraughts) with a spatial extent in the order of the boundary-layer height, which are known to be responsible for the majority of the transport within the CBL (see e.g. Stull, 1988; Chandra et al., 2010). The occurrence of these turbulent scales in the ground-based EC data indicates that during the period p_1, air very close to the ground is able to be transported upwards very efficiently by non-local large-eddy transport processes. The free convective conditions detected simultaneously by the EC measurements also support these findings. By the onset of the up-valley wind these turbulent scales disappear from the data indicating that the turbulent transport of near-ground air became less effective. The effective vertical transport in period p_1 is important because air masses close to the valley bottom are humid, have a characteristic chemical composition, and may possibly be polluted. The effect of the free convective release of surface layer air masses from the valley bottom on ozone measurements at a mountain-top station was recently reported by Mayer et al. (2008).

During these free convective situations in period p_1, the Sodar/RASS observed strong vertical updraughts into the stably stratified valley atmosphere. For illustration, Fig. 4 shows for COPS IOP15b, i.e. 13 August 2007, the morning evolution of vertical wind and virtual potential temperature. In the lower panel of Fig. 4 the observed vertical wind is shown from 0500 to 1300 UTC. The period of low horizontal wind speed in the morning is marked by vertical dashed lines. The times of the profiles plotted in Fig. 4a-d are indicated in the lower panel. At time (a) the stable stratification is shown shortly after sunrise. In (b) the

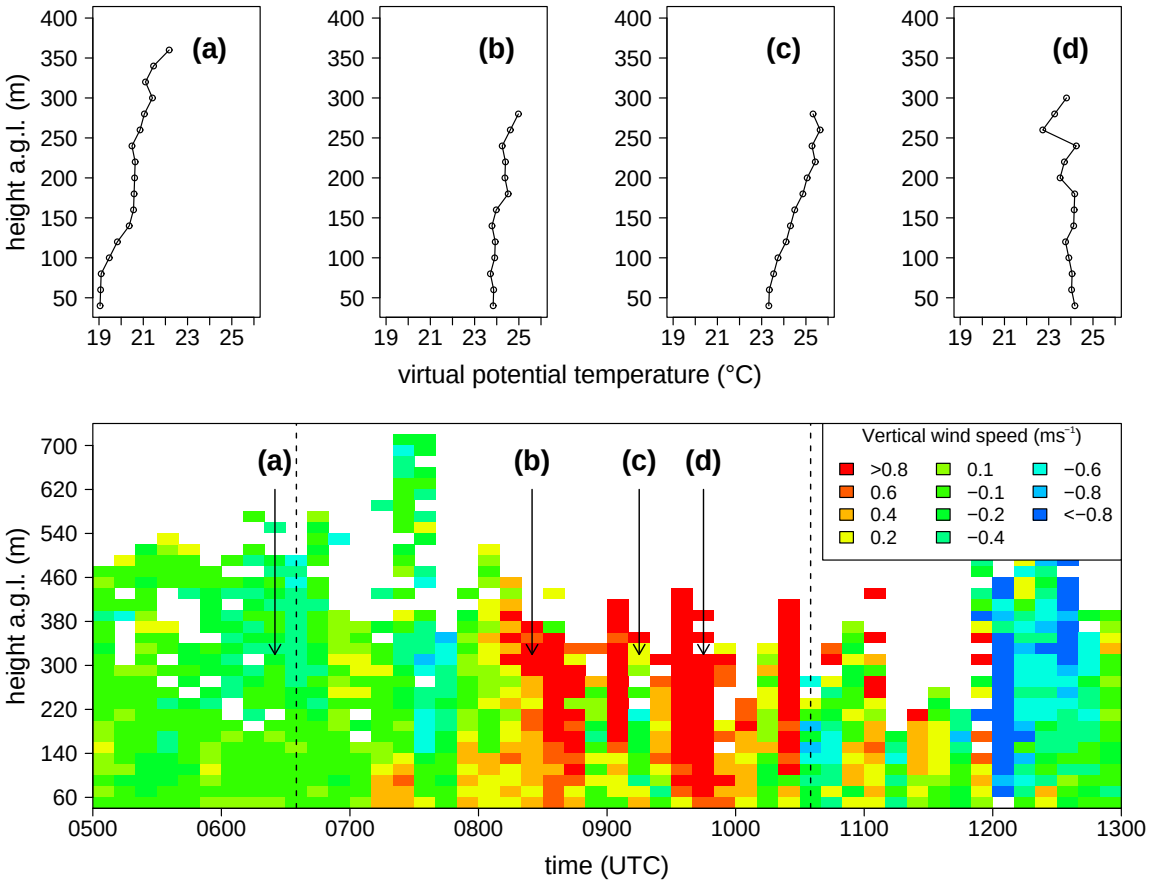

Fig. 4 Upper panel (a-d): Profiles of the virtual potential temperature observed by the Sodar/RASS in the morning hours of COPS IOP15b (13 August 2007). The times of the profiles are marked in the lower panel. Lower panel (from Eigenmann et al., 2009, modified): Vertical wind speeds in colour measured by the Sodar/RASS from 0500-1300 UTC. The black dashed vertical lines indicate the period of vanishing horizontal wind speeds.

profile is representative for a period of strong coherent vertical updraughts. Nearly neutral stratification below 160 m above the valley floor was observed in this period. A weak stable stratification above 160 m can be seen while the corresponding vertical wind speeds remain positive. The strong updraught period is interrupted by a period of weaker vertical winds. The profile in (c) shows that during this short interruption the original stable stratification recovers. After this interruption the vertical wind is again positive and the profile in (d) shows a neutral or slightly unstable profile. In the light of the previous analysis, this individual scene is interpreted as follows: The convection organizes, influenced by the orography, in a way that the updraught and downdraught areas remain quasi-stationary at their spatial location (see Fig. 3). The immobile Sodar/RASS instrument observed this quasi-stationary updraught area for a period of approximately two and a half hours (0800 until 1030 UTC). This period is interrupted by a short period of weaker winds at around 0920 UTC, when the quasi-stationary updraught area slightly moves out of the view of the Sodar/RASS instrument, so that the properties of an attached downdraught area are also observed. In this short period, it can be seen that the stratification of the valley atmosphere outside of the updraughts is still stable (Fig. 4c).

To better understand the state of the boundary layer in which these observations were made, the transient simulation *R*2 (see Sect. 2.2) was carried out and analysed. In Fig. 5, snapshots of the field of the vertical wind speed are shown for two heights and for the time

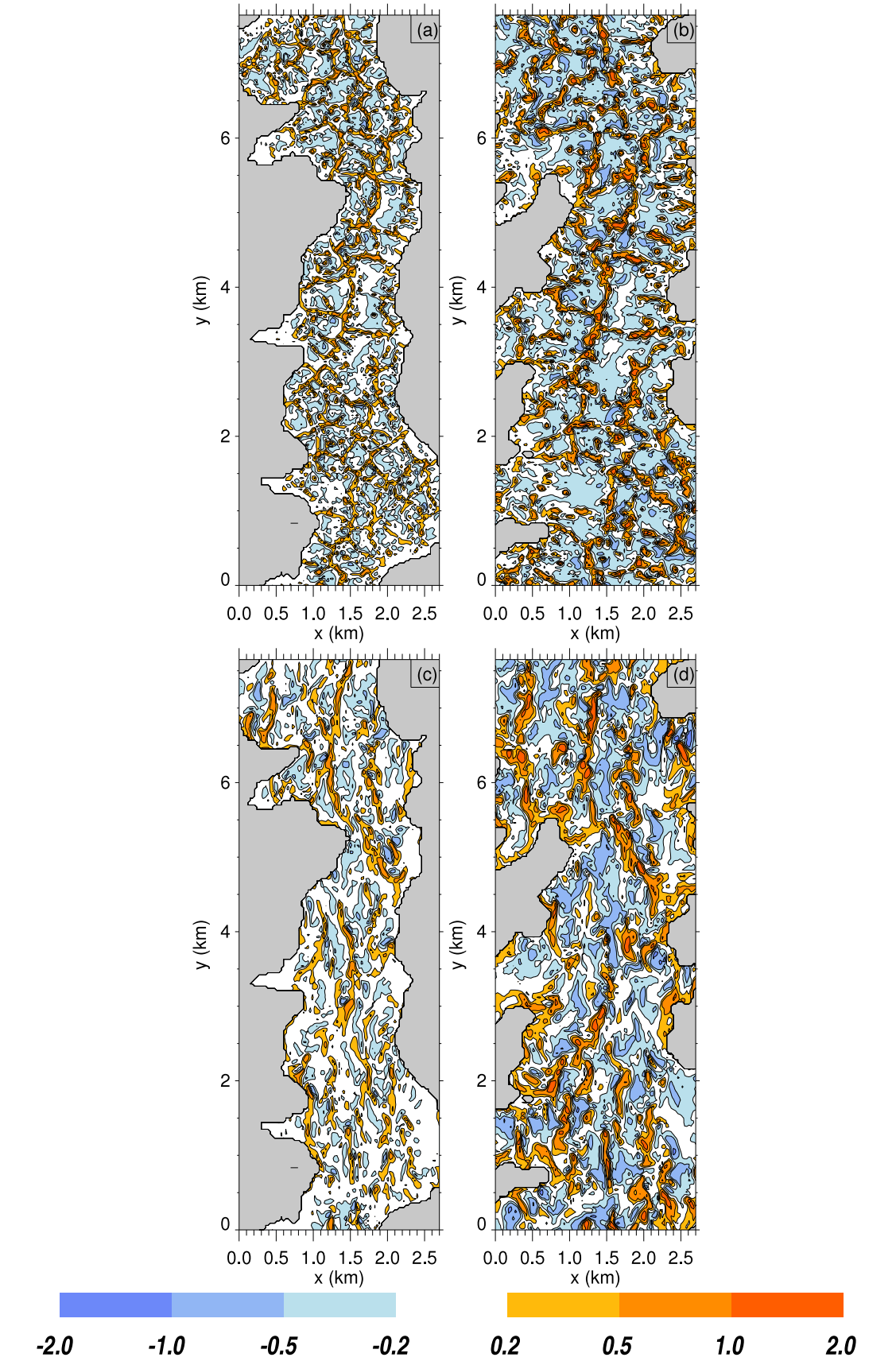

Fig. 5 Instantaneous situations at the time t_1 in the simulated low wind period p_1 (a and b) and for the time t_2 in the simulated up-valley wind period p_2 (c and d) of the simulation *R*2. Vertical wind component w in m s^{-1} is colour-coded. The cross sections are placed at 210 m (a and c) and 300 m a.s.l. (b and d), respectively. The area shown here is marked by the red frame in Fig. 3.

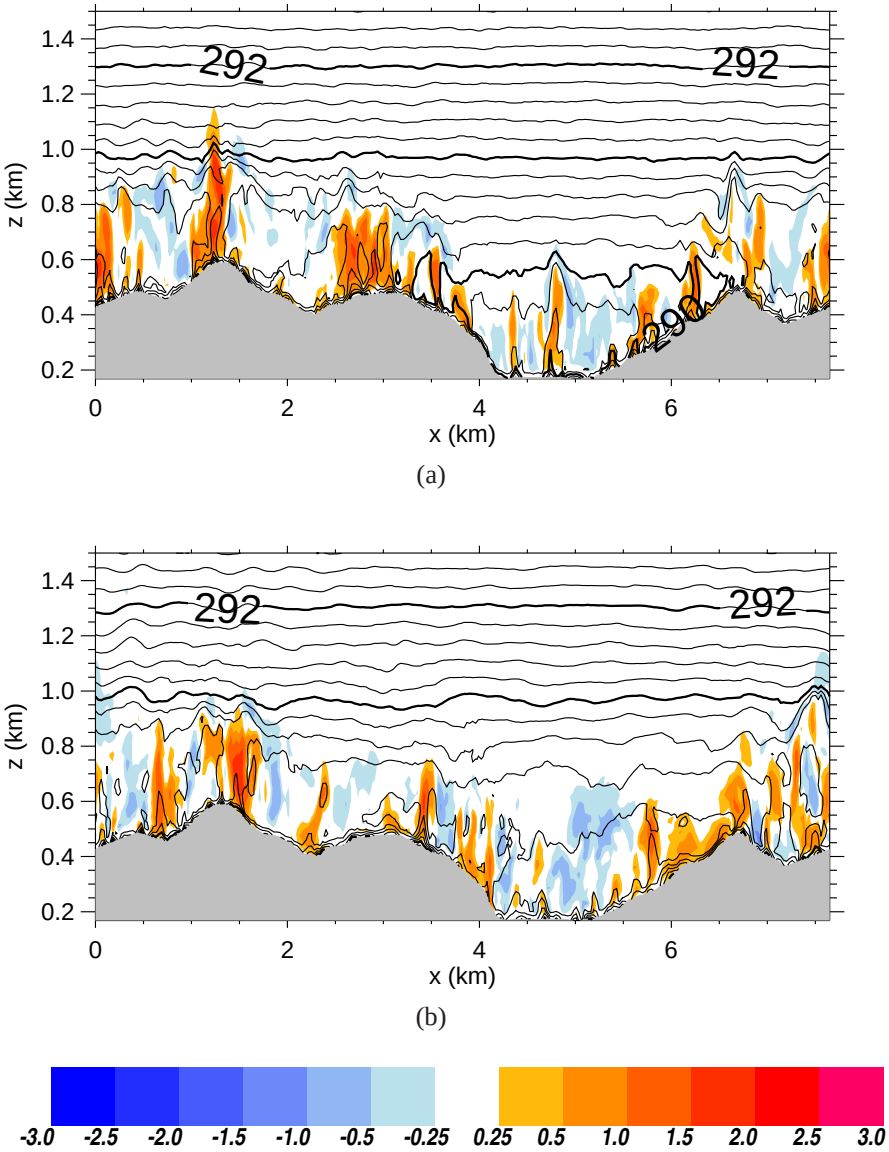

Fig. 6 Vertical cross sections perpendicular to the axis of the valley. Instantaneous situations of the simulation *R2* are shown for the time t_1 in p_1 (a) and for the time t_2 in p_2 (b). Vertical wind w in m s^{-1} is colour-coded. Black lines are isentropes in steps of 0.2 K. Intersection with the orography is shaded in grey.

t_1 in the low wind speed period p_1 and the time t_2 in the up-valley wind period p_2. Figure 5a and b show - especially in the lower height - the typical spoke patterns at time t_1 (e.g. Schmidt and Schumann, 1989). In contrast, at time t_2 (Fig. 5c, d) there are hardly any of these regular patterns left and instead there are now irregular streak-like patterns. The axis of the streak-like structures is aligned roughly in the main wind direction. Roll or streak-like structures in a shear-buoyancy-driven boundary layer are a well-described phenomena in literature (e.g. Moeng and Sullivan, 1994; Weckwerth et al., 1997; Drobinski et al., 1998; Drobinski and Foster, 2003). The locations of updraughts and downdraughts in the instantaneous snapshots at time t_1 in Fig. 5a and b agree well with those found in the ensemble and time mean in Fig. 3. Figure 6 shows the vertical wind and the temperature stratification for instantaneous vertical slices through the model domain at time t_1 (Fig. 6a) and at time t_2 (Fig. 6b). Similar to the observations shown in Fig. 4, strong convective updraught structures can be seen in period p_1 within the valley which penetrate into the stably stratified free at-

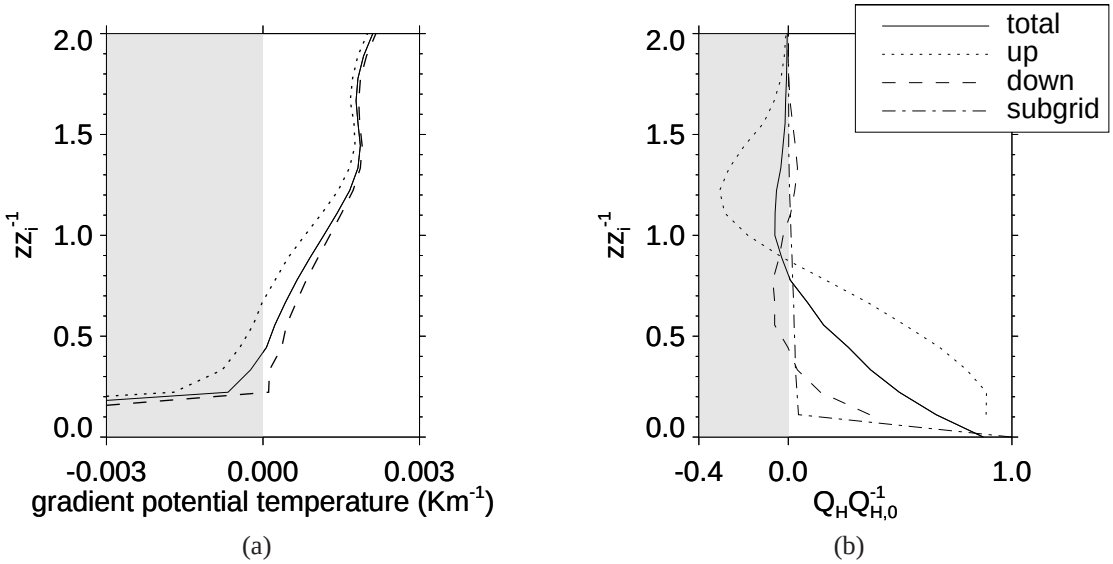

Fig. 7 (a) Vertical profiles of the gradient of the potential temperature and (b) normalized vertical profiles of the heat flux Q_H at time t_1 of the simulation $R2$. Only points in the valley are considered (see red frame in Fig. 3). The solid line shows the values for all points in the valley. The dotted lines shows the profile for places with $w > 0$ (up) and the dashed line for places with $w < 0$ (down). The contribution to the heat flux from the sub-grid model is shown in (b) as dash-dotted line.

mosphere up to a height of about 600 m a.s.l. Within a coherent updraught structure a more neutral stratification is found. In period p_2, more neutral stratification can be seen within the entire valley. The vertical extent of the updraught structures is confined to the neutrally stratified valley atmosphere and does not reach into the stably stratified atmosphere above.

The heat flux profiles and the corresponding vertical gradients of the potential temperature in period p_1 are shown in Fig. 7a and Fig. 7b, respectively. The profiles are calculated as horizontal mean for the area marked with the red frame in Fig. 3. Besides the mean profiles within the valley for all points, profiles for updraught and downdraught areas are analysed separately. In the center of the valley boundary layer between about $0.4z_i$ and $0.8z_i$ the flux of sensible heat, averaged horizontally over all points in the valley, is counter to the temperature gradient. Regarding the updraught area, the heat flux follows the temperature gradient up to a height of $0.65z_i$ due to the unstable to neutral stratification. A counter-gradient flux remains above this height up to approximately $0.9z_i$. Counter-gradient fluxes are a common feature in turbulent flows and are well studied (e.g. Schumann, 1987). The counter-gradient turbulent transfer within forest canopies is discussed, e.g., in Denmead and Bradley (1985). The total heat flux is mainly determined by the flux within the coherent upward motions. Together with the findings in Sec. 3.2 (the orography forces the updraught areas to evolve at specific locations), this result leads to the statement that the majority of the flux takes place at these specific locations.

The change of the flow in the periods $p1$ and $p2$ leads to a modified vertical turbulent transport of TKE. Figure 8 shows the profiles of the transport term of the TKE budget for both times t_1 and t_2. At time t_1, the profile of the turbulent transport of TKE shows negative values in the lower half of the boundary layer and positive values in the upper half (Fig. 8a). Due to the vertical orientation of the flow in p_1, the TKE is redistributed vertically by turbulent eddies. At time t_2 (Fig. 8b), the profile of the turbulent transport of TKE deviates strongly from the situation at t_1. Its values are close to zero up to a height of $0.7z_i$. Above

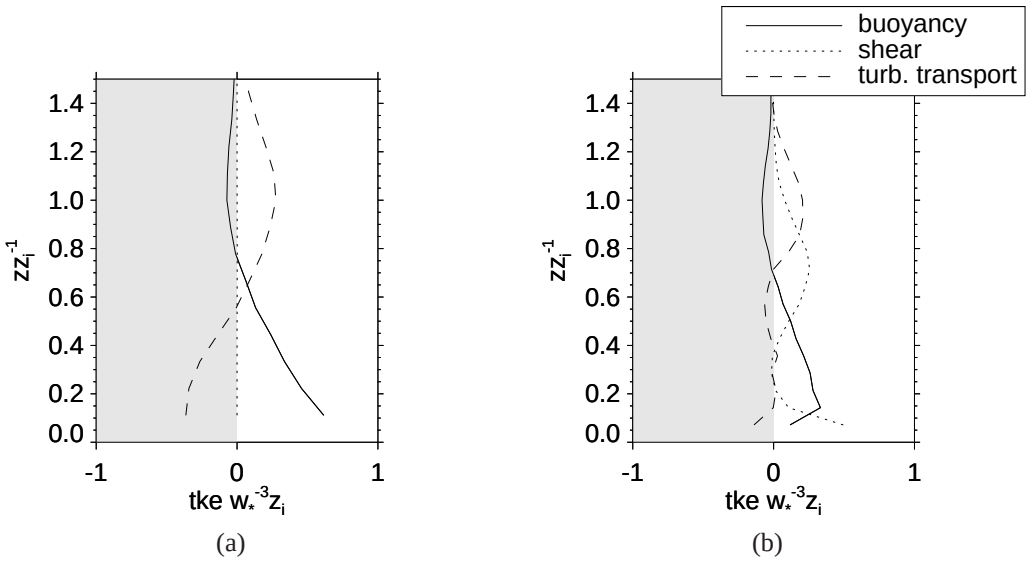

Fig. 8 Vertical profiles of the TKE budget terms of buoyancy, shear and transport for the time t_1 in p_1 (a) and for the time t_2 in p_2 (b) of the simulation *R*2. Only points in the valley are considered (see red frame in Fig. 3).

this height positive values prevail. This means that the vertical turbulent transport of TKE has ceased in the period p_2. The positive values above $0.7z_i$ originate from the production of TKE from outside the valley, i.e. the averaging area (red frame in Fig. 3).

The profiles for the buoyancy term and the shear term of the TKE budget are plotted in Fig. 8 in the same manner as the profiles described above. During the transition from t_1 to t_2, the profile for buoyancy production of TKE remains positive below $0.7z_i$ and negative above. The major change here is that the maximum of the buoyant production of TKE is shifted upwards to $0.15z_i$. This shift is accompanied by an increased shear production of TKE below $0.2z_i$. The maximum in shear production of TKE at $0.7z_i$ at the time t_2 derives from the imposed along valley wind described in Sec. 2.2.2.

4 Conclusions

During the three months of the COPS campaign the surface energy balance at the site in the Kinzig valley was rarely closed, as common for many energy balance measurements. However, the analysis in this study gave the surprising result that the energy balance was closed on average for the low wind period in the morning hours on radiation days. A closed energy balance indicates that all energy containing motions were captured by the instrumentation and that the assumptions for data processing, i.e. stationarity and homogeneity of the flow, were satisfied. It has to be assumed that due to the vanishing horizontal wind speed no missing advective flux components developed over the complex terrain. After the onset of the valley wind, missing advective flux components occurred and the desired closure was no longer met, with the residual of the energy balance going up to values typical for the full data set of this site. The partition of the turbulent heat flux into the contributions of latent and sensible heat indicated that the residual in the considered data occurs due to the reduced relative sensible heat flux.

Large-eddy simulations of the atmosphere in the Kinzig valley were carried out. It was found that the convection in the valley gets organized by the surrounding ridges during the

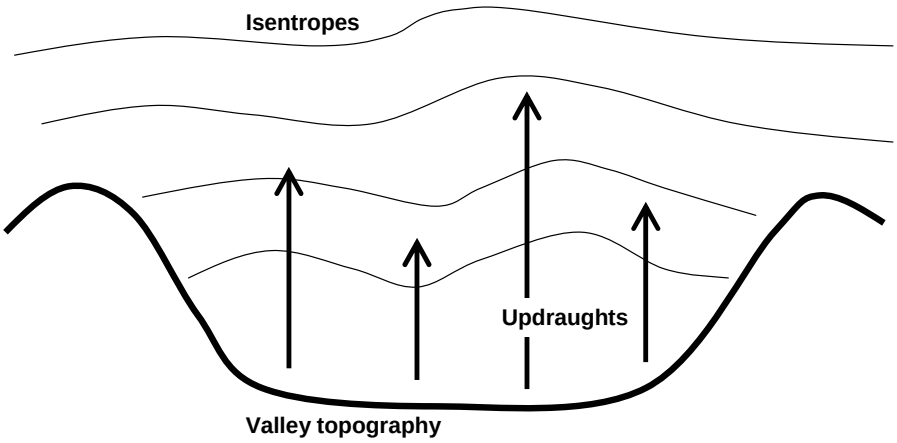

Fig. 9 Schematic view of the turbulent transport during the early-morning low wind speed periods in the Kinzig valley. Strong updraughts exist at specific, preferential locations in the valley which penetrate into the stably stratified valley atmosphere and extend up to about the height of the surrounding ridges.

low-wind period, resulting in quasi-stationary patterns. With this finding the observations of the Sodar/RASS instrument were interpreted in a new way. The distribution of the vertical wind speed, observed by the Sodar/RASS, did not follow the expected pdfs known from literature. While the pdfs derived from the simulations confirmed the results from literature, the pdfs derived from the areas of preferred vertical motion matched well with the observations. This is a strong indication that under the conditions considered here there are orographically induced stationary convection patterns in the valley and further, that the site of the Sodar/RASS was placed in an area of preferred upward motion.

Both the Sodar/RASS observations and the simulations indicate that the turbulent transfer within the valley is counter to the temperature gradient during the early-morning low wind period. This finding is also illustrated schematically in Fig. 9. Surface layer air mass characteristics are transported into higher regions of the stably stratified free atmosphere by strong coherent updraughts in these situations. These coherent updraught structures were shown to occur at specific, preferential locations. The vertical extent of these updraughts happens to be about the height of the surrounding ridges or slightly higher. With the above-valley or large-scale flow at these heights, it can be expected that the vertically transported surface layer air mass characteristics can be translocated horizontally and alter boundary-layer properties elsewhere. As situations of low wind speeds together with high sensible heat fluxes can also develop in different settings of complex terrain (e.g. Hiller et al., 2008; Mayer et al., 2008; Zhou et al., 2011), the observed vertical transport mechanism is not restricted to the conditions in the Kinzig valley. Mayer et al. (2008), e.g., observed the free convective coherent release of surface layer trace gases into upper regions of the boundary layer, which were then advected by the mean wind towards a mountain summit and altered the trace gas observations there significantly. For that reason, the free convective coherent transport of surface layer air mass properties into a stably stratified boundary layer as described in this study should be considered within further boundary-layer experiments.

Acknowledgements This study was funded by the Deutsche Forschungsgesellschaft (DFG) within the special priority program SPP1167 (WI 1685/9-1, WI 1685/10-1, FO 226/19-1, FO 226/23-1). The numerical simulations made for this study were carried out at the high performance computing center of the Deutsches Klima Rechenzentrum (DKRZ) in Hamburg, Germany.

References

Beyrich F (1997) Mixing height estimation from sodar data - A critical discussion. Atmos Environ 31(23):3941–3953, DOI 10.1016/S1352-2310(97)00231-8

Chandra AS, Kollias P, Giangrande SE, Klein SA (2010) Long-term observations of the convective boundary layer using insect radar returns at the SGP ARM climate research facility. J Clim 23(21):5699–5714, DOI 10.1175/2010JCLI3395.1

Charuchittipan D, Babel W, Mauder M, Beyrich F, Leps JP, Foken T (2013) Extension of the averaging time of the eddy-covariance measurement and its effect on the energy balance closure. Boundary-Layer Meteorol to be submitted

Clark T, Farley R (1984) Severe downslope windstorm calculations in 2 and 3 spatial dimensions using anelastic interactive grid nesting - a possible mechanism for gustiness. J Atmos Sci 41(3):329–350, DOI 10.1175/1520-0469(1984)041<0329:SDWCIT>2.0.CO;2

Deardorff J, Willis G (1985) Further results from a laboratory model of the convective planetary boundary layer. Boundary-Layer Meteorol 32:205–236, DOI 10.1007/BF00121880

Deardorff JW (1970) Convective velocity and temperature scales for the unstable planetary boundary layer and for rayleigh convection. J Atmos Sci 27:1211–1213, DOI 10.1175/1520-0469(1970)027<1211:CVATSF>2.0.CO;2

Defant F (1949) Zur Theorie der Hangwinde, nebst Bemerkungen zur Theorie der Berg- und Talwinde. Arch Meteorol Geophys Bioklim A1:421–450

Denmead DT, Bradley EF (1985) Flux-gradient relationships in a forest canopy. In: Hutchison BA, Hicks BB (eds) The forest-atmosphere interaction, D. Reidel Publ. Comp., Dordrecht, Boston, London, pp 421–442

Dörnbrack A, Schumann U (1993) Numerical simulation of turbulent convective flow over wavy terrain. Boundary-Layer Meteorol 65:323–355, DOI 10.1007/BF00707032

Drobinski P, Foster RC (2003) On the origin of near-surface streaks in the neutrally-stratified planetary boundary layer. Boundary-Layer Meteorol 108:247–256, DOI 10.1023/A:1024100125735

Drobinski P, Brown RA, Flamant PH, Pelon J (1998) Evidence of organized large eddies by ground-based doppler lidar, sonic anemometer and sodar. Boundary-Layer Meteorol 88:343–361, DOI 10.1023/A:1001167212584

Eigenmann R, Metzger S, Foken T (2009) Generation of free convection due to changes of the local circulation system. Atmos Chem Phys 9:8587–8600, DOI 10.5194/acp-9-8587-2009

Eigenmann R, Kalthoff N, Foken T, Dorninger M, Kohler M, Legain D, Pigeon G, Piguet B, Schüttemeyer D, Traulle O (2011) Surface energy balance and turbulence network during the Convective and Orographically-induced Precipitation Study (COPS). Q J Roy Meteorol Soc 137(S1):57–69, DOI 10.1002/qj.704

Foken T (2008) The energy balance closure problem: An overview. Ecol Appl 18:1351–1367, DOI 10.1890/06-0922.1

Foken T, Mauder M, Liebethal C, Wimmer F, Beyrich F, Leps JP, Raasch S, DeBruin HAR, Meijninger WML, Bange J (2010) Energy balance closure for the LITFASS-2003 experiment. Theor Appl Climatol 101:149–160, DOI 10.1007/s00704-009-0216-8

Foken T, Aubinet M, Finnigan JJ, Leclerc MY, Mauder M, Paw U KT (2011) Results of a panel discussion about the energy balance closure correction for trace gases. Bull Am Meteorol Soc 92:ES13–ES18, DOI 10.1175/2011BAMS3130.1

Foken T, Aubinet M, Leuning R (2012) The eddy covariance method. In: Aubinet M, Vesala T, Papale D (eds) Eddy Covariance, Springer Atmospheric Sciences, Springer Netherlands, pp 1–19, DOI 10.1007/978-94-007-2351-1-1

Gal-Chen T, Somerville RC (1975) On the use of a coordinate transformation for the solution of the Navier-Stokes equations. J Comput Phys 17:209 – 228, DOI 10.1016/0021-9991(75)90037-6

Hiller R, Zeeman M, Eugster W (2008) Eddy-covariance flux measurements in the complex terrain of an alpine valley in switzerland. Boundary-Layer Meteorol 127:449–467, DOI 10.1007/s10546-008-9267-0

Inagaki A, Letzel MO, Raasch S, Kanda M (2006) Impact of surface heterogeneity on energy imbalance: A study using LES. J Meteorol Soc Jpn 84:187–198, DOI 10.2151/jmsj.84.187

Kalthoff N, Kohler M, Barthlott C, Adler B, Mobbs S, Corsmeier U, Träumner K, Foken T, Eigenmann R, Krauss L, Khodayar S, Di Girolamo P (2011) The dependence of convection-related parameters on surface and boundary-layer conditions over complex terrain. Q J Roy Meteorol Soc 137(S1):70–80, DOI 10.1002/qj.686

Kanda M, Moriwaki R, Kasamatsu F (2004) Large-eddy simulation of turbulent organized structures within and above explicitly resolved cube arrays. Boundary-Layer Meteorol 112(2):343–368, DOI 10.1023/B:BOUN.0000027909.40439.7c

Kühnlein C, Smolarkiewicz PK, Dörnbrack A (2012) Modelling atmospheric flows with adaptive moving meshes. J Comput Phys 231(7):2741–2763, DOI 10.1016/j.jcp.2011.12.012

Mahrt L (2010) Computing turbulent fluxes near the surface: Needed improvements. Agric For Meteorol 150(4):501–509, DOI 10.1016/j.agrformet.2010.01.015

Mauder M, Foken T (2006) Impact of post-field data processing on eddy covariance flux estimates and energy balance closure. Meteorol Z 15(6):597–609, DOI doi:10.1127/0941-2948/2006/0167

Mayer JC, Staudt K, Gilge S, Meixner FX, Foken T (2008) The impact of free convection on late morning ozone decreases on an Alpine foreland mountain summit. Atmos Chem Phys 8:5941–5956, DOI 10.5194/acp-8-5941-2008

Metzger S, Foken T, Eigenmann R, Kurtz W, Serafimovich A, Siebicke L, Olesch J, Staudt K, Lüers J (2007) COPS experiment, Convective and orographically induced precipitation study, 01 June 2007 – 31 August 2007, Documentation. Work Report University of Bayreuth, Department of Micrometeorology, 34, Print: ISSN 1614-8916, 72 pp.

Moeng CH, Sullivan PP (1994) A comparison of shear- and buoyancy-driven planetary boundary layer flows. J Atmos Sci 51:999–1022, DOI 10.1175/1520-0469(1994)051<0999:ACOSAB>2.0.CO;2

NASA Land Processes Distributed Active Archive Center NASA LP DAAC (2001) AST-GTM ASTER Global Digital Elevation Model. LP DAAC, USGS/Earth Resources Observation and Science (EROS) Center, Sioux Falls, South Dakota.

Oncley SP, Foken T, Vogt R, Kohsiek W, DeBruin HAR, Bernhofer C, Christen A, van Gorsel E, Grantz D, Feigenwinter C, Lehner I, Liebethal C, Liu H, Mauder M, Pitacco A, Ribeiro L, Weidinger T (2007) The Energy Balance Experiment EBEX-2000. Part I: Overview and energy balance. Boundary-Layer Meteorol 123:1–28, DOI 10.1007/s10546-007-9161-1

Piotrowski Z, Smolarkiewicz P, Malinowski S, Wyszogrodzki A (2009) On numerical realizability of thermal convection. J Comput Phys 228:6268–6290, DOI 10.1016/j.jcp.2009.05.023

Prusa JM, Smolarkiewicz PK (2003) An all-scale anelastic model for geophysical flows: dynamic grid deformation. J Comput Phys 190:601 – 622, DOI 10.1016/S0021-9991(03)00299-7

Prusa JM, Smolarkiewicz PK, Wyszogrodzki AA (2008) Eulag, a computational model for multiscale flows. Comput Fluids 37(9):1193–1207, DOI 10.1016/J.Compfluid.2007.12.001

Raasch S, Harbusch G (2001) An analysis of secondary circulations and their effects caused by small-scale surface inhomogeneities using large-eddy simulation. Boundary-Layer Meteorol 101:31–59, DOI 10.1023/A:1019297504109

Rotach MW, Andretta M, Calanca P, Weigel AP, Weiss A (2008) Boundary layer characteristics and turbulent exchange mechanisms in highly complex terrain. Acta Geophys 56(1):194–219, DOI 10.2478/s11600-007-0043-1

Schmidt H, Schumann U (1989) Coherent structure of the convective boundary layer derived from large-eddy simulations. J Fluid Mech 200:511–562, DOI 10.1017/S0022112089000753

Schumann U (1987) The countergradient heat flux in turbulent stratified flows. Nucl Eng Des 100(3):255–262, DOI 10.1016/0029-5493(87)90078-1

Segal M, Arritt RW (1992) Nonclassical mesoscale circulations caused by surface sensible heat-flux gradients. Bull Am Meteorol Soc 73(10):1593–1604, DOI 10.1175/1520-0477(1992)073<1593:NMCCBS>2.0.CO;2

Smolarkiewicz PK, Margolin LG (1993) On forward-in-time differencing for fluids: Extension to a curvilinear framework. Mon Weather Rev 121(6):1847–1859, DOI 10.1175/1520-0493(1993)121<1847:OFITDF>2.0.CO;2

Smolarkiewicz PK, Margolin LG (1998) MPDATA: a finite-difference solver for geophysical flows. J Comput Phys 140(2):459–480, DOI 10.1006/jcph.1998.5901

Smolarkiewicz PK, Grubisic V, Margolin LG (1997) On forward-in-time differencing for fluids: Stopping criteria for iterative solutions of anelastic pressure equations. Mon Weather Rev 125(4):647–654, DOI 10.1175/1520-0493(1997)125<0647:OFITDF>2.0.CO;2

Smolarkiewicz PK, Sharman R, Weil J, Perry SG, Heist D, Bowker G (2007) Building resolving large-eddy simulations and comparison with wind tunnel experiments. J Comput Phys 227:633–653, DOI 10.1016/j.jcp.2007.08.005

Sorbjan Z (1996) Numerical study of penetrative and ”solid lid” nonpenetrative convective boundary layers. J Atmos Sci 53:101–112, DOI 10.1175/1520-0469(1996)053<0101:NSOPAL>2.0.CO;2

Stoy P, Mauder M, Foken T, Marcolla B, Boegh E, Ibrom A, Arain M, Arneth A, Aurela M, Bernhofer C, Cescatti A, Dellwik E, Duce P, Gianelle D, van Gorsel E, Kiely G, Knohl A, Mangolis H, McCaughey H, Merbold L, Montagnani L, Papale D, Reichstein M, Serrano-Ortiz P, Sottocornola M, Saunders M, Spano D, Vaccari F, Varlagin A (2013) A data-driven analysis of energy balance closure across FLUXNET research sites: The role of landscape-scale heterogeneity. Agric For Meteorol , accepted

Stull RB (1988) An introduction to boundary layer meteorology. Kluwer Academic Publishers, Dordrecht

Thomas SJ, Hacker JP, Smolarkiewicz PK, Stull RB (2003) Spectral preconditioners for nonhydrostatic atmospheric models. Mon Weather Rev 131(10):2464–2478, DOI 10.1175/1520-0493(2003)131<2464:SPFNAM>2.0.CO;2

Twine TE, Kustas WP, Norman JM, Cook DR, Houser PR, Meyers TP, Prueger JH, Starks PJ, Wesely ML (2000) Correcting eddy-covariance flux underestimates over a grassland. Agric For Meteorol 103:279–300

Walko R, Cotton W, Pielke R (1992) Large-eddy simulations of the effects of hilly terrain on the convective boundary-layer. Boundary-Layer Meteorol 58(1-2):133–150, DOI 10.1007/BF00120755

Weckwerth TM, Wilson JW, Wakimoto RM, Crook NA (1997) Horizontal convective rolls: determining the environmental conditions supporting their existence and characteristics. Mon Weather Rev 125:505–526, DOI 10.1175/1520-0493(1997)125<0505:HCRDTE>2.0.CO;2

Wedi NP, Smolarkiewicz PK (2004) Extending Gal-Chen and Somerville terrain-following coordinate transformation on time-dependent curvilinear boundaries. J Comput Phys 193:1–20, DOI 10.1016/j.jcp.2003.07.034

Weigel A, Chow F, Rotach M (2007) The effect of mountainous topography on moisture exchange between the "surface" and the free atmosphere. Boundary-Layer Meteorol 125:227–244, DOI 10.1007/s10546-006-9120-2

Whiteman CD (1990) Observations of thermally developed wind systems in mountainous terrain. In: Blumen W (ed) Atmospheric processes over complex terrain, Meteorological monographs, vol 23 (45), American Meteorological Society, Boston, Massachusetts, pp 5–42

Whiteman CD (2000) Mountain Meteorology: Fundamentals and Applications. Oxford University Press, USA

Wulfmeyer V, Behrendt A, Kottmeier C, Corsmeier U, Barthlott C, Craig GC, Hagen M, Althausen D, Aoshima F, Arpagaus M, Bauer HS, Bennett L, Blyth A, Brandau C, Champollion C, Crewell S, Dick G, Di Girolamo P, Dorninger M, Dufournet Y, Eigenmann R, Engelmann R, Flamant C, Foken T, Gorgas T, Grzeschik M, Handwerker J, Hauck C, Höller H, Junkermann W, Kalthoff N, Kiemle C, Klink S, König M, Krauss L, Long CN, Madonna F, Mobbs S, Neininger B, Pal S, Peters G, Pigeon G, Richard E, Rotach MW, Russchenberg H, Schwitalla T, Smith V, Steinacker R, Trentmann J, Turner DD, van Baelen J, Vogt S, Volkert H, Weckwerth T, Wernli H, Wieser A, Wirth M (2011) The Convective and Orographically-induced Precipitation Study (COPS): the scientific strategy, the field phase, and research highlights. Q J Roy Meteorol Soc 137(S1):3–30, DOI 10.1002/qj.752

Zardi D, Whiteman CD (2013) Diurnal mountain wind systems. In: Chow FK, De Wekker SF, Snyder BJ (eds) Mountain Weather Research and Forecasting, Springer Netherlands, Dordrecht, pp 35–119

Zhou D, Eigenmann R, Babel W, Foken T, Ma Y (2011) The study of near-ground free convection conditions at nam co station on the tibetan plateau. Theor Appl Climatol 105:217–228, DOI 10.1007/s00704-010-0393-5

Erklärung

Hiermit erkläre ich, dass ich die Arbeit selbständig verfasst und keine anderen als die von mir angegebenen Quellen und Hilfsmittel benutzt habe.

Ferner erkläre ich, dass ich anderweitig mit oder ohne Erfolg nicht versucht habe, diese Dissertation einzureichen. Ich habe keine gleichartige Doktorprüfung an einer anderen Hochschule endgültig nicht bestanden.

Bayreuth, den _____ _____

Rafael Eigenmann